Filip Ljubinković

STRUCTURAL BEHAVIOUR OF COLD-FORMED STEEL BEAMS SUBJECTED TO FIRE

FCTUC 2016

FCTUC DEPARTAMENTO DE ENGENHARIA CIVIL
FACULDADE DE CIÊNCIAS E TECNOLOGIA
UNIVERSIDADE DE COIMBRA

isise Institute for Sustainability and Innovation in Structural Engineering

# STRUCTURAL BEHAVIOUR OF COLD-FORMED STEEL BEAMS SUBJECTED TO FIRE

Filip Ljubinković

Supervisors: Professor Aldina Maria da Cruz Santiago
Professor Rui António Duarte Simões

European Commission
ERASMUS MUNDUS

Thesis Submitted in partial fulfillment of requirements for the degree of Master of Science in Construction of Steel and Composite Structures
European Erasmus Mundus Master
Sustainable Constructions under natural hazards and catastrophic events

University of Coimbra
29.01.2016

# STRUCTURAL BEHAVIOUR OF COLD-FORMED STEEL BEAMS SUBJECTED TO FIRE

Author: Filip Ljubinković

Supervisors: Professor Aldina Maria da Cruz Santiago
Professor Rui António Duarte Simões

University: University of Coimbra


University: University of Coimbra
Date: 29.01.2016

# ACKNOWLEDGMENTS

I would like to thank my advisors Professor Aldina Santiago and Professor Rui Simões for all the help and support they both showed throughout the thesis. Even before the study in this thesis, I had a chance to meet them during my master's program, and their profound knowledge and scientific approach have motivated me a lot, so I can say only words of gratitude that I am given an opportunity to meet them again here at the University of Coimbra and to collaborate with them. Beside they sheared their knowledge unselfishly, they also helped me to solve all technical and institutional problems, so I may say that my expectations were even exceeded and I know the thesis could not be completed without their help. It has been for me an honour and privilege to work and learn from such experts, and I am sure it will help me a lot in the future.

Special acknowledgments are addressed to the Erasmus Mundus SUSCOS_M Consortium, for the Consortium Grant but also to all the people who are a part of this organization and who made it possible to me to participate in the international education exchange program and to improve my knowledge and capacities.

Finally, I would like to thank my parents (Boško Ljubinković, Anita Ljubinković), sisters (Katarina Ljubinković , Ana Ljubinković) and all friends and colleagues whose words of encouragement have always helped me to remain persistent and focused and have also given me the strength to overcome many difficulties throughout the life.

# ABSTRACT

The cold-formed profiles have got recently a significant role in the civil engineering industry. Main reason for this is the fact that these profiles offer numerous advantages in comparison with hot-rolled sections. Cold-forming manufacturing process nowadays makes it possible to have practically any desired shape and dimension of product which considerably increases design flexibility and moreover allows very attractive, economical and sustainable solutions. Another huge advantage is the possibility of prefabrication and mass production, which combined with a very high load capacity-to-weight ratio these profiles have, may naturally lead to enormous construction speed, easy erection and great structural performance. For these reasons, cold-formed profiles found its practical use in numerous building applications.

However, due to the thin shape and thus very slender sections there are several key drawbacks of the cold-formed profiles worth of mentioning; one of them is definitely their sensitivity and vulnerability to buckling phenomenon with often very low critical loading and short buckling lengths. Another problem with the cold-formed profiles is very poor fire resistance. The main reason for this is because steel has high thermal conductivity while the cross sections are not massive and therefore the section factors are several times higher than an average hot-rolled profile. The buckling phenomena of the thin-gauge profiles, however, have been widely examined and the design procedures in which these problems are taken into account are now completely known and can be found in almost every design code. On the other hand, studies on fire performance of cold-formed steel members are still fairly rare and the knowledge in this particular area is rather obscure. The aim of this study is thus to help and stimulate the development of a new knowledge in this particular area of fire safety design and to spur further investigation.

This thesis mainly intends to examine the structural behavior of the cold-formed steel beams in the role of purlins with “Omega - Ω“ shape of the cross-section under the fire condition. For this purpose an industrial building in Portugal is taken as a study case, where 30 minutes resistance is requested by the Portuguese Legislation for purlins above the mezzanine floor where offices are placed. For the considered study case, the zone model curve obtained in Ozone program is used. The analytical approach is conducted according to Eurocode and these results are further compared with the numerical ones, carried out by the use of finite element analysis software – ABAQUS. More specifically, the objective is to determine an adequate fire protection which should aim to help these cold-formed purlins to meet the required fire resistance. Also for this purpose, both analytical and numerical results are obtained and compared. Furthermore, a parametric

study was performed in order to find out the influence of several parameters on the structural performance of the CFS purlins, such as the static scheme of purlin (simply supported beam and continuous beam), initial geometric imperfections, the finite element mesh size and the thickness of both steel section and fire protection. It was established that numerical analysis gives slightly higher resistances of the purlins in comparison with the analytical results, and that the initial imperfections play an important role in overall behavior of the cold-formed profiles subjected to fire by reducing their resistance.

The final goal of this study was to seek for the optimal economical solution taking into account all the mentioned parameters, which should make these purlins a competitive solution on the market and hopefully initiate their mass production. It is concluded that continuous beams are much better solution than simply supported beam, making the savings in expensive fire protection material up to 50%.

***Keywords:*** Fire, Fire protection, Cold-formed profile, Purlin, Buckling, Analytical, Numerical, Imperfection.

# TABLE OF CONTENTS

# FIGURE INDEX

# TABLE INDEX

# NOTATION

*Chapter 2*

| | |
|---|---|
| $b$ | width of cross-section |
| $h$ | height of cross-section |
| $\lambda$ | half-wave length |
| $L$ | length of the member |
| $r$ | fillet radius |
| $t$ | thickness of the cross-section |

*Chapter 3*

| | |
|---|---|
| $A_s$ | the area of stiffener |
| $A_{s,red}$ | the reduced area of stiffener |
| $\alpha$ | the coefficient of thermal expansion |
| $\alpha_c$ | the coefficient of heat transfer by convection (film coefficient) in $[W/m^2K]$ |
| $\alpha_{LT}$ | the imperfection factor |
| $C_i$ | the coefficient depending on the loading and end restraint conditions |
| $c$ | the specific heat |
| $c_a$ | the specific heat of steel |
| $c_p$ | the temperature independent specific heat of the fire protection material |
| $d_p$ | the thickness of fire protection material |
| $\delta$ | the deflection of the stiffener due to the unit load |
| $\phi$ | the configuration factor |
| $E$ | the modulus of elasticity |
| $E_{fi,d,t}$ | the design value of effects of actions under fire |
| $\varepsilon_m$ | the surface emissivity of the member |
| $\varepsilon_f$ | the emissivity of the fire |
| $f_{p0,2,\theta}$ | 0.2 percent proof strength for steel at elevated temperature |
| $f_{yb}$ | the yield strength at 20℃ |
| $f_{y,\theta}$ | the yield strength at elevated temperatures |
| $f_u$ | the ultimate strength at 20℃ |
| $G$ | the shear modulus |

| | |
|---|---|
| $G_k$ | the characteristic values of the permanent action |
| $\dot{h}_{net}$ | the net heat flux |
| $\dot{h}_{net,c}$ | the convective net heat flux |
| $\dot{h}_{net,r}$ | the radiative net heat flux |
| $I_t$ | the torsion constant |
| $I_w$ | the warping constant |
| $I_z$ | the second moment of area about the weak axis |
| $\rho_p$ | the density of the fire protection material |
| $\sigma$ | the Stephan Boltzmann constant ($5{,}67\ 10^{-8}\ W/m^2K^4$) |
| $\sigma_{com,Ed}$ | the compressive stress at the centre-line of the stiffener calculated on the basis of the effective cross-section |
| $\sigma_{cr,s}$ | the critical buckling stress |
| $K$ | the spring stiffness for displacement |
| $k_{E,\theta}$ | the reduction factor for the elastic modulus |
| $k_{p0,2,\theta}$ | the reduction factor for the design yield strength of hot rolled and welded class 4 sections |
| $k_{y,\theta}$ | the reduction factor for the yield strength of steel at the steel temperature $\theta_a$ reached at time $t$ |
| $k_w$ | the effective length factors |
| $k_\sigma$ | the buckling coefficient |
| $L$ | the beam length between points which have lateral restraint |
| $\lambda_a$ | the thermal conductivity of steel |
| $\bar{\lambda}_{LT}$ | the non dimensional slenderness for lateral torsional buckling |
| $\lambda_p$ | the thermal conductivity of fire protection material |
| $\bar{\lambda}_p$ | the relative slenderness of the plate |
| $M_{b,Rd}$ | the design buckling resistance moment |
| $M_{b,fi,t,Rd}$ | the design buckling resistance moment at time t |
| $M_{cr}$ | the elastic critical moment for lateral-torsional buckling |
| $P_k$ | the characteristic values of the pre-stressing action |
| $Q_k$ | the characteristic values of the variable action |
| $\theta_a$ | the temperature in steel |
| $\theta_{cr,d}$ | the critical temperature |
| $\theta_{m,t}$ | the surface temperature of the member in each moment of time in [$°C$] |
| $\theta_{r,t}$ | the radiation temperature in each moment of time which may be taken as the gas temperature $\theta_g$ in [°C] |
| $t$ | the time in fire exposure |
| $t_{red}$ | the reduced thickness of the cross-section |
| $t_{fi,req}$ | the required resistance time |

| | |
|---|---|
| $u$ | the unit load applied at the centroid of the effective part of the stiffness |
| $\psi_{1,1}$ | the coefficient for frequent value of a variable action (dominant variable action) |
| $\psi_{2,i}$ | the coefficient for quasi-permanent value of a variable action |
| $W_{eff,y}$ | the effective section modulus of the Class 4 cross section |
| $z_g$ | the distance between the point of load application and the shear centre |
| $z_j$ | the parameter which takes into account the level of asymmetry at mono-symmetric cross section |
| $\gamma_{M0}$ | the partial factor for resistance of cross-sections |
| $\gamma_{M1}$ | the partial factor for resistance of members |
| $\gamma_{M,fi}$ | the partial factor for the relevant material property, for the fire situation |
| $\chi_d$ | the reduction factor for the distortional buckling resistance |
| $\chi_{LT}$ | the reduction factor for lateral-torsional buckling |
| $\chi_{LT,fi}$ | the reduction factor for lateral-torsional buckling in the fire design situation |
| $\phi_{LT}$ | value to determine the reduction factor $\chi_{LT}$ |

*Chapter 4*

| | |
|---|---|
| $A$ | the area of cross-section |
| $A_{eff}$ | the effective area of a cross-section |
| $\beta_y$ | the mono-symmetry constant about y-axis |
| $\beta_z$ | the mono-symmetry constant about z-axis |
| $E_{a,\theta}$ | the elastic modulus of steel at elevated temperatures |
| $e_c$ | the distance of the extreme fiber in compression |
| $e_t$ | the distance of the extreme fiber in tension |
| $\varepsilon$ | the strain |
| $g_k$ | the characteristic value of the permanent load |
| $I_{eff,y}$ | the second moment of effective area with respect to y-axis |
| $I_{eff,z}$ | the second moment of effective area with respect to z-axis |
| $i_y$ | the radius of gyration about principle y-axis |
| $i_z$ | the radius of gyration about principle z-axis |
| $q_{Ed}$ | the design values of the applied forces for the ultimate limit state |
| $q_{fi,d}$ | the design effect for fire situation |
| $q_k$ | the characteristic value of the imposed load |
| $W_{eff,y}$ | the effective section modulus about principle y-axis |
| $W_{el,y}$ | the elastic section modulus about principle y-axis |

| | |
|---|---|
| $W_{el,z}$ | the elastic section modulus about principle z-axis |
| $y_{sc}$ | the shear centre coordinate in y-direction |
| $z_{sc}$ | the shear centre coordinate in z-direction |
| $\psi$ | the stress or strain ratio |
| $v$ | the Poisson's ratio |

*Chapter 5*

| | |
|---|---|
| $A_m/V$ | the section factor for unprotected steel members |
| $A_p/V$ | the section factor for protected steel members |
| $\alpha_{cr}$ | the minimum force amplifier to reach the elastic critical buckling |
| $f_{bv}$ | the shear buckling strength |
| $h_w$ | the height of the web |
| $I_s$ | the second moment of area of the intermediate stiffener |
| $k_{sh}$ | correction factor for the shadow effect |
| $k_\tau$ | the coefficient of shear buckling |
| $\kappa$ | the adaptation factor |
| $\kappa_1$ | the adaptation factor for non-uniform temperature across the cross-section |
| $\kappa_2$ | the adaptation factor for non-uniform temperature along the beam |
| $\bar{\lambda}_w$ | the relative web slenderness |
| $M_{Ed}$ | the design bending moment |
| $M_{Rd}$ | the characteristic moment resistance of the critical cross section |
| $S$ | the spacing between purlins |
| $s_d$ | the total developed slant height of the web |
| $V_{b,Rd}$ | the design shear resistance |
| $V_{Ed}$ | the design shear force |
| $V_{Ed,web}$ | the design shear force per web |
| $\phi$ | the inclination angle of the web |
| $\theta_{crit}$ | the critical temperature of steel |

*Chapter 6*

| | |
|---|---|
| $\alpha_c$ | the film coefficient of convection |
| $\delta_{global}$ | the global geometric imperfections |
| $\delta_{global}$ | the local geometric imperfections |
| $\sigma_{nom}$ | the nominal value of stress |
| $\sigma_{true}$ | the true value of stress |

| | |
|---|---|
| $\varepsilon_{nom}$ | the nominal value of strain |
| $\varepsilon_{pl}$ | the plastic strains |
| $\varepsilon_{true}$ | the true value of strain |
| $\dot{Q}$ | the rate of transferred heat (heat flux) |
| $dT$ | the temperature difference |
| $\theta_g$ | the gas temperature |
| $\theta_m$ | temperature of the element |

*Appendix A*

| | |
|---|---|
| $A$ | the area of the fire compartment |
| $A_f$ | the floor area of the fire compartment |
| $A_h$ | the area of horizontal openings in roof of compartment |
| $A_{h,v}$ | the total area of openings in enclosure |
| $A_t$ | the total area of enclosure (walls, ceiling and floor, including openings) |
| $A_v$ | the total area of vertical openings on all walls |
| $b$ | the thermal absorptivity for the total enclosure |
| $b_i$ | the thermal absorptivity of layer i of one enclosure surface |
| $\delta_{q1}$ | the factor which considers the risk of fire activation by size of the compartment |
| $\delta_{q2}$ | the factor which considers the fire activation risk due to the type of occupancy |
| $\delta_n$ | the factor which considers the different active protection measures |
| $h_{eq}$ | the weighted average of window heights on all walls |
| $m$ | the combustion efficiency factor (recommended value is 0.8) |
| $O$ | the opening factor of the fire compartment |
| $q_{f,d}$ | the design value of fire load density |
| $q_{f,k}$ | the characteristic value of fire load density |
| $q_{t,d}$ | the design value of the fire load density which refers to the total surface |
| $s_i$ | the thickness of layer i |
| $s_{lim}$ | the limit thickness |
| $t_{max}$ | the time when the maximum temperature occurs |
| $\theta_{max}$ | the maximum temperature developed in the compartment |
| $\Gamma$ | the time factor function of the opening factor $O$ and the thermal absorptivity $b$ |

*Appendix B*

| | |
|---|---|
| $A_s$ | the cross section area of the stiffener cross section |
| $A_{s,red}$ | the reduced effective area of web stiffener |
| $B$ | the width of the bottom flange |
| $B_c$ | the width of the bottom flange (centre line) |
| $b$ | the width of the top flange |
| $b_c$ | the width of the top flange (centre line) |
| $b_{eff}$ | the effective width |
| $b_{p,1}$ | the notional flat width of an outer plane element |
| $b_{p,2}$ | the notional flat width of the central plane element |
| $b_r$ | the overall width of a stiffener |
| $c_{eff}$ | the effective width of the lip |
| $H$ | the height of the section |
| $H_c$ | the height of the section (centre line) |
| $I_s$ | the cross section second moment of area of the stiffener |
| $K_1$ | the linear spring stiffness |
| $k_f$ | coefficient that takes into account partial rotational restraint of the web by the flanges |
| $k_w$ | coefficient that takes into account partial rotational restraint of the flange by the webs |
| $k_\sigma$ | the buckling factor |
| $l_b$ | the flange buckling wavelength |
| $s_{eff,1}$ | the strip of width adjacent to the compression flange |
| $s_{eff,n}$ | the strip of width adjacent to the effective centroidal axis |
| $s_w$ | the slant height of the web |
| $t_n$ | the nominal thickness |
| $t_c$ | the material core thickness |
| $\beta_s$ | the interaction factor for member in bending |
| $\rho$ | the reduction factor |
| $\sigma_{cr,s}$ | the elastic critical buckling stress for compressed flange |
| $\sigma_{cr,sa}$ | the elastic critical buckling stress for the compressed web |
| $\sigma_{cr,mod}$ | the modified elastic critical stress |

# ABBREVIATIONS

| | |
|---|---|
| CEN | European Committee for Standardisation |
| CFD | Computational Fluid Dynamics |
| CFS | Cold-Formed Steel |
| EC | Eurocode |
| ECCS | European Convention for Constructional Steelwork |
| EN | European Norm |
| FEA | Finite Element Analyses |
| FEM | Finite Element Method |
| FSM | Finite Strip Method |
| GMNIA | Geometrically and Materially Nonlinear Analysis with Imperfections Included |
| ISO | International Standard Organization |
| LTB | Lateral Torsional Buckling |
| NCCI | Non-Contradictory Complementary Information |
| NFSC | Natural Fire Safety Concept |
| SUSCOS | Sustainable Construction under natural hazards and catastrophic events |
| UK | United Kingdom |
| USA | United States of America |

# 1 INTRODUCTION

## 1.1 Overview

The slender elements and lightweight structures have got recently an important role in the civil engineering industry. The main reason for such an uprising trend may be the fact that in the previous couple of decades many improvements in the field of production technology, design methodologies and computational techniques have been achieved and even more important, the overall theoretical knowledge about the structural behaviour of this type of structures has been improved and implemented in many design codes. Furthermore, the cold-formed sections have meanwhile proved numerous advantages in comparison with hot-rolled sections. Wide diapason of shapes and dimensions of product are possible due to the cold-forming manufacturing process and it enhances design flexibility with extremely attractive, economical and sustainable solutions. Also cold-formed profiles have one of the highest load capacity-to-weight ratio of any building component currently on the market, which leads to high structural performance (Dubina, 2012). Subsequently, construction speed is highly increased due to possible prefabrication and mass production. For all these reasons these structures have become nowadays the most prestigious ones and they have found practical use in various applications, mostly in buildings, but also in bridge design, hydro-technical constructions, special steel structures etc. Unfortunately, it would be too naive to expect that there exists a perfect solution without any stumbling block. There are several key drawbacks of the cold-formed steel which should be mentioned beside all the advantages. One of them, definitely, is far more complicated design process, often non-linear and iterative, which requires obscure background knowledge and more sophisticated design approaches. The cold-formed profiles face several problems that have to be taken into account. Due to its thin shape and thus very slender sections, cold-formed steel members are more prone to buckling phenomenon with often very low critical loading and short buckling length. All possible buckling modes, which will be explained more detailed later on, have a negative impact on the overall behaviour and resistance of thin-walled cross sections. But beside the buckling phenomena which are maybe the biggest issue with CFS, there are also additional problems such as low torsional stiffness, reduced ductility, but also another noticeable problem is low fire resistance, which is the main subject of this particular project and will be more examined further on.

All these problems and peculiarities with CFS require often a sophisticated time-consuming design approach, broad knowledge but also a certain deal of courage of a

designer, which actually make themselves unique. This often leads to increased likelihood of making mistakes, but on the other hand, this complicated calculation is actually the most challenging part of the design of CFS, and having in mind all the advantages these profiles may offer, a good design might only be admired and respected.

Subsequently, the main goal of this thesis is to provide a detailed study on the structural behaviour of CFS beams (purlins) with unusual shape of the cross-section and moreover, the main emphasis of this work is on the behaviour of these beams under the fire conditions. The final aim is thus to help and encourage the development of a new knowledge in this particular area of fire safety design and to spur further investigation.

## 1.2 Motivation and Thesis Objectives

One of the weaknesses that threat the CFS to lose the market share in relation to hot-rolled steel construction but also concrete construction is definitely very low fire resistance. Therefore, it is clearly of the alarming importance to improve the knowledge in this particular area in order to obtain better and more economical solutions. Before I came to Portugal to work on the thesis, I had found out that this topic is quite popular both at the University of Coimbra and at the University of Aveiro and that several researches had already been performed regarding the behaviour of the Class 4 elements under the elevated temperatures. It has inspired me to investigate further this topic and to contribute to the development of a new knowledge. Nowadays it is a great challenge to use an appropriate fire protection material in order to increase resistance of the steel elements. The main focus, thus, of this research is to examine and justify the use of passive fire protections also in case of CFS and this way to give them chance to retain their place on the market.

The principle goal of this thesis is to examine the structural behaviour of the cold-formed steel beams in the role of purlins under the fire condition. As it is noted before, the currently valid standard for design of cold-formed profiles (EN 1993-1-3, 2004) refers only to the design at the ambient temperature. As such, the intention is to investigate the possible application of the same rules that are established for the fire design of hot-rolled profiles (EN 1993-1-2, 2004) also on the CFS, with appropriate modification due to all peculiarities that these profiles have both at the ambient and elevated temperatures, which are prescribed in Annex E of the same part of the Eurocode. Moreover, in EN 1993-1-2 (2004) it is recommended to consider the critical temperature of class 4 steel members equal to 350°C, so another aim of this work is to verify the validity of this assumption in case of CFS. The analytical results are further compared with the numerical ones, carried out by the use of finite element analysis software – ABAQUS (Abaqus Analysis – User's Manual, 2014).

After, an extensive parametric study was performed, in order to find out the influence of several parameters on the structural performance of the CFS purlin. For that matter, two different static schemes were considered – simply supported and continuous beam. Furthermore, the sensitivity of finite element mesh size on the results was analyzed as well as the influence of the initial geometric imperfections.

More specifically, the objective is to determine an adequate fire protection which should aim to help these cold-formed purlins to meet the required fire resistance. Also for this purpose, both analytical and numerical results are obtained and compared. In order to find the economically optimal solution another parameter study is performed, where the thickness of both steel section and fire protection of the beam is varied.

## 1.3 Contents of the thesis

The thesis consists of a total of seven chapters and the contents of each chapter are briefly described as follows.

**Chapter 1 – Introduction**

In this chapter, a general introduction to this thesis is presented, with a brief overview on the main characteristics and problems regarding cold-formed steel profiles. The motivation for this work, as well as its main objectives is also described in this chapter.

**Chapter 2 – Cold-formed steel profiles**

In Chapter 2, cold-formed steel profiles and their most important characteristics mentioned in the Chapter 1, are presented in more details. The versatility of the shapes and dimensions, as well as a resume of the most common applications is provided. It also focuses particularly on the buckling behaviour of CFS flexural members, including the local, distortional, lateral-torsional buckling and their interactions.

**Chapter 3 – Regulamentar approach**

This chapter may be divided into three huge parts. In the first part, quick overview of all relevant material properties of cold-formed steel and insulation material, both at the ambient and elevated temperature, is illustrated. Secondly, the concept of the fire analysis, according to Eurocode, with all the crucial steps is explained. Finally, a brief description of design approach of CFS beams at the ambient and elevated temperature is summarized. The design approach is given in accordance with EN 1993-1-3 (2004) and EN 1993-1-2 (2004).

**Chapter 4 – Description of the study case**

Chapter 4 provides detailed explanation of the study case. First, the layout of the analyzed industrial building is given, where the studied CFS purlins, their position in the building and static scheme are identified. Further, the chapter also gives information on shape, dimensions, material and geometrical properties of the gross and effective cross-section, as well as the thermal and mechanical actions on the purlins.

**Chapter 5 – Analytical calculations**

This chapter provides analytical calculation of the considered CFS purlins, from the chapter 4. First, purlins are analyzed and designed at the ambient temperature according to EN 1993-1-3 (2004), and then their fire resistance will be checked according to Annex E of EN 1993-1-2 (2004) and French Annex of the same part of the standard. Finally, the these analytical results are compared and discussed.

**Chapter 6 – Numerical analysis**

Chapter 6 explains into details all the steps and techniques used in 3D nonlinear finite element model of cold-formed steel purlins, modelled in ABAQUS program, with particular reference to some general issues in creating the model such as – element type, mesh size, load increment, material stress-strain curve model, magnitude and type of geometric imperfections etc. Also, the influence of the geometric imperfections on the overall fire resistance of the purlins is introduced. The numerical results are later compared and discussed with the ones obtained by analytical results.

**Chapter 7 – Conclusion and future work**

In chapter 7, which is the last one, the main conclusions of the thesis are briefly underlined. Also, some ideas on the possible future work and the further development of this study are pointed out.

# 2 COLD-FORMED STEEL PROFILES

## 2.1 Overview

The use of cold-formed steel profiles (CFS) in construction is relatively "new" branch in the steel sector which began in the middle of 19$^{th}$ century, in the United Kingdom and in the USA (Yu, 2000). Use was mostly experimental, and limited to a few basic structures, due to the lack of adequate technical information about the structural behaviour of cold formed profiles. The always-present need for more effective and faster techniques for building initiated the development of this product, especially in the roofing applications. During the 1920s and 1930s, in the USA, there were several attempts of promoting cold-formed steel as a construction material for prefabricated housing purposes, but acceptance was still limited, since there was not an adequate design standard (Yu, 2000). However, the more intense use of cold-formed steel started approximately in the middle of 20$^{th}$ century, and it was highly affected and spurred by the World War II, when the cold formed steel finally found its use equally competitive as hot-rolled steel, for many advantages it offers.

The cold-formed profiles are characterized by the complexity of the shape which may vary in a wide range, from very simple to enormously complex shapes, both for structural and non-structural applications (*Figure 2.1*). Moreover, structural behaviour of the members is considerably different. Due to its thin shape and thus very slender sections, cold-formed steel members are more prone to local buckling phenomenon with often very low critical loading, but still after this initial buckling, members are able to take more loads before the member yields and collapses.

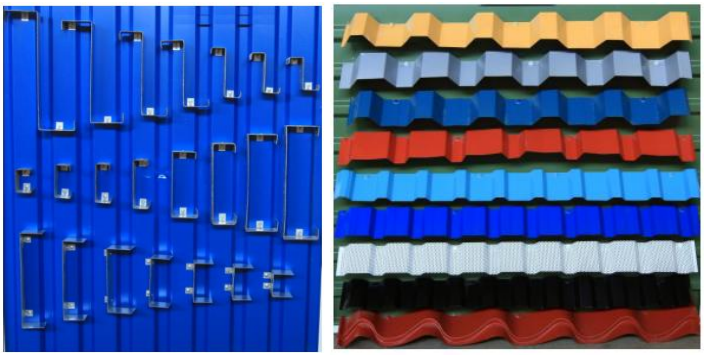

*Figure 2.1* - Various shapes of cold-formed steel sections (Dubina *et al*, 2012):
a) sections of individual structural members;
b) profiled panels, decks and cassettes

## 2.2 Types of cold-formed steel sections

Cold-formed profiled sheets and various members are steel products made from coated or uncoated coils or flat strips. In most cases the cross sections are uniform, with deviations which are limited within the certain tolerances.

Cold-formed structural members may be divided into two main types:

- Panels, decks and cassettes
- Bar members – line elements

Individual structural members also called bar members, are usually manufactured from long products and they can be subdivided into three groups (*Figure 2.2*): open built-up sections, closed built-up sections and typical single cross sections.
The dimensions of bar members vary from 50 mm up to 350 mm and even 400 mm, whereas the thickness is in the range from 0.4 mm up to 6 mm.

On the other hand, panels, decks and cassettes are manufactured from profiled sheets and linear trays (*Figure 2.3*). The depth of decks commonly varies from 20 to 200 mm, whereas the thickness ranges from 0.4 and rarely exceeds 1.5 mm.

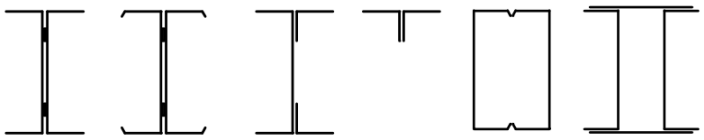

a) built-up cross sections (open and closed)

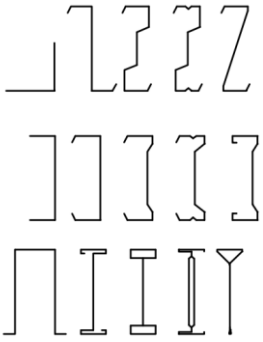

b) typical single cross sections

*Figure 2.2* - Usual forms of sections for cold-formed structural members (EN 1993-1-3, 2004)

As it is already stated before, cold-formed profiles are prone to local buckling phenomenon. In order to increase the stiffness and to improve the overall stability of both bar members and profiled panels, stiffening lips on flanges and intermediate stiffeners in

wide flanges and webs are used (*Figure 2.4*). This allows for another common division of CFS – stiffened and unstiffened elements.

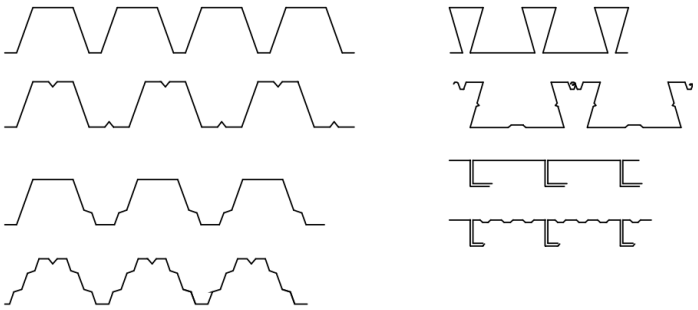

*Figure 2.3* - Usual forms of profiled panels decks and cassettes (EN 1993-1-3, 2004)

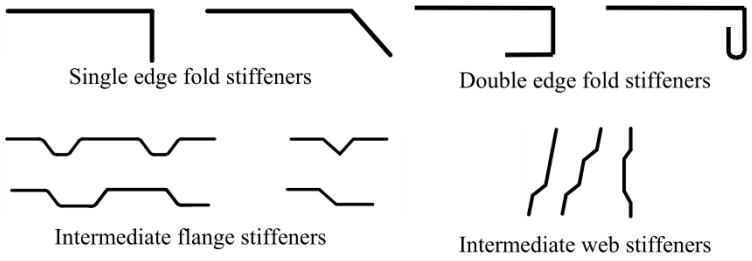


*Figure 2.4* - Most commonly used forms of stiffeners for cold-formed profiles (EN 1993-1-3, 2004)

## 2.3 Application of cold-formed profiles

For many advantages that cold-formed steel elements possess, there are numerous applications where these elements may be used, and here is a brief resume of the most common applications (Dubina *et al.*, 2001a, 2001b).

- Roof and wall members (mostly *C* and *Z*- section purlins and girts as cladding supporters in industrial buildings).
- Steel framing (usually as stand-alone buildings or panels and frames for roofs and walls but also wall partitions of commercial and industrial buildings) (*Figure 2.5*).
- Floor joists for commercial buildings.
- Floor decking (profiled sheeting usually used in composite slabs in substituting also the reinforcement and formwork).
- Roof trusses and portal frames in industrial buildings.
- Other applications (stiffeners for orthotropic bridges, sheet piles for hydro-technical constructions, masts, towers, silos, etc).

*Figure 2.5*- Application of cold-formed profiles as purlins in industrial buildings (ICS, 2012)

## 2.4 Effects of cold-forming

Cold-forming processes lead to several peculiar characteristics of this type of steel profiles, which was not the case with hot-rolled profiles and these effects have to be accounted for. The most significant are:

- Residual stresses
- Strain hardening
- Necking

The residual stresses are commonly appeared in these profiles when cold-rolling type of manufacturing is carried out. The outer fibres tend to elongate when the strip is pressed against the rolls, and this elongation is prevented by the central fibres, thus as an outcome there are residual stresses distributed along the thickness of the cross section with compressive stresses in the outer fibres and tensile stresses in the middle. The similar phenomenon can be observed in hot-rolled profiles, but due to the uneven cooling process, and also the outer fibres are subjected to compressive stresses while the inner to tensile (*Figure 2.6*).

However, these stresses are equilibrated (resultant is equal to zero) and captured inside the cross section so this effect is in the most cases neglected as it has no huge impact on the overall global behaviour, but as a local effect this has to be taken into account, especially when local buckling phenomenon is analysed.

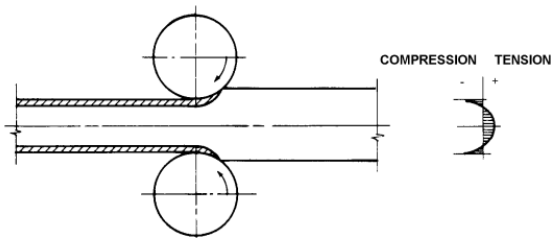


*Figure 2.6* - Residual stresses distribution within the thickness of cold-formed profile (Dubina, 2005)

Unlike the residual stresses which may be considered as "negative" effect of the cold-forming process, one favourable effect emerged. Actually, the cold-forming increases the mechanical properties such as the yielding stress, tensile strength and sometimes the ultimate stress compared to the original material. Consequently, the more the material is exposed to folding the better properties may be achieved in terms of strength (up to 50%), but this also leads to ductility loss, and thus limited use of these profiles in some applications, where ductility is required. This strain-hardening effect depends on geometry of the cross section and on the radius to thickness ratio (*r/t*). As a consequence, the stress strain curve of cold formed elements is modified (*Figure 2.7*).

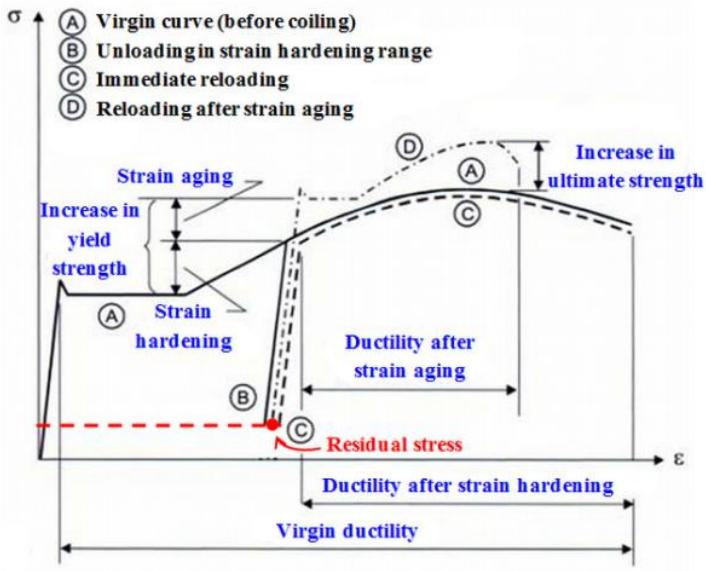


*Figure 2.7* – Effects of cold forming – strain hardening (Chajes *et al.*, 1963; Rondal and Dubina, 2005; Moen *et al.*, 2008)

Another effect of cold-forming is so called "necking" or "thinning" of the corners of cross section due to the small fillet radius ($r \approx t$). Consequently, this may lead to modified properties of the cross section. However, this effect may be neglected since the corners itself present only small part of the gross area of the cross section. If detailed and more accurate calculation is required, this necking effect of the corners may be taken into account.

## 2.5 Buckling of the cold-formed steel members

One of the main problems which are consisting part of practically every steel member and so cold-formed profile is stability. Depending on member properties, boundary conditions (restraints) and type of loading the basic buckling modes of a steel section that may occur are: local, distortional, global and shear.

Due to its thin shape and thus very slender sections, cold-formed steel members are more prone to local buckling phenomenon with often very low critical loading and short buckling length, which may be compared with the dimensions of width and height of cross sections ($\lambda \approx \min(b, h)$). This buckling mode is characterized by cross sections which change their shape while nodes remain fixed.

Distortional buckling is characterized by cross sections which also change their shape but unlike local buckling mode, some nodes (fold-lines) are displaced from their original position. The half-wave length of distortional buckling is normally in between that of local buckling and global buckling, which also may be compared with the dimensions of width and height of cross sections ($\lambda \approx \min(b, h)$).

Global buckling is a unique name for several phenomena that may occur, depending on member properties and type of loading. Therefore there are: flexural (Euler), torsional and flexural-torsional buckling of the members mainly exposed to the axial loading, and lateral-torsional buckling of the beams. The half-wave length of any global buckling is generally the longest in comparison with that of local buckling and distortional buckling, and may be compared with the dimensions of the length of a member ($\lambda \approx L$).

Local and distortional buckling are both regarded as modes of the cross section, and their interaction is also quite common phenomenon, as well as their interaction with global buckling, which is commonly called “coupled buckling”.

For better visual understanding of all the buckling modes mentioned before, they are gathered in the following figure (*Figure 2.8)*, both single and coupled, using a lipped channel as an example (Dubina, 1996). These buckling modes have been obtained by software which works with finite elements method.

For the certain geometrical properties of a cross section the buckling modes depend only upon the length of a member which determines the buckling length (*Figure 2.9*) (Hancock, 2001). As it is expected and explained before, the local buckling mode occurs at shorter wavelengths, which is in the example of *Figure 2.9* equal to 65 mm (point A), whereas for the longer wavelengths cross section undergoes distortional buckling mode (point B), and for the longest buckling lengths global buckling will occur (flexural-torsional and flexural in points D and E, respectively).

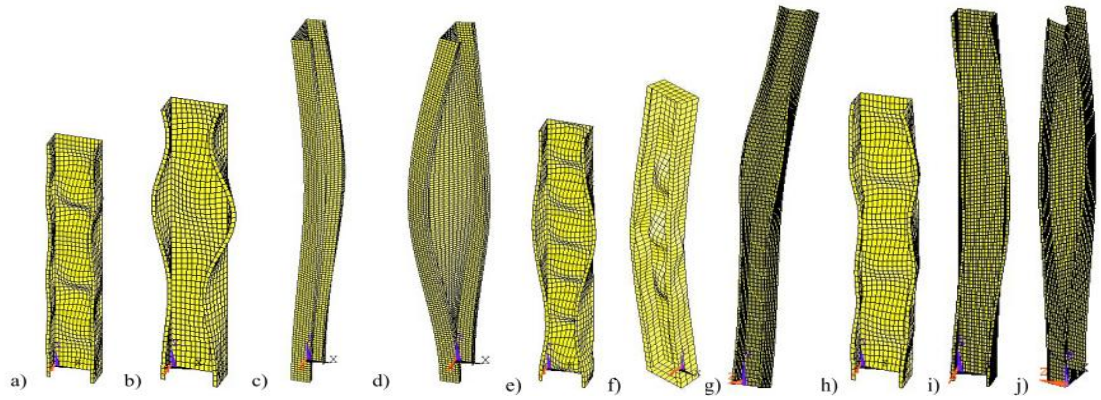


*Figure 2.8* - Buckling modes for a lipped channel in compression
Single modes: a) local; b) distortional; c) flexural; d) flexural-torsional;
Coupled modes: e) local and distortional; f) flexural and local; g) flexural and distortional; h) flexural-torsional and local; i) flexural-torsional and distortional; j) flexural and flexural-torsional (Dubina, 2002)

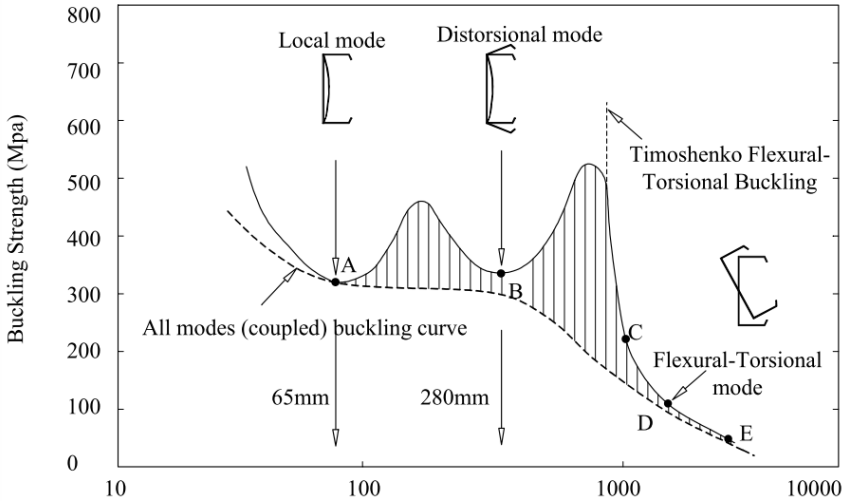


*Figure 2.9* - Buckling strength versus half-wavelength for a lipped channel in compression (Hancock, 2001)

All these "sectional" buckling modes (local and distortional) have a negative impact on the overall behaviour and resistance of thin-walled cross sections such as cold-formed profiles. This is well explained in the following figure (*Figure 2.10*).

It may be observed that local buckling phenomena may occur even before the plastification starts, with very low force ($N_L < N_{el}$), which is not the case with the thick-walled profiles. However, thin-walled bar still have capacity to carry more load, but the stiffness is significantly decreased. This increase of resistance in post-buckling phase is due to favourable influence of spatiality, which is typical plate buckling behaviour and it allows the application of concept of effective width. After the sections reach the

maximum load ($N_U$), in both cases the load declines and the curves advance toward the theoretical rigid-plastic curve.

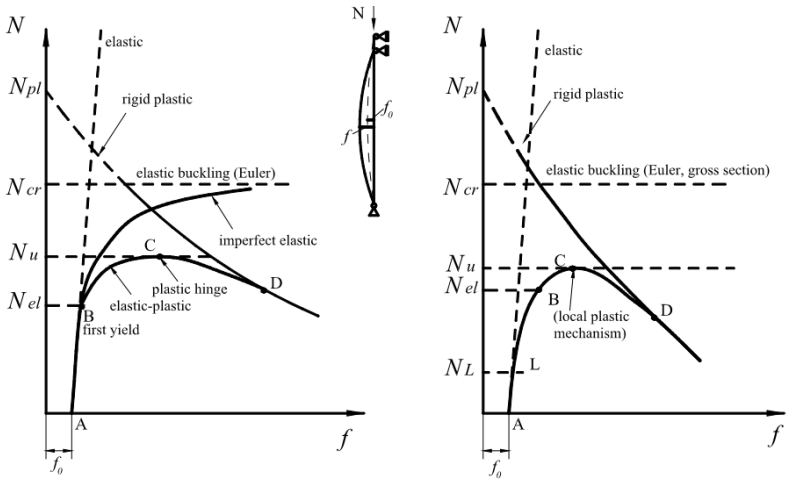


*Figure 2.10* - Comparison in overall behaviour of slender thick-walled (left) and thin- walled (right) compression bar (Murray, 1985; Dubina, 2000)

# 3 REGULAMENTAR APPROACH

## 3.1 Overview

As it is marked out in Chapter 1, the main focus of this work is the structural behaviour of cold-formed beams under fire condition. This chapter represents a quick overview of all important material properties of steel and insulation material both at the ambient and elevated temperature, that are used later on in analytical and numerical analysis. Furthermore, the brief description of analytical calculations of cold-formed beams is summarized, both at the ambient and elevated temperature.

## 3.2 Material Properties of Cold-Formed Steel at Ambient Temperature

As described in Chapter 2, cold-forming process leads to several peculiar characteristics of this type of steel profiles, which was not the case with hot-rolled profiles. Actually, the cold-forming increases the mechanical properties such as the yielding stress, tensile strength and sometimes the ultimate stress compared to the original material. As a consequence, the stress strain curve of cold formed elements is modified (*Figure 3.1*), which means it is no longer "sharp-yielding" but "gradually-yielding".

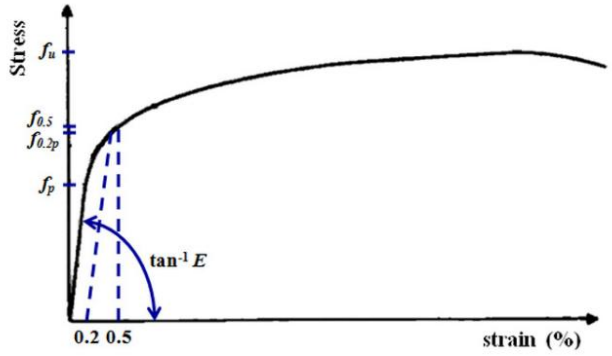


*Figure 3.1* - Stress-strain curve of steel elements produced by cold-worked (Yu, 2000)

In this thesis, S280GD+Z steel grade is used, that is designation for continuous hot dip zinc coated carbon steel, which nominal values, according to EN 10326 standard, for yield strength and ultimate tensile strength are $f_{yb} = 280\ N/mm^2$ and $f_u = 360\ N/mm^2$.

## 3.3 Material Properties of Cold-Formed Steel at Elevated Temperature

At the higher temperatures, steel changes its properties considerably. For this particular purpose the most important thermal and mechanical properties variations at elevated temperatures will be presented. Properties of steel at the elevated temperature may be found in different literature sources, as well as in many building codes. For the purposes of this thesis, the properties of carbon steel at elevated temperatures will be taken from corresponding valid standard - EN 1993-1-2 (2004).

### 3.3.1 Mechanical Properties of Carbon Steel

At elevated temperatures, both the stiffness (modulus of elasticity) and the yield strength are reduced compared to the ambient temperature of 20°C. Moreover, this leads to the significant change in the shape of the stress-strain curve, which is characterized by the loss of the recognisable yield-plateau which exists at room temperature, and also the material shows non-linear behaviour tendency even at the low stresses. Eurocode takes into account these changes of material properties using the so-called reduction factors. In the following table (*Table 3.1*), are listed reduction factors for modulus of elasticity, yield strength and proportional limit at elevated temperature, which are applied to appropriate material property at the ambient temperature of 20°C.

*Table 3.1* - Reduction factors for mechanical properties according to EN 1993-1-2 (2004)

| Steel Temperature $T$ (°C) | Reduction factor for yield strength $k_{y,T}$ | Reduction factor for proportional limit $k_{p,T}$ | Reduction factor for elastic modulus $k_{E,T}$ |
|---|---|---|---|
| 20 | 1.0000 | 1.0000 | 1.0000 |
| 100 | 1.0000 | 1.0000 | 1.0000 |
| 200 | 1.0000 | 0.8070 | 0.9000 |
| 300 | 1.0000 | 0.6130 | 0.8000 |
| 400 | 1.0000 | 0.4200 | 0.7000 |
| 500 | 0.7800 | 0.3600 | 0.6000 |
| 600 | 0.4700 | 0.1800 | 0.3100 |
| 700 | 0.2300 | 0.0750 | 0.1300 |
| 800 | 0.1100 | 0.0500 | 0.0900 |
| 900 | 0.0600 | 0.0375 | 0.0675 |
| 1000 | 0.0400 | 0.0250 | 0.0450 |
| 1100 | 0.0200 | 0.0125 | 0.0225 |
| 1200 | 0.0000 | 0.0000 | 0.0000 |

It is important to stress that at the ambient temperature, the proportional limit ($f_p$) is presumed to be equal to the yield strength ($f_{yb}$). However, this assumption is lost at the elevated temperatures, as the proportional limit is reached at a lower stress than the yield

strength, which corresponds to the fact that the stress-strain curve becomes rounded, and the material starts to show non-linear behaviour in an early stage. This is particularly important for the calculation of cold-formed profiles, where for the design under fire conditions the design yield strength of steel should be taken as the 0.2 percent proof strength. In Annex E of EN 1993-1-2 (2004)a table is provided in which reduction factors for cold-formed profiles as well as for the hot-rolled class 4 cross sections at elevated temperatures are presented (*Table 3.2*).

*Table 3.2*- Reduction factors for mechanical properties of cold formed and hot rolled class 4 steel sections at elevated temperatures (EN 1993-1-2, 2004)

| Steel Temperature ($\Theta_a$) | Reduction factor (relative to $f_{yb}$) for the design yield strength of cold-formed class 4 sections ($k_{p0.2,\Theta}$) |
|---|---|
| 20 °C | 1.00 |
| 100 °C | 1.00 |
| 200 °C | 0.89 |
| 300 °C | 0.78 |
| 400 °C | 0.65 |
| 500 °C | 0.53 |
| 600 °C | 0.30 |
| 700 °C | 0.13 |
| 800 °C | 0.07 |
| 900 °C | 0.05 |
| 1000 °C | 0.03 |
| 1100 °C | 0.02 |
| 1200 °C | 0.00 |

For better visual understanding, the reduction factors for cold-formed steel sections which are used in this thesis in particular, have been plotted below (*Figure 3.2*). As it may be observed from the previous figure, according to EN 1993-1-2 (2004) there is no reduction in yield strength until the temperature goes beyond 400°C, whereas, the elastic modulus and proportional limit are reduced even when the temperature exceeds 100°C.

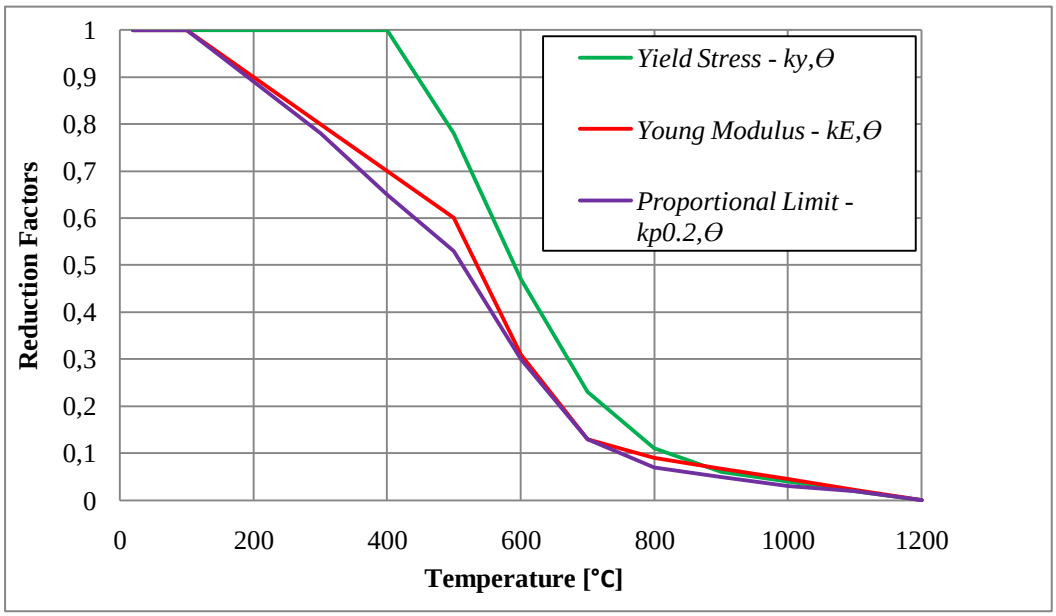


*Figure 3.2* - Reduction factors for mechanical properties of cold- formed sections at elevated temperatures (EN 1993-1-2, 2004)

The French National Annex of EN 1993-1-2, uses another material law model, and therefore the reduction factors for steel at elevated temperature are slightly different (see *Table 3.3*)

*Table 3.3* - Reduction factors for mechanical properties of cold formed and hot rolled class 4 steel sections at elevated temperatures according to French National Annex of EN 1993-1-2 (Vila Real *et al.*, 2013)

| Temperature (°C) | $k_{0.2p,\Theta}$ (EN 1993-1-2) | $k_{0.2p,\Theta}$ (French Annex) | Relative difference (%) |
|---|---|---|---|
| 20 | 1.00 | 1.00 | 0.00 |
| 100 | 1.00 | 1.00 | 0.00 |
| 200 | 0.89 | 0.896 | 0.67 |
| 300 | 0.78 | 0.793 | 1.67 |
| 400 | 0.65 | 0.694 | 6.77 |
| 500 | 0.53 | 0.557 | 5.09 |
| 600 | 0.3 | 0.318 | 6.00 |
| 700 | 0.13 | 0.15 | 15.38 |
| 800 | 0.07 | 0.078 | 11.43 |
| 900 | 0.05 | 0.048 | -4.00 |
| 1000 | 0.03 | 0.032 | 6.67 |
| 1100 | 0.02 | 0.026 | 30.00 |
| 1200 | 0.00 | 0.00 | 0.00 |

Recently, new properties of CFS at elevated temperatures are proposed (Craveiro *et.al.*, 2016). However, this proposal was not considered in this thesis.

### 3.3.2 Stress-strain curves

At elevated temperatures, as it is previously stated, beside the reduction in strength and stiffness, the significant change in the shape of the stress-strain curve occurs, which is characterized by the loss of the recognisable yield-plateau which exists at room temperature, and also the material shows non-linear behaviour tendency even at the low stresses. At the ambient temperature, the standard allows simplification of strain-stress curve into a bilinear one. However, in this case not the bilinear curve but more accurate estimation of the behaviour of steel will be used (*Figure 3.3*). On the other hand, it would be a huge mistake to idealize stress-strain curve at elevated temperatures into a bilinear curve, since the steel shows a remarkable nonlinear behaviour at these temperatures. This nonlinearity plays a specifically important role when it comes to stability problems, since the buckling strength is directly related to the tangent modulus. Equations needed to model the stress-strain curves for carbon steel at different elevated temperatures are given in EN 1993-1-2 (2004). For the different values of temperatures, the stress-strain curves are plotted using the previously mentioned equations, and gathered together in the following figure (*Figure 3.3*). It is obvious from these stress-strain curves that nonlinear behaviour of steel takes place in an early stage when exposed to elevated temperatures.

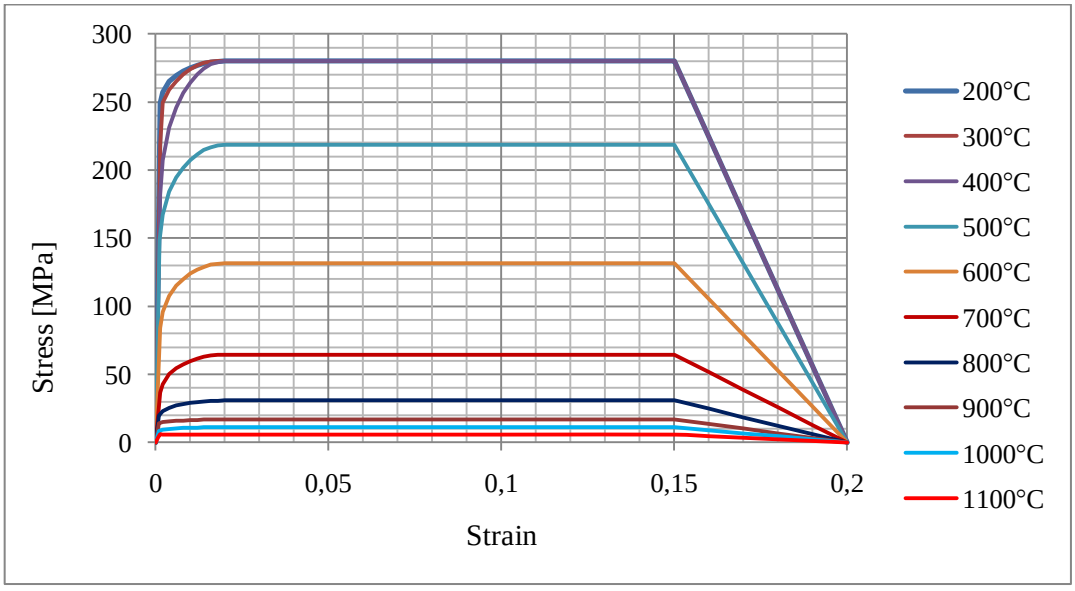


*Figure 3.3* – Stress-strain curves of steel at elevated temperatures (EN 1993-1-2, 2004)

### 3.3.3 Coefficient of Thermal Expansion

In EN 1993-1-2 (2004) are not provided explicitly the equations for calculation of the coefficient of thermal expansion ($\alpha$). However, knowing the physical meaning of this

parameter it can be obtained from the equations for thermal elongation (ΔL/L), which are provided in the standard as follows:

$$\frac{\Delta L}{L} = 1.2 \cdot 10^{-5} \cdot T + 0.4 \cdot 10^{-8} \cdot T^2 - 2.416 \cdot 10^{-4}\ , \quad 20℃ \leq T < 750℃ \qquad (3.1)$$

$$\frac{\Delta L}{L} = 1.1 \cdot 10^{-2}\ , \qquad 750℃ \leq T \leq 860℃ \qquad (3.2)$$

$$\frac{\Delta L}{L} = 2 \cdot 10^{-5} \cdot T - 6.2 \cdot 10^{-3}, \qquad 860℃ < T \leq 1200℃ \qquad (3.3)$$

The thermal strain (elongation) as a function of temperature ($\frac{\Delta L}{L}(T) = f(T)$) is plotted in the following figure (*Figure 3.4*), and it can be observed that the thermal strain rises as the temperature rises almost linearly.

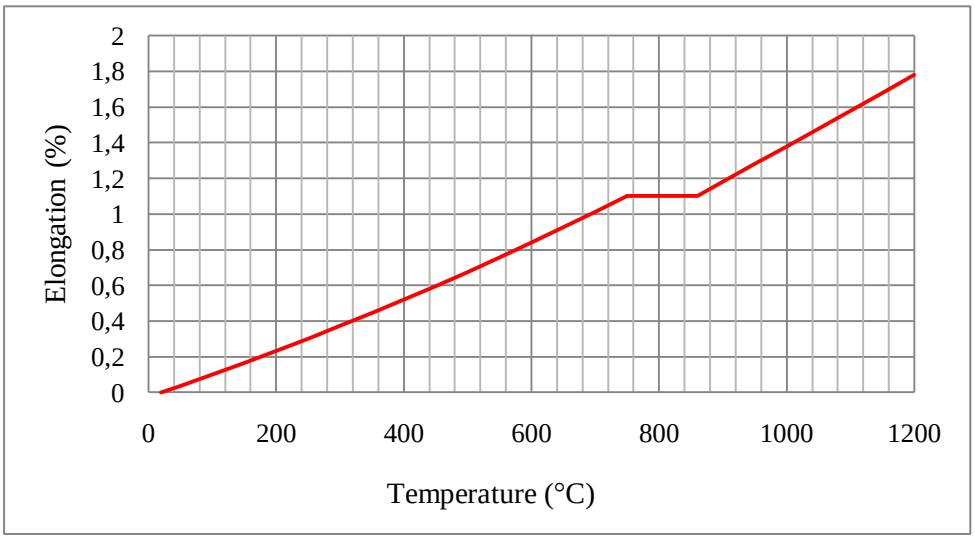


*Figure 3.4* - Thermal strain of carbon steel at elevated temperatures (EN 1993-1-2, 2004)

Now that the thermal elongation is known, the coefficient of thermal expansion ($\alpha$) may be obtained as the first derivative of the previous function, which leads to following results:

$$\alpha = 1{,}2 \cdot 10^{-5} + 0{,}8 \cdot 10^{-8} \cdot T \quad [1/℃]\ , \qquad 20℃ \leq T < 750℃ \qquad (3.4)$$

$$\alpha = 0 \quad [1/℃]\ , \qquad 750℃ \leq T \leq 860℃ \qquad (3.5)$$

$$\alpha = 2 \cdot 10^{-5} \quad [1/℃]\ , \qquad 860℃ < T \leq 1200℃ \qquad (3.6)$$

Coefficient of thermal expansion of steel at elevated temperature is plotted against the temperature in the following figure (*Figure 3.5*).

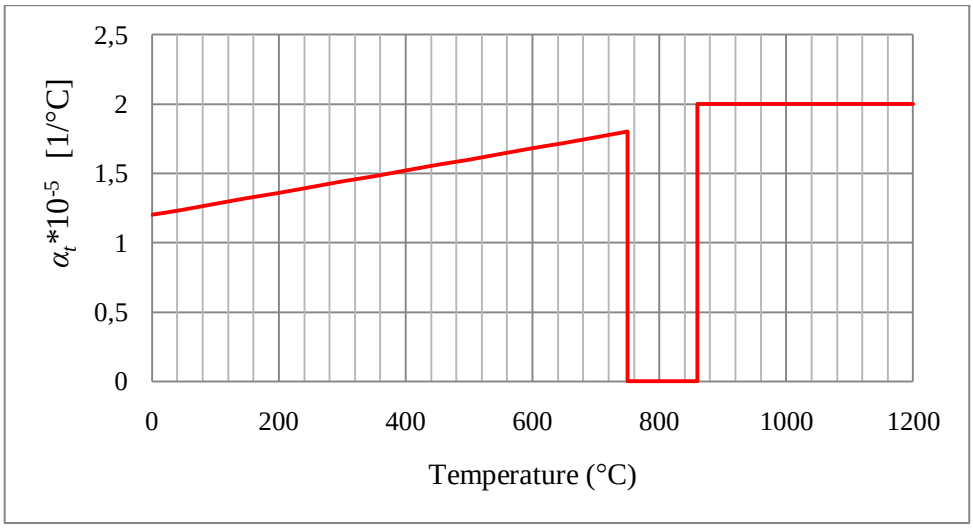


*Figure 3.5* - Coefficient of thermal expansion against temperature (EN 1993-1-2, 2004)

### 3.3.4 Thermal Properties of Carbon Steel

Here is presented the influence of the elevated temperatures on the specific heat and thermal conductivity, as these two parameters are of the greatest importance for the heat transfer analysis. According to EN 1993-1-2 (2004), the specific heat of carbon steel at the ambient temperature is considered to be $c_a$ = 439.8 J/kgK, whereas the thermal conductivity is $\lambda_a$ = 53.33 W/mK. However, with the change of temperature in steel ($\theta_a$), Eurocode provides the equations in which specific heat and thermal conductivity are presented as a function of temperature, and this functions are illustrated below (*Figure 3.6* and *Figure 3.7*).

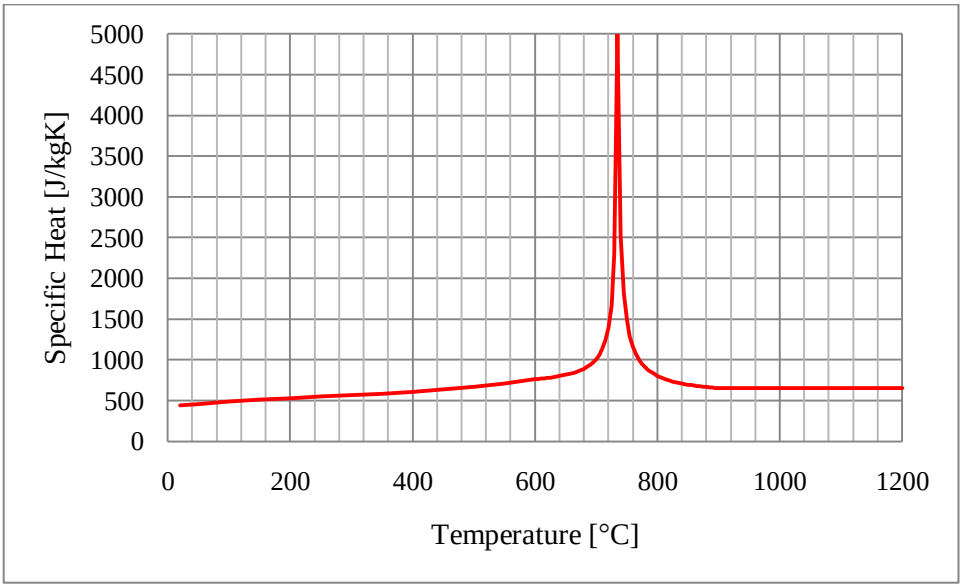


*Figure 3.6* - Specific heat of steel as a function of temperature (EN 1993-1-2, 2004)

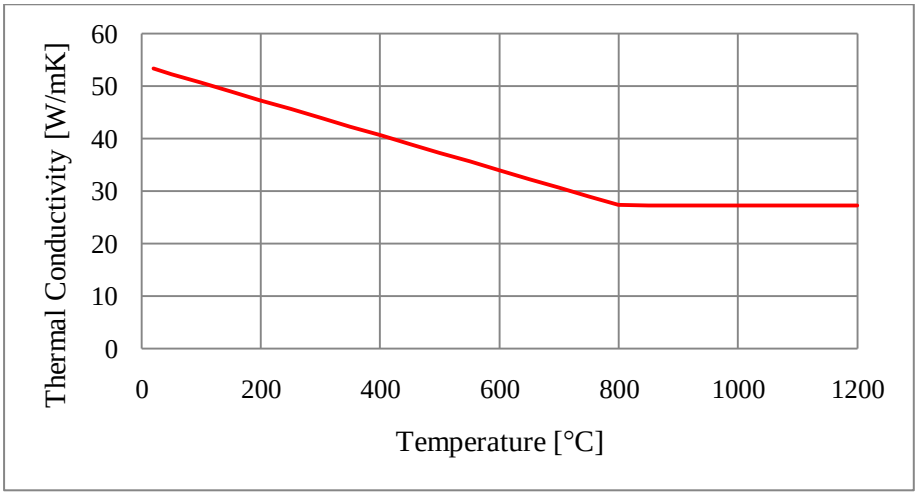


*Figure 3.7* - Thermal conductivity as a function of temperature (EN 1993-1-2, 2004)

## 3.4 Material Properties of Insulation

In this research instumescent coating is used as a fire protection. These coatings are mostly used in applications where lower fire protection requirements are required (R15-R60), such as offices, warehouses, residential buildings etc. The intumescent coatings are proven to be extremely effective in fire situations which are precisely defined, even in natural and localized fires, where with thin layer of coating it is possible to keep the temperature in steel below the critical temperature. However, the real potential of the intumescent coatings is still obscure, due to the uncertainties regarding the technological issues.

In this thesis, SteelProst coating was considered for fire protection, which was developed during FP7 Research Programme, funded by European project. FP7 is basically focused on validation, manufacturing and certification of intumescent coatings, with the aim to develop innovative and quality spraying system, which should provide necessary fire protection and eventually reduce the cost.

The thermal properties of the SteelProst coating which is used in this case are given below. The thermal conductivity of the coating material $\lambda_p$ depends on the temperature of the fire protection which is more precisely calculated as an average value of gas temperature $\theta_{g,t}$ and steel temperature $\theta_{a,t}$ (*Table 3.4*). Detailed information may be found in Deliverable 4.2 – "Fire Criteria Definition" [SteelProst, 2015]. Density of the intumescent coating is taken as $\rho_p$ = 1375 kg/m$^3$, while the specific heat at the ambient temperature is $c_p$ = 0 J/kgK.

*Table 3.4* - Thermal conductivity of the SteelProst intumescent coating (SteelProst, 2015)

| Average temperature of the coating $\theta_{p,t}$ (°C) | Thermal conductivity $\lambda_p$ (W/mK) |
|---|---|
| 0-50 | 0.029 |
| 50-100 | 0.0144 |
| 100-150 | 0.0144 |
| 150-200 | 0.0144 |
| 200-250 | 0.0144 |
| 250-300 | 0.0133 |
| 300-350 | 0.0147 |
| 350-400 | 0.0131 |
| 400-450 | 0.0094 |
| 450-500 | 0.0050 |
| 500-550 | 0.0041 |
| 550-600 | 0.0043 |
| 600-650 | 0.0049 |
| 650-700 | 0.0055 |
| 700-750 | 0.0067 |
| 750-800 | 0.0080 |
| 800-850 | 0.0212 |
| 850-900 | 0.041 |
| 900-950 | 0.022 |

## 3.5 Fire analysis

### 3.5.1 Introduction

Generally, there are two basic approaches in the fire safety design, prescriptive and engineered (performance-based) approach. The prescriptive approach has been prevalent and the only one existing for many years, even today in many non-European countries this approach prevails. This simple approach consists of prescriptive rules and recommendations that have to be applied for fire safety according to appropriate building code, and commonly the engineering calculation component is missing. The mentioned rules are obtained individually for each structural elements of a building - beams, columns, connections, etc. The standard furnace test is used, in which the fire resistance rate of all these elements is examined when subjected to standard ISO-834 fire. Unlike the prescriptive approach, in the engineered approach the building is designed in such a way to sustain the fire condition and to satisfy a certain requirements regarding the overall structural performance. Fire is considered as a load case, in the same way as any other load (permanent load, imposed load, snow load, etc), then the response of a structure for this particular "load" is calculated and finally the suitable measures are adopted to provide structural performance. Such an approach is considered far more rational and closer to reality, allows us to follow and control the behaviour of a structure under fire, thus gives more precise and in the most cases the more economical structural fire safety design (Buchanan, 2002).

In some building codes, Eurocodes for instance, the fire safety design guidance is already implemented for typical and most usual steel structures, while in the U.S the development of these standards has recently begun. The fundamental concept of all these standards is basically the same – they have to be straightforward and simple design guidance, understandable for everyone, in which calculation of reduced strength of an element is provided. This reduced strength of a structural element arises from deterioration of the steel as a material at the elevated temperatures, in which both the strength and the stiffness of the material are decreased.

The fire analysis is a complex problem which in thesis will be conducted completely according to prescriptions given in Eurocodes, which are currently the valid standards. For that purpose, several parts of this standard have to be considered and here is a brief list of them:

- EN 1990 (bases of design)
- EN 1991-1-1 (mechanical actions on structure)
- EN 1991-1-2 (mechanical actions acting on the structures in fire condition; thermal actions)
- EN 1993-1-1 (structural stability of steel structures at ambient temperature)
- EN 1993-1-2 (structural behaviour of steel structures subjected to fire)
- EN 1993-1-3 (supplementary rules for cold-formed members and sheeting)

The concept of the fire analysis is based on the verification of the mechanical resistance of elements, which has to be higher of the applied design loads under fire when ultimate limit state occurs. Fire safety is thus guaranteed if the element is able to sustain applied loads longer than required fire resistance time.

The whole fire analysis may be divided into 3 main steps, as it is presented in the following scheme (*Figure 3.8*) (Franssen and Vila Real, 2010).

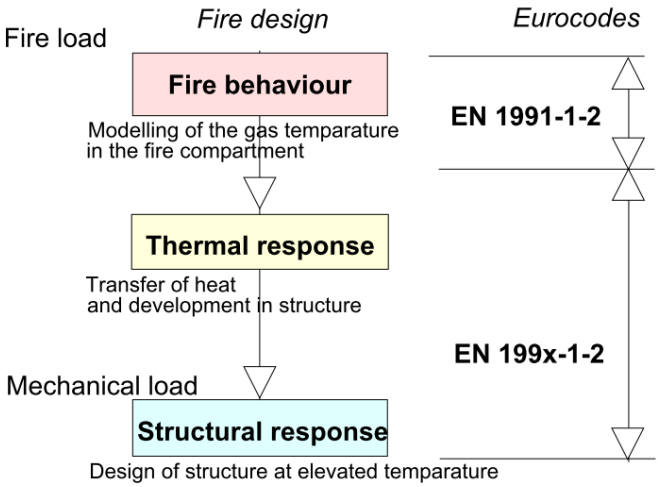


*Figure 3.8* - Fire analysis steps according to Eurocode

All the steps previously mentioned in the *Figure 3.8* are explained into detail in the following section.

### 3.5.2 Fire Load

The fire load is consisted of two components: thermal action and mechanical loading acting under fire conditions.

- *Thermal Action:*

Thermal action of fire is presented usually as a time-temperature curve in which development of the gas temperature in time is shown within the considered compartment. There are several different models of compartment fire that can be used for analysis, but generally they are divided into 2 main groups according to EN 1991-1-2 (2002):

- Nominal fire curves
  - Standard ISO 834 curve
  - Hydrocarbon fire curve
  - External temperature-time curve

- Natural fire curves:
  - Parametric fire curve (Annex A)
  - Zone models (Annex D)
  - Computational Fluid Dynamics CFD (Annex D)
  - Localized fires

In this thesis, 3 different fire curves will be considered and the results will be compared and discussed- Standard ISO 834 curve, parametric fire curve and zone model natural fire curve.

- *Mechanical Fire Loading:*

Mechanical actions at the elevated temperatures are the same as the ones at the ambient temperatures. However, for the fire conditions the accidental design situation should be considered, according to EN 1990 (2002), and the design effect for fire ($E_{fi,d,t}$) can be obtained as follows:

$$E_{fi,d} = G_k + P_k + \psi_{1,1} Q_{k1} + \sum_{i>1} \psi_{2,i}\, Q_{ki} \tag{3.7}$$

$$E_{fi,d} = G_k + P_k + \sum_{i>1} \psi_{2,i}\, Q_{ki} \tag{3.8}$$

Where $G_k$ is the characteristic value of permanent action; $P_k$ is the characteristic value of prestressing load; $Q_{ki}$ are the characteristic values of variable actions $i$, and $\psi_{1,1}$ and $\psi_{2,i}$

are coefficients for combination for frequent values and quasi-static values of variable actions. These coefficients ($\psi$) for buildings are listed in the table A1-1 of EN 1990 (2002).

### 3.5.3 Thermal response

Once the fire curve is obtained, the next step is to see what will be the thermal response of the steel member, or in other words, what will be the distribution of the temperature inside the steel when subjected to fire. EN 1991-1-2 (2002) provides the formula which allows easy calculation of the heat flux reaching the steel member, and the formula actually consists of two parts – convective and radiative net flux, as follows

$$\dot{h}_{net} = \dot{h}_{net,c} + \dot{h}_{net,r} \tag{3.9}$$

$$\dot{h}_{net} = \alpha_c \cdot (\theta_{g,t} - \theta_{m,t}) + \varepsilon_m \cdot \sigma \cdot \left[(\theta_{g,t} + 273)^4 - (\theta_{m,t} + 273)^4\right] \tag{3.10}$$

Where

$\alpha_c$ is the coefficient of heat transfer by convection (film coefficient) in [W/m$^2$K]

$\theta_{r,t}$ is the radiation temperature in each moment of time which may be taken as the gas temperature $\theta_g$ in [°C]

$\theta_{m,t}$ is the surface temperature of the member in each moment of time in [°C]

$\phi$ is the configuration factor (may be taken as 1,0)

$\varepsilon_m$ is the surface emissivity of the member (for steel $\varepsilon_m = 0{,}75 \sim 0{,}85$)

$\varepsilon_f$ is the emissivity of the fire (may be taken as 1,0)

$\sigma$ is the Stephan Boltzmann constant (= 5,67x10$^{-8}$ W/m$^2$K$^4$)

Further, in the EN 1993-1-2 (2004) are given equations for manual calculation of the heat transfer of the unprotected steelwork (clause 4.2.5.1 of EN 1993-1-2), as well as for the steelwork insulated by fire protection (clause 4.2.5.2 of EN 1993-1-2).

### 3.5.4 Structural response – mechanical analysis

After the calculation of fire resistance, the verification has to be done. According to EN 1991-1-2 (2002), the verification of fire resistance of the element or structure should be done using one of the following three strategies.

1. Time domain: $t_{fi,d} \geq t_{fi,req}$
2. Load domain: $R_{fi,d,t} \geq E_{fi,d,t}$
3. Temperature domain: $\theta_{cr,d} \geq \theta_{d,t}$

The most commonly used strategy in steel structure subjected to nominal fire curve is load domain. The aim is to obtain first the critical temperature for required resistance time and then for that critical temperature the material properties and then fire resistance have to be determined and compared with design fire load. However, in this thesis, the natural fire was used and thus the time domain as an alternative and more complex approach is applied and the detailed calculation will be presented in the chapter 4.

## 3.6 Design Approach of Cold-Formed Beams

### 3.6.1 Ambient Temperature

This section presents the general design approach of cold formed beams, which is provided in the Eurocode 3 and which will be used in this thesis. For the analytical calculation of the cold-formed beams, several parts of the Eurocode 3 will be used: *General rules and rules for building* are provided in EN 1993-1-1 (2004); *Supplementary rules for cold-formed members and sheeting* are given in EN 1993-1-3 (2004) and also *Design of plated structural elements* is needed and it is provided in EN 1993-1-5 (2006). Through these three separate parts of Eurocode 3, all buckling phenomena (local, distortional and lateral-torsional) of cold-formed beams are taken into account. Local buckling is accounted for by using effective cross-sectional properties, based on the concept of effective widths given in the EN 1993-1-5. On the other hand, the distortional buckling for elements with edge or intermediate stiffeners is accounted for in section 5.5.3 of EN 1993-1-3, where the concept of reduced thickness of stiffeners (edge and/or intermediate) or other parts of the cross-section undergoing distortional buckling according to the minimum distortional buckling stress is used. Finally, for the global stability problem, which is in this case lateral-torsional buckling, the same rules as for the hot-rolled beams are used (EN 1993-1-1, 2004), and again repeated in EN 1993-1-3 (2004). Taking all these things into consideration, the whole procedure of calculation of resistance of cold-formed beams at the ambient temperature may be divided into following steps:

1) First, the elastic buckling stress has to be determined for all the wavelengths up to the nominal length of the beam and according to this critical stress the corresponding buckling mode has to be found.

2) Then, local buckling effects have to be checked for all the parts of the cross section exposed to compression, by calculation of the effective widths and eventually effective cross section properties according to EN 1993-1-5 (2006).

3) Afterwards, the distortional buckling effects have also to be considered by calculation of the reduced thickness of stiffeners (edge and/or intermediate) or other parts of the cross-section undergoing distortional buckling, according to the minimum distortional buckling stress (EN 1993-1-3, 2004)

4) Finally, the overall buckling resistance of the cold-formed beam has to be calculated taking into account the global buckling mode obtained in the first step for wavelength equal to nominal length of the beam, and also accounting for previously calculated effective cross-section in the step 2 and 3.

Below, these methodologies for calculation of local, distortional and lateral-torsional buckling of CFS, prescribed in Eurocode 3 are briefly presented, whereas the more detailed calculation for a particular cross-section which will be used in this thesis is given in the chapter 5.

- *Local buckling:*

The local buckling could occur in an early stage in compressed parts of the section prevents the development of full plastic moment and thus affect the overall performance and resistance of the beam. This is typical phenomenon for the thin-gauge elements such as CFS and thus the classification of these cross-sections is excluded from EN 1993-1-3 (2004), as they are commonly considered class 4. For this reason, the determinant limit state is the elastic buckling one, which means that even the yielding of the extreme fibres will not occur, which is the basic assumption for the Class 3 cross-sections. Due to local buckling effects, the stiffness is reduced in these parts, which leads to redistribution of the stresses in the cross-section towards the stiffer parts. This distribution of the stresses is nonlinear, but standard takes it into account as a linear distribution of the stresses which act only on the effective parts of the cross section, while the buckled parts are completely omitted from the calculation, and they are not contributing to the cross section resistance (*Figure 3.9*). Therefore, to take into account local buckling means to calculate the effective widths which still participate in section resistance for all parts of the cross section exposed to compressive stresses. In EN 1993-1-5 (2006) is provided well defined procedure how to calculate these effective widths, using a reduction factor ($\rho < 1.0$) which multiplied with the total width gives the effective one. In order to calculate the reduction factor, first the relative slenderness of the plate ($\overline{\lambda_p}$) should be determined.

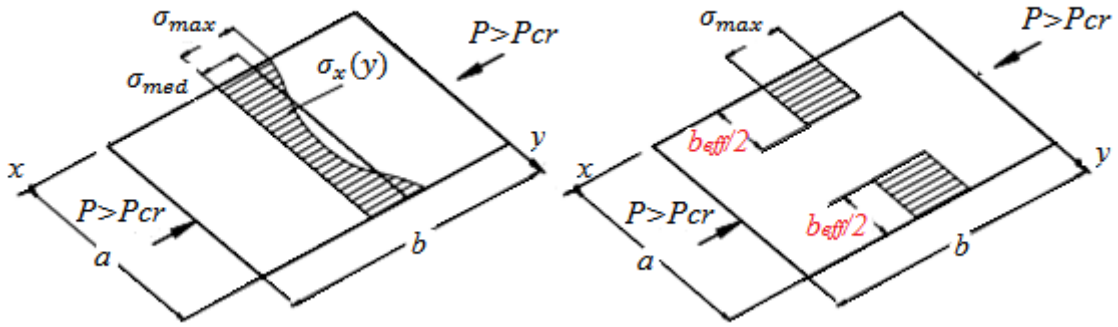


*Figure 3.9*- Distribution of stresses due to local buckling of the plate (Dubina *et al.*, 2012)

The relative slenderness depends on the mechanical properties of steel (yield strength, in particular), geometry of considered plate (width ($b$) and thickness ($t$)), boundary conditions of the plate (outstand or internal) and stress distribution that is taken into account by buckling coefficient ($k_\sigma$), as follows:

- For internal compression parts:

$$\rho = \begin{cases} 1.0 & if \quad \overline{\lambda_p} \leq 0.5 + \sqrt{0.085 - 0.055\psi} \\ \dfrac{\overline{\lambda_p} - 0.055(3+\psi)}{\overline{\lambda_p}^2} \leq 1.0 & if \quad \overline{\lambda_p} > 0.5 + \sqrt{0.085 - 0.055\psi} \end{cases} \tag{3.11}$$

- For outstand compression parts:

$$\rho = \begin{cases} 1.0 & if \quad \overline{\lambda_p} \leq 0.748 \\ \dfrac{\overline{\lambda_p} - 0.188}{\overline{\lambda_p}^2} \leq 1.0 & if \quad \overline{\lambda_p} > 0.748 \end{cases} \tag{3.12}$$

Where $\psi$ is the stress ratio obtained from the tables given in the EN 1993-1-5 (2006) (see *Table 3.5* and *Table 3.6*)

Relative plate slenderness is calculated as follows:

$$\overline{\lambda_p} = \frac{\bar{b}/t}{28.4\varepsilon\sqrt{k_\sigma}} \tag{3.13}$$

Where $\bar{b}$ is the width of considered plate, $t$ is the thickness of plate and $k_\sigma$ is buckling coefficient determined according to EN 1993-1-5 (see *Table 3.4*, *Table 3.5*)

- *Distortional buckling:*

Unlike the local buckling phenomenon, which is more straightforward and easier for understanding, the distortional buckling is not that plain. The main reason is the fact that local buckling critical stress depends practically only on the *b/t* ratio, while distortional buckling is more complex phenomenon and depends on the rotational stiffness at the junction of two adjacent plates. As it is stressed before, the half-wave length of distortional buckling is normally in between that of local buckling and global buckling, which also may be compared with the dimensions of width and height of cross sections ($\lambda \approx \min(b, h)$) (see *Figure 2.9*).

*Table 3.5* - Internal compression elements (EN 1993-1-5, 2006)

| Stress distribution (compression positive) | | | | Effective width $b_{eff}$ | | |
|---|---|---|---|---|---|---|
| 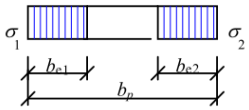 | | | | $\psi = 1$<br>$b_{eff} = \rho \cdot b_p$<br>$b_{e1} = 0.5 \cdot b_{eff}; b_{e2} = 0.5 \cdot b_{eff}$ | | |
| 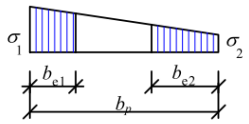 | | | | $1 > \psi \geq 0$<br>$b_{eff} = \rho \cdot b_p$<br>$b_{e1} = \frac{2}{5-\psi} \cdot b_{eff}; b_{e2} = b_{eff} - b_{e1}$ | | |
| 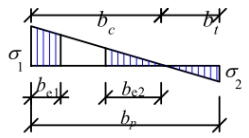 | | | | $\psi < 0$<br>$b_{eff} = \rho \cdot b_c = \rho b_p / (1-\psi)$<br>$b_{e1} = 0.4 \cdot b_{eff}; b_{e2} = 0.6 b_{eff}$ | | |
| $\psi = \sigma_2 / \sigma_1$ | 1 | $1 > \psi > 0$ | 0 | $0 > \psi > -1$ | $-1$ | $-1 > \psi \geq -3$ |
| Buckling factor $k_\sigma$ | 4.0 | $8.2/(1.05+\psi)$ | 7.81 | $7.81 - 6.29\psi + 9.78\psi^2$ | 23.9 | $5.98(1-\psi)^2$ |

*Table 3.6* - Outstand compression elements (EN 1993-1-5, 2006)

| Stress distribution (compression positive) | | | Effective width $b_{eff}$ | |
|---|---|---|---|---|
| 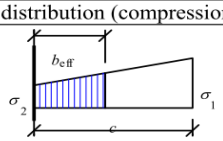 | | | $1 > \psi \geq 0$<br>$b_{eff} = \rho \cdot c$ | |
| 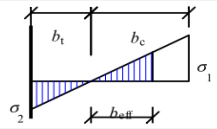 | | | $\psi < 0$<br>$b_{eff} = \rho \cdot b_c = \rho c / (1-\psi)$ | |
| $\psi = \sigma_2 / \sigma_1$ | 1 | 0 | $-1$ | $1 \geq \psi \geq -3$ |
| Buckling factor $k_\sigma$ | 0.43 | 0.57 | 0.85 | $0.57 - 0.21\psi + 0.07\psi^2$ |
| 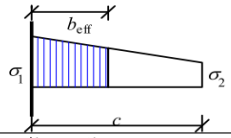 | | | $1 > \psi \geq 0$<br>$b_{eff} = \rho \cdot c$ | |
| 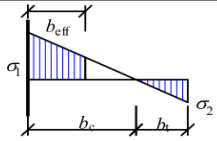 | | | $\psi < 0$<br>$b_{eff} = \rho \cdot b_c = \rho c / (1-\psi)$ | |
| $\psi = \sigma_2 / \sigma_1$ | 1 | $1 > \psi > 0$ | 0 | $0 > \psi > -1$ | $-1$ |
| Buckling factor $k_\sigma$ | 0.43 | $0.578/(\psi + 0.24)$ | 1.70 | $1.7 - 5\psi + 17.1\psi^2$ | 23.8 |

The local buckling stress can be easily obtained using the simple equations provided in literature and standards, whereas the hand calculation of the distortional buckling is usually rather awkward and inappropriate for practical use. For some cross-sections which shape is simple (e.g lipped channel), the hand calculation methods for the elastic distortional buckling may be found. However, even these methods are usually impractical for regular use and thus the numerical methods are recommended. The most used numerical methods are finite element methods (FEM) or even more appropriate finite strip method (FSM).

One of the most used software for calculation of the elastic buckling analysis of the thin-gauge elements is CUFSM (Schafer *et.al.*, 2006), and this software also uses finite strip method (FSM). CUFSM is extremely practical for quick computation of the critical loads and corresponding buckling modes (local, distortional and global) and moreover, it allows the user to predict the geometrically non-linear behaviour (stability) of thin-gauge profiles and to analyse the influence and importance of each mode on the overall behaviour of the beam. This way, it is also possible to take into consideration the initial geometrical imperfections in the analysis, since these imperfections are usually modelled in such a way to have the same shape as the buckling modes. In this thesis, the CUFSM program is also used for the above mentioned purposes.

Speaking of calculation of distortional buckling according to EN 1993-1-3 (2004), there are no explicitly given rules for manual calculation. Nevertheless, there is an alternative procedure provided, which is actually based on the same rules as for plane elements with edge or intermediate stiffeners.

The calculation of elements with edge or intermediate stiffeners exposed to compression is based on the theory of beams on elastic foundations in which the stiffener is considered as a beam carried by springs. The stiffness of the springs is calculated from the deflection of the considered part of the cross section, and subsequently depends on the boundary conditions and the flexural stiffness of the adjoining element. The stiffness of the spring can be calculated by applying a unit load, as it is presented in *Figure 3.10*.

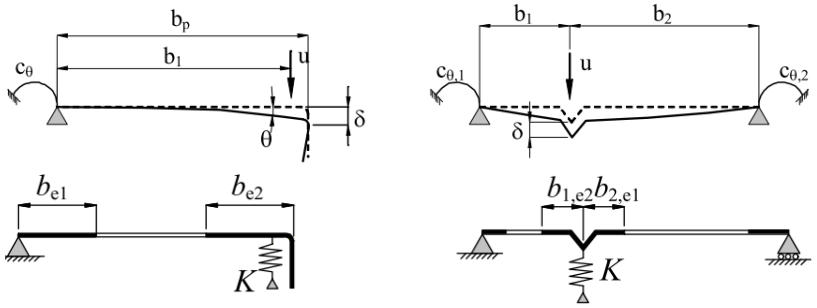


*Figure 3.10* - Examples of the elements with edge and intermediate stiffeners with corresponding calculation models (EN 1993-1-3, 2004)

The complexity of this approach is contained now in the computation of the stiffness of the spring (*K*). It can be derived from the following equation (Eq. 3.14):

$$K = \frac{u}{\delta} \tag{3.14}$$

Where $u$ presents the unit load applied at the centroid of the effective part of the stiffness and $\delta$ presents the deflection of the stiffener due to the unit load (see *Figure 3.10*), which can be calculated as follows:

- For an edge stiffener:

$$\delta = \theta \cdot b_p + \frac{u \cdot {b_p}^3}{3} \cdot \frac{12(1-\nu^2)}{E \cdot t^3} \tag{3.15}$$

- For an intermediate stiffener:

$$\delta = \theta \cdot b_p + \frac{u \cdot {b_1}^2 \cdot {b_2}^2}{3(b_1 + b_2)} \cdot \frac{12(1-\nu^2)}{E \cdot t^3} \tag{3.16}$$

Once the string stiffness is determined, EN 1993-1-3 (2004) provides further instructions how to obtain elastic critical buckling stress ($\sigma_{cr,s}$). Depending on the type of the cross section and the position and number of stiffeners, different cases are possible.

1. For the plane elements with edge stiffeners elastic critical buckling stress is calculated according to EN 1993-1-3 (clause 5.5.3.2).
2. For plane elements with intermediate stiffeners elastic critical buckling stress is calculated according to EN 1993-1-3 (clause 5.5.3.3).
3. For trapezoidal sheeting profiles with intermediate stiffeners critical buckling stress is calculated according to EN 1993-1-3 (clause 5.5.3.4).

In this thesis, the trapezoidal "omega" profile with intermediate stiffeners both on the web and flange is used, and detailed analytical calculation with all steps provided in clause 5.5.3.4 of EN 1993-1-3 (2004) will be shown in the following chapter.

After computation of the elastic critical buckling stress, the following step is calculation of the relative slenderness ($\overline{\lambda_d}$), by the following formula (Eq. 3.17):

$$\overline{\lambda_d} = \sqrt{f_{yb} / \sigma_{cr,s}} \tag{3.17}$$

And finally, the reduction factor $\chi_d$ for the distortional buckling resistance (flexural buckling of a stiffener) ought to be calculated according to the previously obtained relative slenderness:

If $\overline{\lambda_d} \leq 0.65$: $\chi_d = 1.0$
If $0.65 < \overline{\lambda_d} < 1.38$: $\chi_d = 1.47 - 0.723\overline{\lambda_d}$ (3.18)
If $\overline{\lambda_d} \geq 1.38$: $\chi_d = 0.66/\overline{\lambda_d}$

Distortional buckling effects are then accounted for by calculation of the reduced thickness of stiffeners (edge and/or intermediate) or other parts of the cross-section undergoing distortional buckling, according to the minimum distortional buckling stress. Reduced area and thickness of effective stiffener section is calculated as follows:

$$A_{s,red} = \chi_d A_s \frac{f_{yb}/\gamma_{M0}}{\sigma_{com,Ed}} \quad (3.19)$$

Where:
$\sigma_{com,Ed}$ is compressive stress at the centreline of the stiffener calculated on the basis of the effective cross-section

The reduced effective area $A_{s,red}$ should be then represented by using a reduced thickness $t_{red}$ for all the elements included in the effective area of the stiffeners ($A_s$).

$$t_{red} = t \cdot \frac{A_{s,red}}{A_s} \quad (3.20)$$

- *Global (lateral-torsional) buckling:*

Finally, the global buckling is also taken into account according to provisions given in EN 1993-1-1 (2004), where the usual procedure for beams is followed as for any other hot-rolled Class 4 section. The design procedure for Class 4 cross section is practically the same as for the Class 3, just instead of gross cross section the effective cross section is used which means that the determinant limit state is the elastic one. Accordingly, the design buckling resistance moment of a beam prone to lateral-torsional buckling is calculated as follows:

$$M_{b,Rd} = \frac{\chi_{LT} \cdot W_{eff,y} \cdot f_{yb}}{\gamma_{m,1}} \quad (3.21)$$

The reduction factor $\chi_{LT}$ for is given by:

$$\begin{cases} \chi_{LT} = \dfrac{1}{\phi_{LT} + \sqrt{{\phi_{LT}}^2 - \bar{\lambda}_{\mathrm{LT}}{}^2}} & if \quad \left(\bar{\lambda}_{\mathrm{LT}} > 0.4\right) \\ \chi_{LT} = 1.0 & if \quad \left(\bar{\lambda}_{\mathrm{LT}} \leq 0.4\right) \end{cases} \quad (3.22)$$

Where,

$$\phi_{LT} = 0.5\left[1 + \alpha_{LT}\left(\bar{\lambda}_{LT} - 0.2\right) + \bar{\lambda}_{LT}^{\,2}\right] \quad (3.23)$$

$$\bar{\lambda}_{LT} = \sqrt{\frac{W_{eff,y} \cdot f_y}{M_{cr}}} \quad (3.24)$$

And here,

$W_{eff,y}$ is effective section modulus of the Class 4 cross section

$\alpha_{LT}$ is the imperfection factor of the

$M_{cr}$ is elastic critical moment for lateral-torsional buckling, which for the double-symmetric and mono-symmetric section subjected to bending about the symmetry axis may be calculated according to following formula: (NCCI: Elastic critical moment for lateral torsional buckling SN003a-EN-EU), or using an appropriate software for more complex problems (e.g. LTBeam or CUFSM)

$$M_{cr} = C_1 \cdot \pi^2 \cdot \frac{EI_z}{(kL)^2} \cdot \left[\sqrt{\left(\frac{k}{k_w}\right)^2 \cdot \frac{I_w}{I_z} + \frac{(kL)^2 \cdot GI_t}{\pi^2 EI_z} + \left(C_2 z_g - C_3 z_j\right)^2} - \left(C_2 z_g - C_3 z_j\right)\right] \quad (3.25)$$

Where,

$E$ is the Young modulus ($E$ = 210000 N/mm$^2$)

$G$ is the shear modulus (G = 80770 N/mm$^2$)

$I_z$ is the second moment of area about the weak axis

$I_t$ is the torsion constant

$I_w$ is the warping constant

$L$ is the beam length between points which have lateral restraint

$k_w$ is effective length factor (may be considered as 1.0)

$z_g$ is the distance between the point of load application and the shear centre

$z_j$ is the parameter which takes into account the level of asymmetry at mono-symmetric cross section

$C_1, C_2, C_3$ are coefficients depending on the loading and end restraint conditions evaluated in accordance with NCCI SN003 (2005).

### 3.6.2 Elevated Temperature

As it is already stressed before, the fire resistance of the thin-walled profiles is considerably lower than of the thick-walled ones. Moreover, the instability phenomena which are already significant, at the elevated temperatures are even more amplified.

However, the knowledge of the performance of Class 4 steel elements (which is common case for CFS) under the fire is still limited. In the part 4.2.3.6 of EN 1993-1-2 (2004), it is indicated that the critical temperature for Class 4 steel members is equal to 350°C and some additional information are provided in the Annex E of the same part of the Eurocode. France, for instance, considers that these prescriptions are too conservative and thus modified design approach for CFS under fire is provided in its National Annex of EN 1993-1-2 (NF EN 1993-1-2, 2007).

Here will be presented the fire design approach for lateral-torsional buckling of CFS beams according to EN 1993-1-2 (2004), which is compared with the French National Annex of EN 1993-1-2.

- *Eurocode 3 procedure:*

For the Class 4 steel beams exposed to fire , the prescriptions are given in Annex E of EN 1993-1-2 (2004), where the standard allows the user either to use Advanced calculation models (E.1) or Simple manual calculation models (E.2), which is here of the greatest interest.

According to the E.2 (1), the LTB resistant moment for Class 4 cross-sections should be calculated in the same manner as for the Class 3 cross sections (clause 4.2.3.4 of the same code), in which the elastic section modulus is replaced by the effective section modulus.

The calculation of the effective cross section was explained above (section 3.4.1), where both local and distortional buckling have to be taken into consideration using the material properties at 20°C. However, for the design under fire conditions, design yield strength of steel should be taken as the 0.2 percent proof strength. In Annex E of EN 1993-1-2 (2004) is given a table in which reduction factors for cold-formed profiles as well as for the hot-rolled class 4 cross sections at elevated temperatures are presented (*Figure 3.2)*. So, the lateral-torsional resistant moment for Class 4 sections is calculated as follows:

$$M_{b,fi,t,Rd} = \frac{M_{b,fi,Rd}}{\kappa_1 \kappa_2} = \frac{\chi_{LT,fi} \cdot W_{eff,y} \cdot k_{0.2p,\theta} \cdot f_{yb}}{\gamma_{M,fi}} \cdot \frac{1}{\kappa_1 \kappa_2} \qquad (3.26)$$

Where

$\kappa_1$ is a coefficient that takes into account non-uniform distribution of temperature across the cross section, and may be taken as:

$$\kappa_1 = \begin{cases} 1.0 - \text{for a beam exposed to fire on all four sides (general case)} \\ 0.70 - \text{for an unprotected beam exposed to fire on three sides with concrete or composite slab on the fourth} \\ 0.85 - \text{for an protected beam exposed to fire on three sides with concrete or composite slab on the fourth} \end{cases}$$

$\kappa_2$ is a coefficient that takes into account non-uniform distribution of temperature along the beam, and may be taken as:

$$\kappa_2 = \begin{cases} 0.85 - \text{at the supports of a statically indeterminate beam} \\ 1.0 - \text{for all other cases} \end{cases}$$

$W_{eff,y}$ is effective section modulus of the cross-section about the stronger axis, and $\chi_{LT,fi}$ is calculated using the following formula:

$$\chi_{LT,fi} = \frac{1}{\phi_{LT,\theta} + \sqrt{\phi_{LT,\theta}{}^2 - \bar{\lambda}_{\mathrm{LT},\theta}{}^2}} \tag{3.27}$$

with

$$\phi_{LT,\theta} = 0.5\left[1 + \alpha \cdot \bar{\lambda}_{\mathrm{LT},\theta} + \bar{\lambda}_{\mathrm{LT},\theta}{}^2\right] \tag{3.28}$$

The imperfection factor $\alpha$ depends on the steel grade and is determined with the yielding strength at the room temperature as follows:

$$\alpha = 0.65\sqrt{235/f_{yb}} \tag{3.29}$$

Finally, the non-dimensional slenderness for lateral-torsional buckling at elevated temperatures is given by:

$$\bar{\lambda}_{\mathrm{LT},\theta} = \bar{\lambda}_{\mathrm{LT}}\sqrt{k_{0.2p,\theta}/k_{E,\theta}} \tag{3.30}$$

In this expression, $\bar{\lambda}_{LT}$ is the non-dimensional slenderness at ambient temperature and for the Class 4 cross-sections is calculated as follows:

$$\bar{\lambda}_{LT} = \sqrt{\frac{W_{eff,y} \cdot f_y}{M_{cr}}} \tag{3.31}$$

- *French national annex of EN 1993-1-2:*

The procedure itself is practically the same as in EN 1993-1-2 (2004). The crucial changes in these annex are the use of Ayrton-Perry formula as:

$$\phi_{LT,\theta} = 0.5\left[1 + \alpha \cdot \left(\bar{\lambda}_{\mathrm{LT},\theta} - 0.2\right) + \bar{\lambda}_{\mathrm{LT},\theta}{}^{2}\right] \quad (3.33)$$

This formula enables the appearance of a plateau until the value of slenderness of 0.2 on the buckling curve, which allows less conservative results.

And another difference is that the imperfection factor is obtained from EN 1993-1-1 (2004) using the buckling curve for hot rolled sections, which is in this case $\alpha_{LT} = 0.34$ (value from Table 6.1, cause 6.3.2.2 of EN 1993-1-1, lateral buckling curve b). Also the reduction factors for steel at elevated temperature ($k_{0.2p,\theta}$) are slightly different than ones provided in EN 1993-1-2, since the French National Annex refers to modified material law model (see Table 3.3).

## 3.7 State of the art

Currently, in Europe, the valid standard for fire safety design of steel structures is EN 1993-1-2 (2004). This standard provides guidance for typical hot-rolled steel sections, and regarding the CFS, it is stated that "The methods given are also applicable to cold-formed steel members and sheeting within the scope of EN 1993-1-3 (2004)". In contrast to this, EN 1993-1-3 (2004), which is standard for design of CFS, provides only the prescriptions for design at the ambient temperature, while it does not provide strict design rules for the fire design of CFS and about the behaviour of these elements under the elevated temperatures. Only few rules are provided in the Annex E of the same standard, which aim to point out the differences between hot-rolled and cold-formed steel members. For instance, for the design under fire conditions the design yield strength of steel should be taken as the 0.2 proof strength. Also, the reduction factors, which take into account degradation of the material at the elevated temperatures, are slightly modified. Moreover, in EN 1993-1-2 (2004), it is recommended to consider the critical temperature of class 4 steel members equal to 350°C. This may lead to the rather unsafe results, since CFS excited by high temperatures may have entirely different performance compared to hot-rolled, so it is of the utmost importance to take these differences into account in design procedures in a proper way. For that reason, for instance, The French engineers have realized that these results are too conservative, so in their national annex, they propose different design formulae and a different steel constitutive law for cold-formed profiles at elevated temperatures.

Studies on fire performance of CFS members are still fairly rare, and mostly of a numerical nature. Furthermore, they are based usually on the structural behaviour of single and short elements at elevated temperatures, as the experimental tests require expensive equipments and furnaces for the fire simulation. However, this topic has recently become popular in Portugal, at the University of Aveiro and University of Coimbra, where several researches have been performed. At the University of Aveiro numerous experimental and numerical analysis on behaviour and resistance of CFS beams with lipped channel sections under fire conditions have been recently performed (Flávio and Arrais, 2012; Vila Real *et.al.*, 2015). In these studies, it was aimed to analyze the fire behaviour of steel beams and columns, where several parameters were taken into consideration, such as different steel grades, cross-section slenderness and various bending diagrams. Also, the influence of geometric imperfections and residual stresses in their ultimate loads were evaluated. The numerical models are calibrated using the experimental results and the results obtained by SAFIR software (developed at the University of Liège in Belgium) are compared with the resistances determined by EN 1993-1-2 (2004), considering also the French National Annex. Following these comparisons, new design formulae are tested and he results showed a good agreement with this new methodology, revealing that the current design expressions are indeed too conservative. FN Annex showed a better approximation to the numerical results, but stills having too safe results for beams subjected to non-uniform bending diagrams.

Another similar numerical study on the thin-walled welded stainless steel I-beams with Class 4 cross-sections subjected to fire was performed at the University of Aveiro (Lopes and Vila Real, 2014). It is also proven, that some small adjustments could be made in order to improve the approximations to the numerical results.

Also, at the University of Coimbra it has been investigated the behaviour of cold-formed sections with various shapes under fire (Laim, 2013). In this work, four-point bending tests on cold-formed steel C-, lipped I-, R- and 2R-section beams were performed, both under fire conditions, under flexural loading conditions and under simply supported boundary conditions. So the aim was to analyze the influence of the cross-sections, the axial restraining to the thermal elongation of the beam and the rotational stiffness of the beam supports. A numerical study was performed by the FE program ABAQUS and the models are calibrated with the experimental tests. Also in this study, it is concluded that the CFS beams may have higher critical temperature than 350°C, which is proposed by the standard. However, it is obtained that the boundary conditions may have huge impact on the fire behaviour of the CFS beams. For instance, if the thermal elongation is restrained in the axial direction, the critical temperature may drop even up to 30%.

On the other hand, in the most recent researches, also performed at the University of Coimbra (Craveiro, 2015; Craveiro *et.al.*, 2016), an extensive experimental and numerical analysis on single and built-up CFS columns at both ambient and elevated temperatures

was performed in scope of a National Research Project entitled *FireColdFSteel*. It was also intended to investigate the influence of cross-section shape, initial applied load, end-support conditions and level of restraint to thermal elongation imposed by the surrounding structures on the overall behaviour of the CFS columns. As one of the most interesting conclusions, it is obtained that the level of restraint to the thermal elongations significantly affects the behaviour of the CFS beams. Higher level of restraint to thermal elongation results in higher values of restraining forces, which eventually lead to decline of critical temperatures. Also, in this study, new reduction factors are proposed, which are result of the detailed experimental investigation on steel grade S280GD+Z both at ambient and elevated temperatures.

As it may be seen from the previous studies, there are many parameters that are not considered in the current design methods and that may significantly affect the structural behaviour of the CFS members under fire conditions. Therefore, it is of the urgent importance to develop further the knowledge on this subject and eventually to establish new design guidance in some of the following editions of standard.

# 4 DESCRIPTION OF THE CASE STUDY

## 4.1 Scope

In order to analyze the structural behaviour of CFS beams exposed to bending under fire conditions, a realistic application is considered. Since the cold-formed profiles are often used as purlins in roof applications, an industrial building is taken as a study case. In this chapter, the detailed description of the study case is provided. The purlins, as the supporters of the claddings, are designed to sustain static load, whereas the design values of the applied forces are obtained from the fundamental load combinations.

Single storey buildings, such as industrial buildings, do not normally require structural fire resistance (see pp. 9050-9127 from P nº1532/2008 and pp. 7903-7922 from D-L nº220/2008). For this reason, the fire safety design for the purlins is normally excluded in most cases. However, exceptions may occur and one of the examples is quite common use of mezzanine floor inside the industrial building, as it is shown in the *Figure 4.1*. In such a case, the purlins may be subjected to fire, and thus structural fire resistance requirements have to be provided. In this work, a free-standing intermediate floor which is held up by metal columns extending from the floor is supposed to be placed in one of the corner of the examined industry building.

*Figure 4.1* - Mezzanine floor inside the industrial building (PortaFab Inplant Offices, 2014)

The mezzanine floor in this case is meant to be used to create new space for offices with all the features of a regular office which includes electrical devices (sockets, computers, etc), heating and lights. For this reason, fire is possible to occur and furthermore, the adequate fire safety design of the unprotected purlins above has to be provided in order to meet desired fire resistance requirements, which are given in *Table 4.1* according to Portuguese legislation (point 2 of P1537, 2008).

*Table 4.1* - Structural fire resistance requirements according to Portuguese legislation

| Purpose group of building | Minimum periods of fire resistance (minutes) in a: | | | | | |
|---|---|---|---|---|---|---|
| | Basement storey [5] including floor over | | Ground or upper storey | | | |
| | Depth (m) of a lowest basement | | Height (m) of top floor above ground, in a building or separated part of a building | | | |
| | More than 10 | Not more than 10 | Not more than 5 | Not more than 18 | Not more than 30 | More than 30 |
| 1. Residential: | | | | | | |
| a. Block of flats | | | | | | |
| – not sprinklered | 90 | 60 | 30* | 60**† | 90** | Not permitted |
| – sprinklered | 90 | 60 | 30* | 60**† | 90** | 120** |
| b. Institutional | 90 | 60 | 30* | 60 | 90 | 120# |
| c. Other residential | 90 | 60 | 30* | 60 | 90 | 120# |
| 2. Office: | | | | | | |
| – not sprinklered | 90 | 60 | 30* | 60 | 90 | Not permitted |
| – sprinklered [2] | 60 | 60 | 30* | 30* | 60 | 120# |
| 3. Shop and commercial: | | | | | | |
| – not sprinklered | 90 | 60 | 60 | 60 | 90 | Not permitted |
| – sprinklered [2] | 60 | 60 | 30* | 60 | 60 | 120# |
| 4. Assembly and recreation: | | | | | | |
| – not sprinklered | 90 | 60 | 60 | 60 | 90 | Not permitted |
| – sprinklered [2] | 60 | 60 | 30* | 60 | 60 | 120# |
| 5. Industrial: | | | | | | |
| – not sprinklered | 120 | 90 | 60 | 90 | 120 | Not permitted |
| – sprinklered [2] | 90 | 60 | 30* | 60 | 90 | 120# |
| 6. Storage and other non-residential: | | | | | | |
| a. any building or part not described elsewhere: | | | | | | |
| – not sprinklered | 120 | 90 | 60 | 90 | 120 | Not permitted |
| – sprinklered [2] | 90 | 60 | 30* | 60 | 90 | 120# |
| b. car park for light vehicles: | | | | | | |
| i. open sided car park [3] | Not applicable | Not applicable | 15*+ | 15*+ [4] | 15*+ [4] | 60 |
| ii. any other car park | 90 | 60 | 30* | 60 | 90 | 120# |

For the offices with the height less than 5.0 m, the required fire resistance time is 30 minutes (R30).

## 4.2 Industrial building description

The industrial building is placed in Coimbra in Portugal. It is 60 m long and has a span (centre to centre) of 40 m, with equal rafters of 20 m each, a height of 7.90 m, a rafter slope of $\alpha = 8º$ and a spacing between frames of 5.0 m (*Figure 4.2*). The office area is partly placed outside the envelope of the building and partly indoors, with overall length of 20 m and width of 14.60 m from the frontal side.

Inside the building is free-standing intermediate floor, 4.20 m above the ground, which is held up by metal columns extending from the floor. The length of 16.50 m and width of 5.20 m provide the total area of 85.8 $m^2$, which are used as a space for offices (*Figure 4.3*).

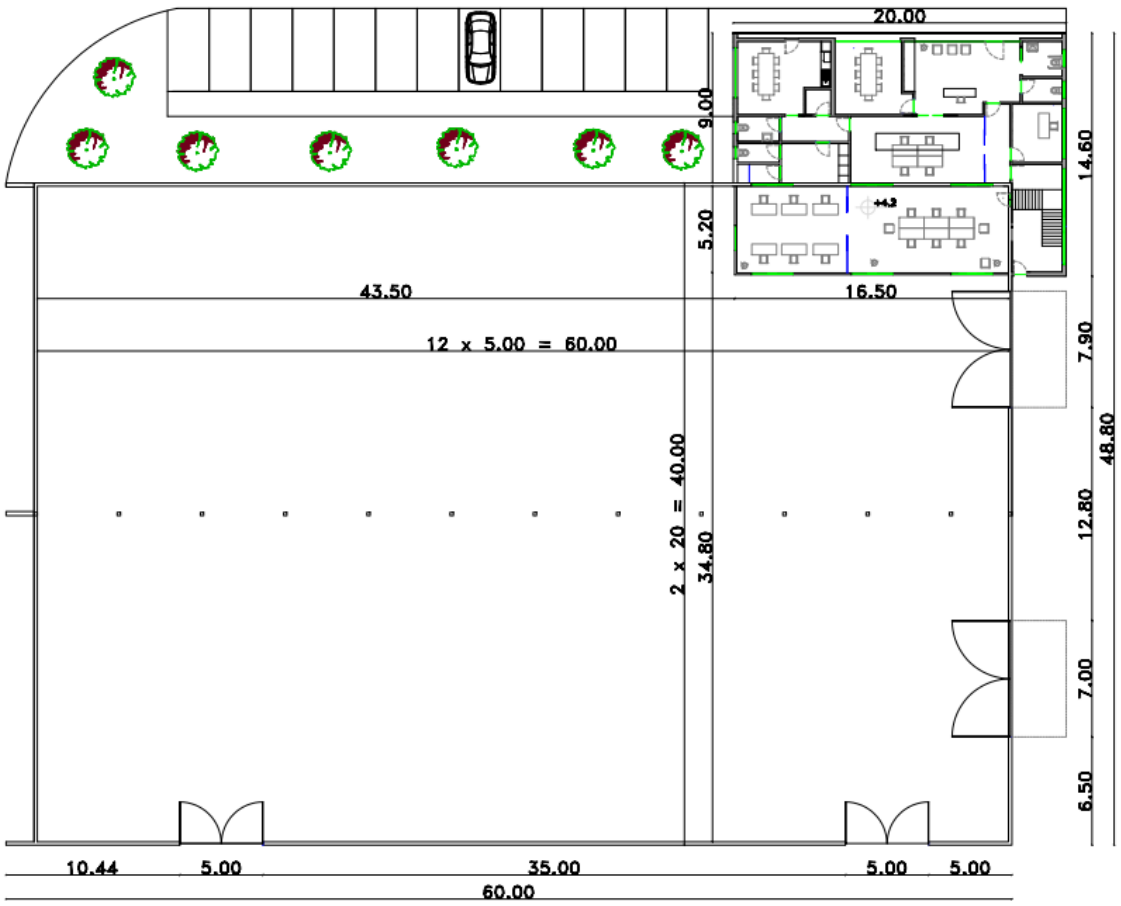


a) Layout of the industrial building with adjacent offices

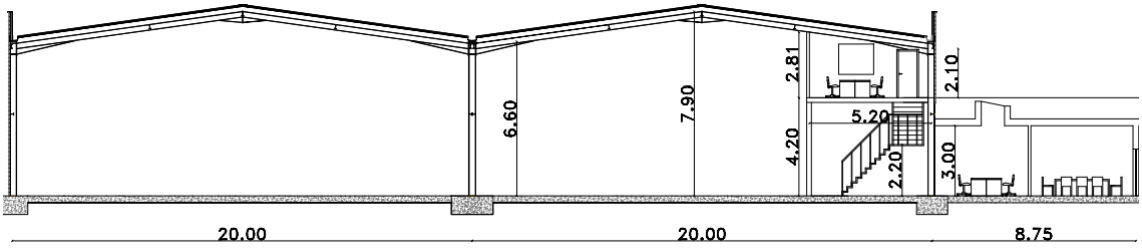


b) Transversal frame – 2 bays (side view)

*Figure 4.2* - Study case – industrial building

The walls and roof are thermally insulated. The roof is composed by, from exterior to interior: external membrane, rigid gypsum roof boards (12.5 mm thick), insulation (rock wool, 100 mm thick), vapour retarder, structural deck (1 mm thick), and the supporting steelwork. Walls are made by, from exterior to interior: external profile sheeting (1 mm thick), insulation (rock wool, 100 mm thick), gypsum board (12.5 mm thick).

It is also worth of mentioning that the purlins are considered as though they are not laterally constrained by means of roof steel sheeting as the level of constraint is not known, so this has been adopted as a safety-side solution.

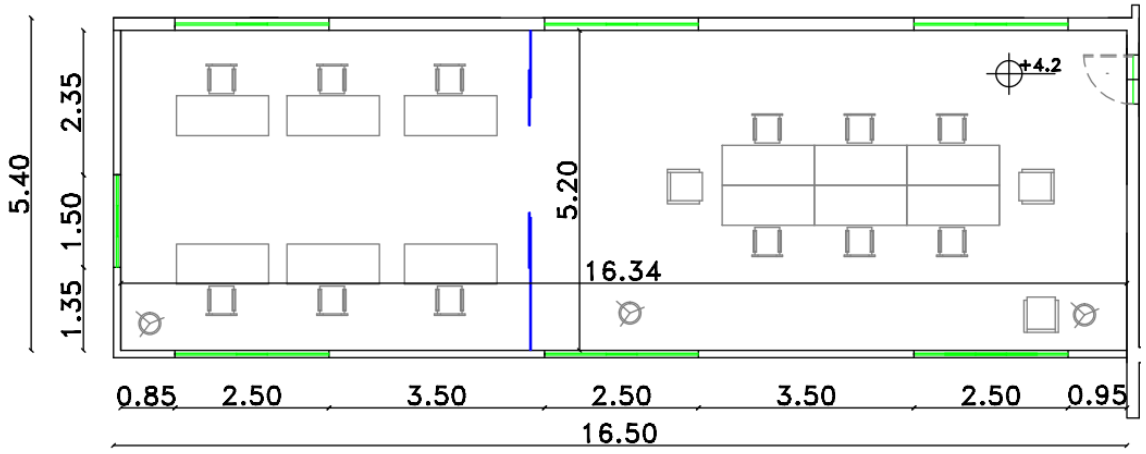


*Figure 4.3* - Layout of the mezzanine floor

## 4.3 Action and combinations

### 4.3.1 Thermal actions

Based on chapter 3.4.1, three different temperature-time fire curves are used for the studied example (*Figure 4.4*): i) standard ISO 834 fire curve; ii) parametric curve calculated based on the Annex A and Annex E of EN 1991-1-2 and iii) zone curve calculated by the program OZone V2 (Cadorin and Franssen, 2001).

The detailed calculation of the parametric fire curve is shown in Appendix A of this thesis. This curve presents the fire action more realistically, and unlike the nominal curve both heating and cooling phase are included. However, the main disadvantage of this curve is that it also assumes uniform temperature in the entire apartment. It is necessary to say that this curve may be applied only for fire compartments up to 500 m² of floor area, maximum height of 4.0 m without openings in the roof.

For the considered study case, the zone model curve obtained in Ozone program will be used for further calculation, as a curve that is approximate to the reality in a best way. This curve is obtained from more sophisticated mass and energy balance model which also takes into account pre-flashover phase, which for instance is not considered in parametric fire curve. However, even in this curve uniform temperature in each zone is assumed. OZone software is based on the natural fire safety concept design (NFSC), in which the basic inputs zone models need are the heat release rate RHR($t$) [W], the pyrolisis rate $\dot{m}_{fi}$(t) [kg/s] and the fire area $A_{fi}(t)$ as a function of time. The program also allows user to take into account active fire fighting measures. All the data used for the definition of the fire curve are given in Annex A of the thesis, where the same parameters are used for calculation of parametric fire curve.

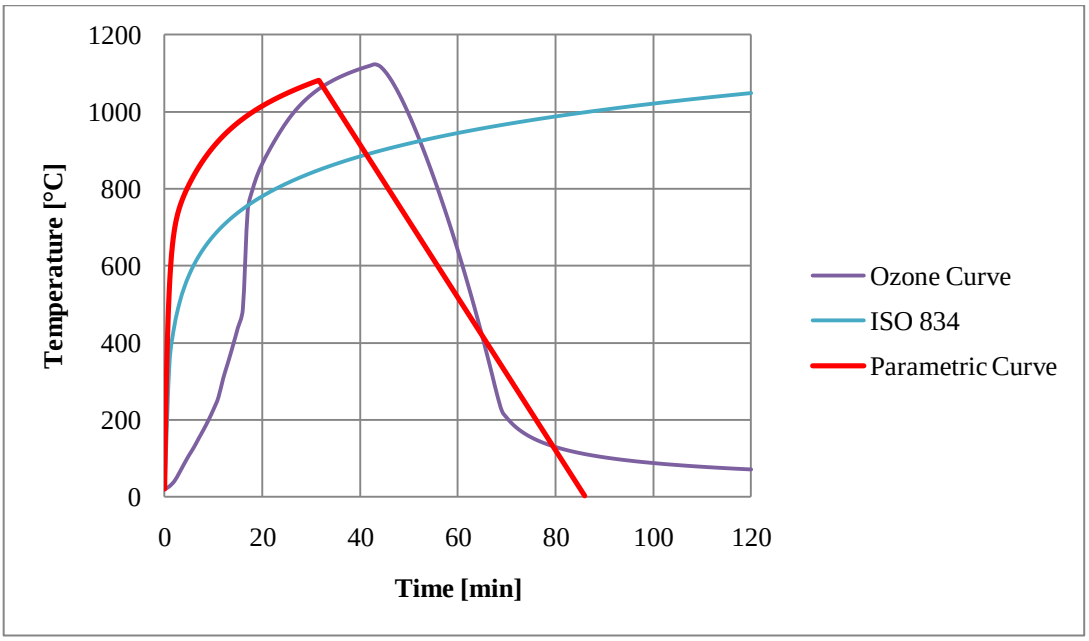


*Figure 4.4* - Temperature-time fire curves of the study case

Normally it is assumed that the nominal fire curve (ISO 834) is always on a safety side, as there is an abrupt jump in temperature in an early phase and the temperature constantly increases in time. However, that does not have necessary always to be the case as it can be observed in this case (*Figure 4.4*). Here, for instance, in zone model curve the temperature rises slower than ISO curve, but after approximately 20 minutes from the ignition, the temperature exceeds the ISO curve and hits the peak of 1123°C after 43minutes and 15 seconds from the ignition, and after that point comes the cooling phase which is not considered in the nominal curve.

### 4.3.2 Mechanical actions

In this section, the considered mechanical actions that act on the purlin are listed with their values.

Permanent actions:

- roof weight.....$g_r = 0.40$ kN/m$^2$
- purlin weight.....$g_p = 0.15$ kN/m$^2$
- installations..... $g_i = 0.05$ kN/m$^2$
- bracings.....$g_b = 0.075$ kN/m$^2$

Total: $g_k = 0.675$ kN/m$^2$

Imposed load:

The imposed load on the roof is given according to EN 1991-1-1 (2002). Considering that the roof is not accessible, except for repairing and maintenance (H category), the characteristic value of the uniformly distributed imposed load, varies between 0.0 kN/m$^2$ and 1.0 kN/m$^2$. In this case it is adopted:

$$q_k = 0.40 \text{ kN/m}^2$$

Since the industrial building is located in Coimbra in Portugal, the snow loads are neglected. In EN 1990 it is defined that the coefficient for combination for imposed load ($\psi_1$ and $\psi_2$) should be taken as zero for the H category buildings. Speaking of wind load, it is prescribed that coefficient for combination $\psi_1$ should be taken as 0.2. However, in this case it is obtained that wind load has favorable effect, and thus it is neglected from the load combination in order to obtain the most unfavorable load situation.

### 4.3.3 Fundamental and accidental combinations

The design values of the applied forces for the ultimate limit state are obtained from the fundamental combination, given by (EN 1990, 2002).

$$q_{Ed} = 1.35 \cdot g_k = 1.35 \cdot 0.675 = 0.92 \text{ kN/m}^2$$

According to EN 1990 (2002), the fire is considered as an accidental design situation and the design effect for fire ($q_{fi,d}$) can be obtained as follows (EN 1991, 2002):

$$q_{fi,d} = 1.0 \cdot g_k = 1.0 \cdot 0.675 = 0.675 \text{ kN/m}^2$$

Where, the coefficients for combination ($\psi$) are listed in the table A1-1 of EN 1990 (2002).

## 4.4 Geometrical and material data of the studied purlin

### 4.4.1 Shape and the dimensions of the cross-section

The shape of the cross-section is trapezoidal (Ω160) and it is taken from the previous study done (Ferraz, 2014), for the purlins subjected to bending in ambient temperatures of 20°C. That study aimed to optimize the shape, by means of intermediate stiffeners in such a way to make the section as much effective as possible (*Figure 4.5*).

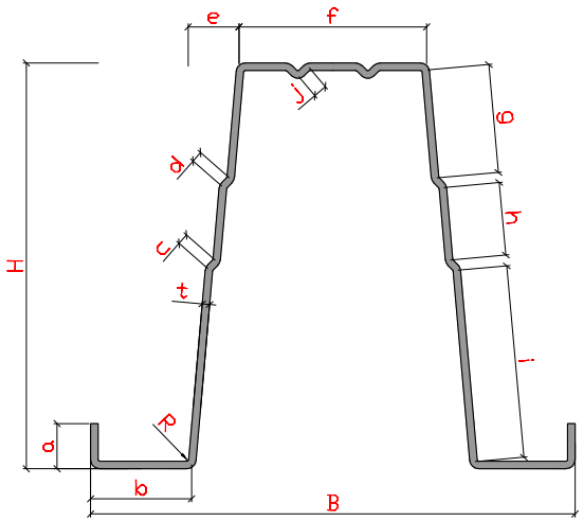


*Figure 4.5* - Omega (Ω160) cross-section (Ferraz, 2014)

All the dimensions of the cross section are presented here in general numbers. However, all of them have fixed value except the thickness ($t$) which will be varied in the range between 1 mm and 2.4 mm accordingly, in order to find the optimal solution. The exact values of the other dimensions are given in the Table below:

*Table 4.2* - Legend of dimensions of Omega 160 cross-section

| Symbol | Dimension [mm] |
|---|---|
| $H$ | 160 |
| $B$ | 195 |
| $a$ | 20 |
| $b$ | 40 |
| $c$ | 4.24 |
| $d$ | 4.24 |
| $e$ | 20 |
| $f$ | 75 |
| $g$ | 45 |
| $h$ | 30 |
| $i$ | 78.6 |
| $j$ | 5.66 |
| $t$ | 1 to 2.4 |
| $R$ | 1.5 |

### 4.4.2 Material properties

Below are listed the mechanical material properties of the steel S280GD+Z:

-Young's module of elasticity: $E$ =210000 N/mm$^2$

-Poisson ratio: $\nu$ = 0.3

-Shear modulus: $G$=80770 N/mm$^2$

-Nominal yield strength (S280GD+Z): $f_{yb}$ = 280 N/mm$^2$

-Partial factor for cross-section checks (EN 1993-1-3, 2004): $\gamma_{M0}$ = 1.0

-Partial factor for member checks (EN 1993-1-3, 2004): $\gamma_{M1}$ = 1.0

-Elastic strain: $\varepsilon = \sqrt{235/f_{yb}}$ $\varepsilon$ = 0.92

-Partial safety factor in fire situation (EN 1993-1-2, 2004): $\gamma_{M,fi}$ = 1.0

-Elastic strain at elevated temperatures:

$$\varepsilon = \sqrt{\frac{E_\theta}{f_{y,\theta}}} = \sqrt{\frac{k_{E,\theta} \cdot E}{k_{y,\theta} \cdot f_{yb}}} = \sqrt{\frac{k_{E,\theta}}{k_{y,\theta}}} \sqrt{\frac{E}{f_{yb}}} \cong 0.85\sqrt{235/f_{yb}} = 0.78$$

- Reduction factor for proportional limit ($k_{0.2p,\theta}$) *Figure 3.2* (3.3.1)

- Reduction factor for proportional limit ($k_{E,\theta}$) *Figure 3.2* (3.3.1)

### 4.4.3 Geometrical properties of gross cross-section

Here are given the geometrical properties of the purlin with thickness of 1 mm (*Figure 4.6*), since an example of analytical calculation will be done in chapter 5, using these cross section properties.

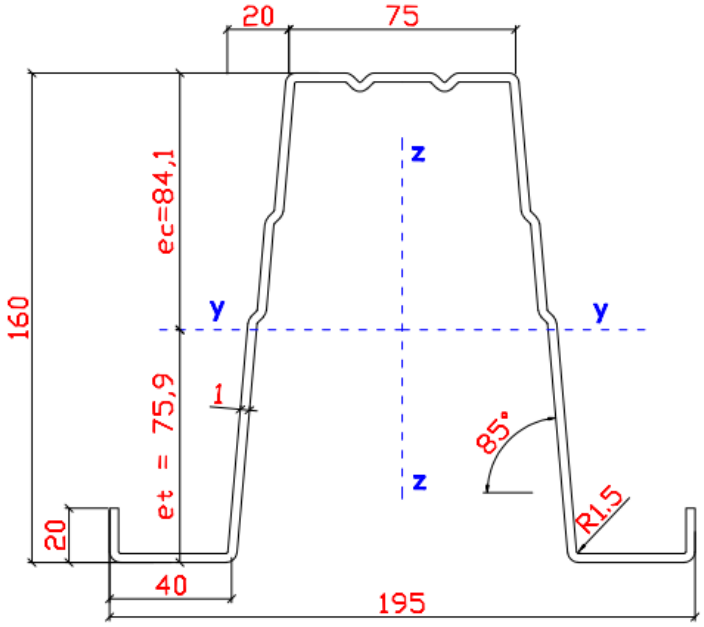


*Figure 4.6* - Gross cross-section - Ω160 (t = 1 mm)

- Area of cross-section: $A$ = 5.158 cm$^2$
- Distance of the extreme fiber in compression: (with respect to gravity centre) $e_c$ = 84.09 mm
- Distance of the extreme fiber in tension: (with respect to gravity centre) $e_t$ = 75.925 mm
- Second moment of area with respect to y-axis: $I_y$ = 183.1 cm$^4$
- Second moment of area with respect to z-axis: $I_z$ = 153.04 cm$^4$
- Radius of gyration about principle y-axis: $i_y$ = 60 mm
- Radius of gyration about principle z-axis: $i_z$ = 54 mm
- Elastic section modulus about principle y-axis: $W_{el.y}$ = 21.77 cm$^3$
- Elastic section modulus about principle z-axis: $W_{el.z}$ = 15.96 cm$^3$
- Shear centre coordinate in y-direction: (measured from gravity centre) $y_{sc}$ = 0 mm
- Shear centre coordinate in z-direction: (measured from gravity centre) $z_{sc}$ = 123 mm
- Torsional constant: $I_t$ = 171.93 mm$^4$
- Warping constant: $I_w$ = 2218.2 cm$^6$
- Mono-symmetry constant about y-axis: $\beta_y$ = - 271 mm
- Mono-symmetry constant about z-axis: $\beta_z$ = 0 mm

### 4.4.4 Geometrical properties of effective cross-section

The effective cross section is calculated as it is described in chapter 3.5.1 of this work. The detailed calculation of effective cross section Ω160, when subjected to positive and negative bending moment, according to Section 5.5.3.4 of EN 1993-1-3 (2004), is presented in Appendix B of this work. Here are presented only the final results of the geometrical properties of the cross-section important for further calculations of the design buckling resistance moment ($M_{b,Rd}$).

- *Positive bending moment:*

- Effective Area of cross-section: $A_{eff}$ = 4.95 cm$^2$
- Distance of the extreme fiber in compression: $e_c$ = 87.584 mm

(with respect to gravity centre)

- Distance of the extreme fiber in tension: $e_t$ = 72.432 mm
  (with respect to gravity centre)

- Second moment of effective area with respect to y-axis: $I_{eff\ .y}$ = 168.162 cm$^4$

- Second moment of effective area with respect to z-axis: $I_{eff\ .z}$ = 152.53 cm$^4$

- Effective section modulus about principle y-axis: $W_{eff\ .y}$ = 19.2 cm$^3$

- *Negative bending moment:*

- Effective Area of cross-section: $A_{eff}$ = 4.59 cm$^2$

- Distance of the extreme fiber in compression: $e_c$ = 81.0 mm
  (with respect to gravity centre)

- Distance of the extreme fiber in tension: $e_t$ = 79.0 mm
  (with respect to gravity centre)

- Second moment of effective area with respect to y-axis: $I_{eff\ .y}$= 165.52 cm$^4$

- Second moment of effective area with respect to z-axis: $I_{eff\ .z}$ = 132.44 cm$^4$

- Effective section modulus about principle y-axis: $W_{eff\ .y}$ = 20.435 cm$^3$

# 5 ANALYTICAL CALCULATIONS

## 5.1 Introduction

In this chapter, analytical calculation of the considered CFS purlin will be provided. Two different cases of purlins are analyzed:

- simply supported beam (5 m)
- two-span continuous beam (5 m + 5 m)

First, these purlins will be analyzed and designed at the ambient temperature according to EN 1993-1-3 (2004), and then their fire resistance will be checked according to Annex E of EN 1993-1-2 (2004).

## 5.2 Steel beam at the ambient temperature

The design buckling resistance moment ($M_{b,Rd}$) is calculated for considered study case using EN 1993-1-1 (2004), EN 1993-1-3 (2004) and EN 1993-1-5 (2006), as it is described in chapter 3.4.1 of this thesis. In EN 1993-1-3 (chapter 10) are provided special rules for purlins which are restrained by sheeting. However, as it is previously explained in this case purlins are considered as non-restrained so these rules are not applicable in this case. The detailed calculation will be presented only for one case - for the section Ω160 with thickness of 1mm. For the other cases the same principles will be applied, and the results will be given in the tabular manner.

### 5.2.1 Simply supported beam

- **Load analysis:**

Span of purlin $L = 5.0\ m$
Spacing between purlins $S = 1.0\ m$

With spacing between the purlins of 1.0 m, according to chapter 4.3.2, it is obtained:

$$q_{Ed} = S \cdot (1.35 \cdot g_k) = 1.0 \cdot (1.35 \cdot 0.675) = 0.92\ \text{kN/m}$$

And the design values of forces acting on the purlin are calculated as

$$M_{Ed} = \frac{q_{Ed} \cdot L^2}{8} = 3.3 \text{ kNm}$$

$$V_{Ed} = \frac{q_{Ed} \cdot L}{2} = 2.3 \text{ kN}$$

- **Geometrical and material data:**

All the necessary data regarding material and geometrical properties are provided in chapter 4.4.

- **Design buckling resistance moment:**

Critical elastic moment for lateral-torsional buckling is calculated using the CUFSM software, specialized for cold-formed profiles, which allows practical and quick computation of the critical loads. After that, the usual procedure is used for calculation of the design buckling resistance moment, as it is described in chapter 3.5.1.

- Critical elastic moment for LTB: $M_{cr} = \alpha_{cr} \cdot M_{Rd} = 21.99$ kNm

Where $\alpha_{cr}$ presents the load factor, obtained from the CUFSM software, and $M_{Rd}$ presents the plastic resistance moment.

- Non-dimensional slenderness:

$$\bar{\lambda}_{LT} = \sqrt{\frac{W_{eff,y} \cdot f_{yb}}{M_{cr}}} = \sqrt{\frac{19.2 \cdot 28.0}{21.99 \cdot 10^2}} = 0.494$$

- Imperfection factor: ($\alpha_{\mathrm{LT}}$)

According to Clause 6.2.4(1) of EN 1993-1-3 (2004) the design buckling resistance moment of a member that is susceptible to lateral-torsional buckling should be determined according to EN 1993-1-1 (2004), section 6.3.2.2 using the lateral buckling curve *b*, which leads to the value of the imperfection factor of $\alpha_{\mathrm{LT}}$ =0.34.

$$\phi_{LT} = 0.5\left[1 + \alpha_{LT}\left(\bar{\lambda}_{LT} - 0.2\right) + \bar{\lambda}_{LT}^{\,2}\right] = 0.672$$

- The reduction factor $\chi_{LT}$: ($\bar{\lambda}_{LT} > 0.4$)

$$\chi_{LT} = \frac{1}{\phi_{LT} + \sqrt{\phi_{LT}^{\,2} - \bar{\lambda}_{\mathrm{LT}}^{\,2}}} = 0.887$$

And finally, the design buckling resistance moment is calculated:

$$M_{b,Rd} = \frac{\chi_{LT} \cdot W_{eff,y} \cdot f_{yb}}{\gamma_{M,1}} = \frac{0.887 \cdot 19.2 \cdot 28.0}{1.0} = 4.77 \text{ kNm}$$

- Verification:

$$\frac{M_{Ed}}{M_{b,Rd}} = 0.76 < 1.0$$

- **Verification of the shear forces:**

The shear forces should be checked since the shear buckling is also common phenomenon in CFS. The procedure for calculation of the design shear resistance for the inclined web with the intermediate longitudinal stiffeners is provided in 6.1.5 of EN 1993-1-3 (2004), and the necessary parameters of the cross section are given in the Apendix B of this thesis.

-Total developed slant height of the web:

$$s_d = s_a + s_{sa} + s_b + s_{sb} + s_p = 45 + 4.24 + 30 + 4.24 + 78.6 = 162.1\ mm$$

-Coefficient of shear buckling:

$$k_\tau = 5.34 + \frac{2.1}{t}\sqrt[3]{\left(\frac{\sum I_s}{s_d}\right)} = 5.34 + \frac{2.1}{0.96}\sqrt[3]{\left(\frac{2 \cdot 96.3293}{162.1}\right)} = 7.657$$

-Relative web slenderness: ($\bar{\lambda}_w$)

$$\bar{\lambda}_w = 0.346\frac{s_d}{t}\sqrt{\frac{5.34 \cdot f_{yb}}{k_\tau \cdot E}} = 1.7814 \quad > \quad 0.346\frac{s_p}{t}\sqrt{\frac{f_{yb}}{E}} = 1.0344$$

-Shear buckling strength: ($f_{bv}$) (Table 6.1 of EN 1993-1-3)

$$\bar{\lambda}_w = 1.7814 \quad > 1.4 \quad \rightarrow \quad f_{bv} = \frac{0.67 \cdot f_{yb}}{\bar{\lambda}_w{}^2} = 59.116 \text{ MPa}$$

-Design shear resistance: ($V_{b,Rd}$)

$$V_{b.Rd} = \frac{\frac{h_w}{\sin\phi} \cdot t \cdot f_{bv}}{\gamma_{M0}} = \frac{\frac{159}{\sin 85} \cdot 0.96 \cdot 59.116}{1.0} = 9.06 \text{ kN}$$

- Verification:

$$\frac{V_{Ed,web}}{V_{b,Rd}} \approx \frac{V_{Ed}/2}{V_{b,Rd}} = \frac{1.15}{9.06} = 0.15 < 1.0$$

### 5.2.2 Continuous beam

- **Load analysis:**

The same characteristic values of permanent and imposed loads, as for the simply supported beam, are applied here.

Span of purlin $L = 2 \text{ x } 5.0\ m$
Spacing between purlins $S = 1.0\ m$

With spacing between the purlins of 1.0 m it is obtained according to chapter 4.3.2:

$q_{Ed} = S \cdot (1.35 \cdot g_k) = 1.0 \cdot (1.35 \cdot 0.675) = 0.92 \text{ kN/m}$

And the design values of forces acting on the purlin are calculated as

$$M^{-}_{Ed,max} = \frac{q_{Ed} \cdot L^2}{8} = \frac{0.92 \cdot 5.0^2}{8} = 3.3 \text{ kNm}$$

$$M^{+}_{Ed,max} = \frac{9 \cdot q_{Ed} \cdot L^2}{128} = \frac{9 \cdot 0.92 \cdot 5.0^2}{128} = 1.74 \text{ kNm}$$

$$V_{Ed,1} = \frac{3 \cdot q_{Ed} \cdot L}{8} = \frac{3 \cdot 0.92 \cdot 5.0}{8} = 1.725 \text{ kN}$$

$$V_{Ed,2} = \frac{5 \cdot q_{Ed} \cdot L}{8} = \frac{5 \cdot 0.92 \cdot 5.0}{8} = 2.875 \text{ kN}$$

- **Geometrical and material data:**

All the necessary data regarding material and geometrical properties are provided in chapter 4.4

- **Design buckling resistance moment:**

Critical elastic moment for lateral-torsional buckling is calculated using the CUFSM software, specialized for cold-formed profiles, which allows practical and quick computation of the critical loads. After that, the usual procedure is used for calculation of the design buckling resistance moment, as it is described in chapter 3.5.1.

- Critical elastic moment for LTB: $M_{cr} = \alpha_{cr} \cdot M_{Rd} = 28.22 \text{ kNm}$

- Non-dimensional slenderness:

$$\bar{\lambda}_{LT} = \sqrt{\frac{W_{eff,y} \cdot f_{yb}}{M_{cr}}} = \sqrt{\frac{20.435 \cdot 28.0}{28.22 \cdot 10^2}} = 0.45$$

- Imperfection factor: ($\alpha_{\mathrm{LT}}$)

According to Clause 6.2.4 of EN 1993-1-3 (2004) the design buckling resistance moment of a member that is susceptible to lateral-torsional buckling should be determined according to clause 6.3.2.2 of EN 1993-1-1 (2004), using the lateral buckling curve b, which leads to the value of the imperfection factor of $\alpha_{\mathrm{LT}}$ =0.34.

$$\phi_{LT} = 0.5\left[1 + \alpha_{LT}\left(\bar{\lambda}_{LT} - 0.2\right) + \bar{\lambda}_{LT}{}^2\right] = 0.644$$

- The reduction factor $\chi_{LT}$: ($\bar{\lambda}_{\mathrm{LT}} > 0{,}4$)

$$\chi_{LT} = \frac{1}{\phi_{LT} + \sqrt{\phi_{LT}{}^2 - \bar{\lambda}_{\mathrm{LT}}{}^2}} = 0.9055$$

And finally, the design buckling resistance moment is calculated:

$$M_{b,Rd} = \frac{\chi_{LT} \cdot W_{eff,y} \cdot f_{yb}}{\gamma_{M,1}} = \frac{0.9055 \cdot 20.435 \cdot 28.0}{1.0} = 5.18 \text{ kNm}$$

- Verification:

$$\frac{M_{Ed}}{M_{b,Rd}} = 0.7 < 1.0$$

- **Verification of the shear forces:**

-Design shear resistance ($V_{b,Rd}$) has the same value as for the simply supported beam, which is previously calculated.

$$V_{b,Rd} = \frac{\frac{h_w}{\sin\phi} \cdot t \cdot f_{bv}}{\gamma_{M0}} = \frac{\frac{159}{\sin 85} \cdot 0.96 \cdot 59.116}{1.0} = 9.06 \text{ kN}$$

- Verification:

$$\frac{V_{Ed,web}}{V_{b,Rd}} \approx \frac{V_{Ed,2}/2}{V_{b,Rd}} = \frac{1.44}{9.06} = 0.16 < 1.0$$

- **Interaction of shear forces and bending moment:**

Since the utilization of the shear forces in the middle support is 16% which is less than 50%, there is no need to check interaction of bending moment and shear force.

## 5.3 Unprotected steel beam at the elevated temperature

The lateral-torsional resistant moment for CFS under elevated temperatures ($M_{b,fi,t,Rd}$) is calculated for considered study case using, as it is described in chapter 3.5.2 of this thesis (see Eq. 3.26). The detailed calculation will be presented only for one case - for the section Ω160 with thickness of 1mm as it was shown at the ambient temperature. Moreover, two methods will be used, one prescribed in EN 1993-1-2 (2004) and the other one according to French annex of the same standard. For the other cases the same principles will be applied, and the results will be given in the tabular manner.

### 5.3.1 Simply supported beam

- **Load analysis:**

The same characteristic values of permanent and imposed loads that are used at the ambient temperatures, will be used here.

Span of purlin $L = 5.0\ m$
Spacing between purlins $S = 1.0\ m$

With spacing between the purlins of 1.0 m it is obtained according to chapter 4.3.2:

$q_{fi,d} = S \cdot (1.0 \cdot g_k) = 1.0 \cdot (1.0 \cdot 0.675) = 0.675$ kN/m

And the design values of forces acting on the purlin under fire condition are calculated as

$$M_{fi,Ed} = \frac{q_{fi,d} \cdot L^2}{8} = \frac{0.675 \cdot 5.0^2}{8} = 2.11 \text{ kNm}$$

$$V_{fi,Ed} = \frac{q_{fi,d} \cdot L}{2} = \frac{0.675 \cdot 5.0}{2} = 1.6875 \text{ kN}$$

- **Geometrical properties of gross cross-section:**

All the necessary data regarding material and geometrical properties are provided in chapter 4.4

- **Calculation of the critical temperature:**

According to EN 1991-1-2 (2004), the verification of fire resistance of the element or structure should be done using one of three strategies (chapter 3.4.3). In this case the time domain strategy is used, which considers comparison of the resistance of the element measured in time with required fire resistance time in minutes (in this case R30).

*I) Eurocode procedure:*

Critical elastic moment for lateral-torsional buckling is calculated using the CUFSM software (the same value are already given in 5.1)

- Critical elastic moment: $M_{cr} = \alpha_{cr} \cdot M_{Rd} = 21.99$ kNm

- Non-dimensional slenderness at ambient temperature: ($\bar{\lambda}_{LT}$)

$$\bar{\lambda}_{LT} = \sqrt{\frac{W_{eff,y} \cdot f_{yb}}{M_{cr}}} = \sqrt{\frac{19.2 \cdot 28.0}{21.99 \cdot 10^2}} = 0.494$$

- Non-dimensional slenderness at elevated temperature: ($\bar{\lambda}_{LT,\theta}$)

Since the non-dimensional slenderness in the fire situation depends directly on the temperature which is at this moment still unknown, an iterative procedure has to be conducted. However, convergence can be reached quite fast if the following recommendation is used for assuming the first critical temperature:

***1. Iteration:***

$$\bar{\lambda}_{\mathrm{LT},\theta}{}^{(1)} = \bar{\lambda}_{LT} \sqrt{\frac{k_{0.2p,\theta}}{k_{E,\theta}}} = 1.2 \cdot \bar{\lambda}_{LT} = 0.593$$

- Imperfection factor: ($\alpha$)

$$\alpha = 0.65\sqrt{235/f_{yb}} = 0.595$$

$$\phi_{LT,\theta}{}^{(1)} = 0.5\left[1 + \alpha \cdot \bar{\lambda}_{LT,\theta}{}^{(1)} + \left(\bar{\lambda}_{LT,\theta}{}^{(1)}\right)^2\right] = 0.852$$

- Reduction factor: ($\chi_{LT,fi}$)

$$\chi_{LT,fi}{}^{(1)} = \frac{1}{\phi_{LT,\theta}{}^{(1)} + \sqrt{\left(\phi_{LT,\theta}{}^{(1)}\right)^2 - \left(\bar{\lambda}_{LT,\theta}{}^{(1)}\right)^2}} = 0.683$$

The appropriate value of reduction factor $k_{0.2p,\theta}$ is calculated from the following condition:

$$M_{b,fi,t,Rd} = M_{fi,Ed}$$

$$\frac{\chi_{LT,fi}{}^{(1)} \cdot W_{eff,y} \cdot k_{0.2p,\theta} \cdot f_{yb}}{\gamma_{M,fi}} = 2.11\text{kNm} \qquad \rightarrow \qquad k_{0.2p,\theta}{}^{(1)} = 0.575$$

The corresponding value of the critical temperature is obtained using the table E.1 of Annex E of EN 1993-1-2 (here *Table 3.2*). Using linear interpolation, the following critical temperature is calculated:

$$\theta_{crit}{}^{(1)} = 462.5\ °\text{C}$$

Now that the critical temperature of steel is obtained, non-dimensional relative slenderness can be calculated. But first, for this particular temperature the reduction factor for the modulus of elasticity has to be found, using the *Table 3.1*.

$$\theta_{crit}{}^{(1)} = 462.5\ °\text{C} \ \rightarrow \quad k^{(1)}{}_{E,\theta} = 0.6375$$

The remaining iterations are given in tabular manner, where the same procedure was used as for the first iteration (*Table 5.1*)

*Table 5.1* - Calculation of critical temperature according to EN 1993-1-2 (2004)

| | $\bar{\lambda}_{LT,\theta}$ | $\phi_{LT,\theta}$ | $\chi_{LT,fi}$ | $k_{0.2p,\theta}$ | $\theta_{crit}$ (°C) | $k_{E,\theta}$ |
|---|---|---|---|---|---|---|
| ***2. Iteration*** | 0.469 | 0.7495 | 0.7495 | 0.4669 | 502.6 | 0.593 |
| ***3. Iteration*** | 0.465 | 0.746 | 0.7521 | 0.522 | 503.3 | 0.59 |
| ***4. Iteration*** | 0.464 | 0.7462 | 0.7518 | 0.522 | **503.5** | 0.59 |

As it may be observed from the table, the critical temperature is:

$$\boldsymbol{\theta_{crit} = 503.5}\ °\text{C}$$

*II) <u>French national annex of Part 1-2 of EN 1993-1-2</u>:*

The calculation according to French national annex is given in tabular manner (*Table 5.2*). The calculation procedure is explained in chapter 3.5.2 of the thesis.

*Table 5.2* - Calculation of critical temperature according to French national annex

| | $\bar{\lambda}_{LT,\theta}$ | $\phi_{LT,\theta}$ | $\chi_{LT,fi}$ | $k_{0.2p,\theta}$ | $\theta_{crit}$ (°C) | $k_{E,\theta}$ |
|---|---|---|---|---|---|---|
| ***1. Iteration*** | 0.593 | 0.7426 | 0.8406 | 0.549 | 537.7 | 0.4907 |
| ***2. Iteration*** | 0.5225 | 0.6913 | 0.874 | 0.449 | 545.2 | 0.469 |
| ***3. Iteration*** | 0.4834 | 0.665 | 0.8915 | 0.44 | 548.85 | 0.4583 |
| ***4. Iteration*** | 0.484 | 0.6654 | 0.8912 | 0.4404 | **548.8** | 0.4585 |

With imperfection factor obtained from EN 1993-1-1 (2004) using the buckling curve for hot rolled sections, which in this case means buckling curve B ($\alpha = 0.34$) (Table 6.4 of EN 1993-1-1). The reduction factors are given in the chapter 3.3.1 (Table 3.3).

As it may be observed from the table, this method indeed gives less conservative results and thus higher critical temperature:

$$\boldsymbol{\theta_{crit} = 548.8 \approx 549\ ℃}$$

- **Fire resistance verification:**

In this case, as it shown, the time domain strategy is used, which considers comparison of the resistance of the element measured in time with required fire resistance time in minutes (in this case R30).

To do so, it is necessary to calculate thermal response of the steel member or in other words, the distribution of the temperature inside the steel when subjected to fire. The fire curve, which presents the thermal action of fire, is given in chapter 4.3 (*Figure 4.4*), and the thermal response is manually calculated according to the procedure described in chapter 3.5.2. The calculation of the heat transfer is done in Excel (*Figure 5.1*).

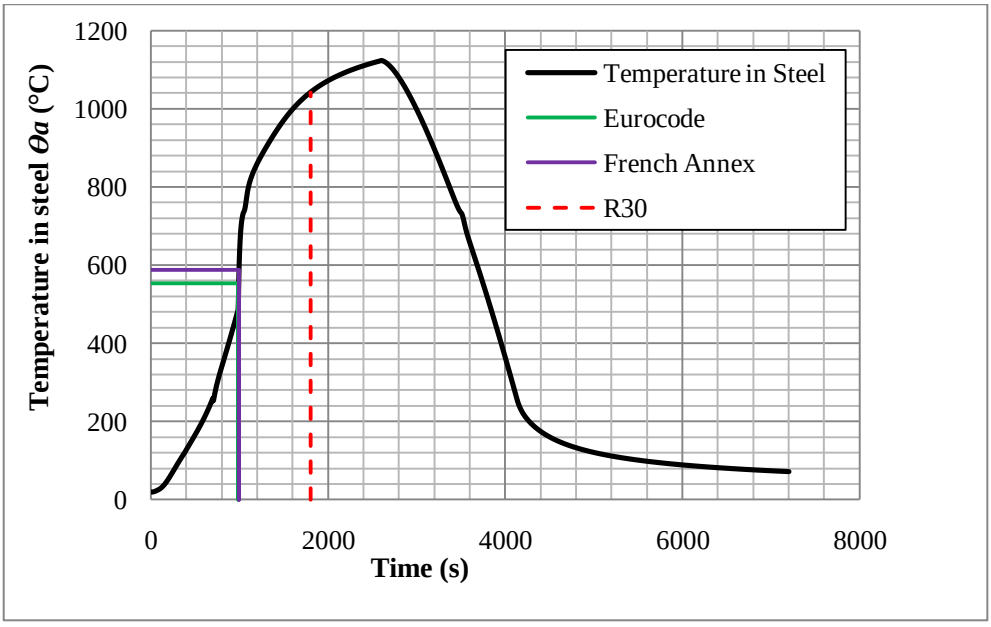


*Figure 5.1*- Thermal response of the Ω160 subjected to fire

Where the section factor $A_m/V$ due to the uncertainty is conservatively calculated considering that in the case of fire all the sides of the cross section are exposed, and this value is given as:

$A_m/V = O/A = 1042\,mm/5.158\ cm^2 = 2020.16\,m^{-1}$

The coefficient that takes into account shadow effect is conservatively taken as $k_{sh}$ =1.0, while the film coefficient of convection is taken as 35 W/m$^2$K, which is prescribed in clause 3.3.2 of EN 1991-1-2 (2002), for advanced natural fire models.

As it may be seen (*Figure 5.1*), the curve which describes the thermal response of the purlin is affine to the compartment fire curve (*Figure 4.4*). The reason for such a small difference is the fact that the thickness of the considered purlin is only 1.0 mm, and the steel is heated almost immediately.

The time resistance of the purlin is obtained from the *Figure 5.1*. For the previously calculated critical temperatures of steel (Y-axis), it is easy to read the time resistance (X-axis). The following results are obtained:

Eurocode: $t_{fi,d} = 981s = 16.35\,min \leq t_{fi,req} = 30\,min$

French Annex: $t_{fi,d} = 987s = 16.45\,min \leq t_{fi,req} = 30\,min$

In both cases the required fire resistance time is not satisfied, which means that fire protection measures have to be applied and that is presented in the following chapter 5.2.

- **Verification of the shear forces:**

The verification of the shear forces under fire conditions is done according to 4.2.3.3 of EN 1993-1-2 (2004), where the shear resistance of the gross cross-section for normal temperature design is calculated according to EN 1993-1-3 (2004) and it is given in chapter 4.4.1.

-Design shear resistance at room temperature: ($V_{b,Rd}$)

$$V_{b,Rd} = \frac{\frac{h_w}{\sin\phi} \cdot t \cdot f_{bv}}{\gamma_{M0}} = 9.06\ \text{kN}$$

-Design shear resistance $V_{fi,t,Rd}$ at time *t*, is calculated using the following expression:

$$V_{fi,t,Rd} = \frac{k_{0.2p,web,\theta} \cdot V_{b,Rd}}{\gamma_{M,fi}} \qquad (5.1)$$

The appropriate value of reduction factor $k_{0.2p,web,\theta}$ is calculated from the following condition:

$V_{fi,t,Rd} = \mathrm{V}_{fi,Ed}$

$$\frac{k_{0.2p,web,\theta} \cdot V_{b,Rd}}{\gamma_{M,fi}} = \mathrm{V}_{fi,Ed,web} \approx \mathrm{R}_{fi,Ed}/2 = 0.84375\ \text{kN} \quad \rightarrow \quad k_{0.2p,web,\theta} = 0.093$$

The corresponding value of the critical temperature is then:

$\theta_{crit}{}^{(V_{fi,Ed})} = 761.66\ °C \quad \gg \quad \theta_{crit}{}^{(M_{fi,Ed})} = 503.5\ °C$

Since the critical temperature of the web subjected to shear force is significantly higher than the critical temperature of the element subjected to bending ($\theta_{crit}{}^{(V_{fi,Ed})} > \theta_{crit}{}^{(M_{fi,Ed})}$), the required fire resistance time is certainly higher and thus shear forces are not the governing ones for the overall design.

### 5.3.2 Continuous beam

- **Load analysis:**

The same characteristic values of permanent and imposed loads, as for the simply supported beam, are applied here.

Span of purlin $L = 2$ x $5.0\ m$
Spacing between purlins $S = 1.0\ m$

With spacing between the purlins of 1.0 m it is obtained according to chapter 4.3.2:

$q_{fi,d} = S \cdot (1.0 \cdot g_k) = 1.0 \cdot (1.0 \cdot 0.675) = 0.675$ kN/m

And the design values of forces acting on the purlin under fire conditions are calculated as

$$M_{fi,Ed}{}^{-} = \frac{q_{fi,d} \cdot L^2}{8} = \frac{0.675 \cdot 5.0^2}{8} = 2.11\ kNm$$

$$M_{fi,Ed}{}^{+} = \frac{9 \cdot q_{fi,d} \cdot L^2}{128} = \frac{9 \cdot 0.675 \cdot 5.0^2}{128} = 1.1865\ kNm$$

$$V_{fi,Ed,1} = \frac{3 \cdot q_{fi,d} \cdot L}{8} = \frac{3 \cdot 0.675 \cdot 5.0}{8} = 1.265\ kN$$

$$V_{fi,Ed,2} = \frac{5 \cdot q_{fi,d} \cdot L}{8} = \frac{5 \cdot 0.675 \cdot 5.0}{8} = 2.11\ kN$$

- **Geometrical properties of gross cross-section:**

All the necessary data regarding material and geometrical properties are provided in chapter 4.4

- **Calculation of the critical temperature:**

According to EN 1991-1-2 (2004), the verification of fire resistance of the element or structure should be done using one of three strategies (*Figure 3.14*). In this case again the time domain strategy is used, which considers comparison of the resistance of the element measured in time with required fire resistance time in minutes (in this case R30).

*I) Eurocode procedure:*

Critical elastic moment for lateral-torsional buckling is calculated using the CUFSM software (the same value are already given in 5.1)

- Critical elastic moment: $M_{cr} = \alpha_{cr} \cdot M_{Rd} = 28.22$ kNm

- Non-dimensional slenderness at ambient temperature: ($\bar{\lambda}_{LT}$)

$$\bar{\lambda}_{LT} = \sqrt{\frac{W_{eff,y} \cdot f_{yb}}{M_{cr}}} = \sqrt{\frac{20.435 \cdot 28.0}{28.22 \cdot 10^2}} = 0.45$$

The same iterative procedure that was used in a case of simply supported beam is conducted here, and results are given in tabular manner (*Table 5.3*).

*Table 5.3* - Calculation of critical temperature according to EN 1993-1-2 (2004)

| | $\bar{\lambda}_{LT,\theta}$ | $\phi_{LT,\theta}$ | $\chi_{LT,fi}$ | $k_{0.2p,\theta}$ | $\theta_{crit}$ (°C) | $k_{E,\theta}$ |
|---|---|---|---|---|---|---|
| ***1. Iteration*** | 0.54 | 0.8066 | 0.7114 | 0.4406 | 538.86 | 0.4873 |
| ***2. Iteration*** | 0.428 | 0.719 | 0.7712 | 0.4064 | 553.73 | 0.4442 |
| ***3. Iteration*** | 0.4304 | 0.7207 | 0.77 | 0.407 | **553.5** | 0.445 |

Where the appropriate value of reduction factor $k_{0.2p,\theta}$ is calculated from the following condition:

$$M_{b,fi,t,Rd} = M_{fi,Ed}$$

$$\frac{\chi_{LT,fi} \cdot W_{eff,y} \cdot k_{0.2p,\theta} \cdot f_{yb}}{\gamma_{M,fi}} \frac{1}{\kappa_1 \kappa_2} = 2.11 kNm$$

According to EN 1993-1-2, the value of $\kappa_2 = 0.85$ at the supports of a statically indeterminate beam is taken.

The critical temperature according to *Table 4.4* is

$$\boldsymbol{\theta_{crit} = 553.5}\ °C$$

*II) French national annex of EN 1993-1-2:*

The calculation according to French national annex is given in tabular manner (*Table 5.4*).

*Table 5.4* - Calculation of critical temperature according to French national annex

| | $\bar{\lambda}_{LT,\theta}$ | $\phi_{LT,\theta}$ | $\chi_{LT,fi}$ | $k_{0.2p,\theta}$ | $\theta_{crit}$ (°C) | $k_{E,\theta}$ |
|---|---|---|---|---|---|---|
| ***1. Iteration*** | 0.54 | 0.7036 | 0.8661 | 0.362 | 581.62 | 0.3633 |
| ***2. Iteration*** | 0.4492 | 0.6433 | 0.906 | 0.346 | 588.3 | 0.344 |
| ***3. Iteration*** | 0.4514 | 0.6446 | 0.9052 | 0.3463 | **588.2** | 0.3443 |

As it may be observed from the table, this method indeed gives slightly less conservative results and thus higher critical temperature:

$$\boldsymbol{\theta_{crit} = 588.2\ ℃ \approx 588\ ℃}$$

- **Fire resistance verification:**

The same way as it is presented in the case of the simply supported beam, the thermal response of the steel beam subjected to fire is calculated. Since the same cross section is used (1 mm thick) and the same fire curve, the same the same response is obtained. (*Figure 5.2*)

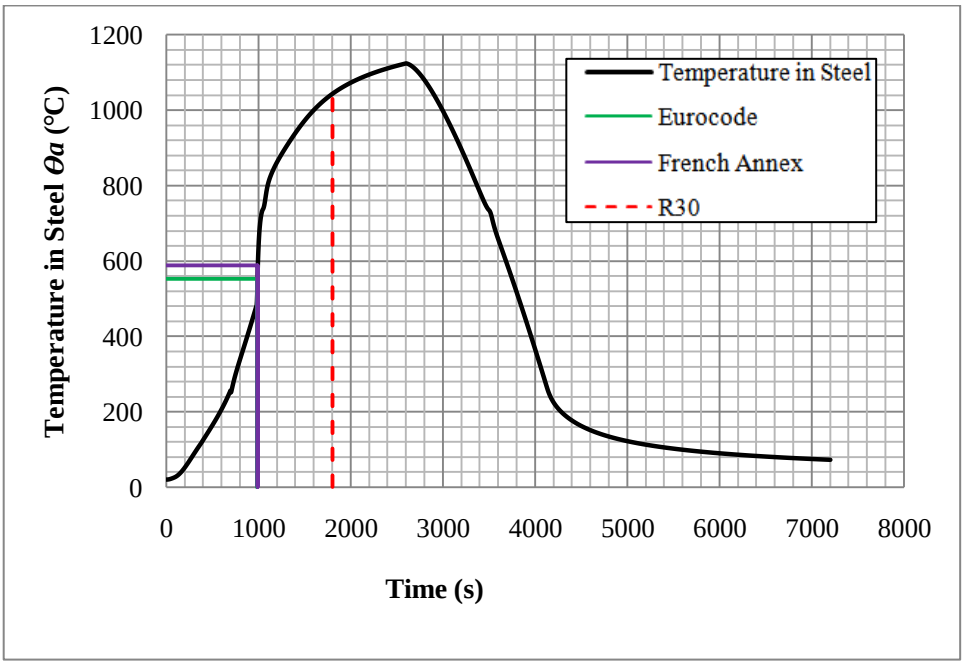


*Figure 5.2* - Thermal response of the Ω160 subjected to fire

The resistance of the purlin is checked and presented also in the *Figure 5.1*, and the following results are obtained:

Eurocode: $t_{fi,d} = 987s = 16.45\ min \leq t_{fi,req} = 30\ min$

French Annex: $t_{fi,d} = 993s = 16.55\ min \leq t_{fi,req} = 30\ min$

In both cases the required fire resistance time is not satisfied, which means that fire protection measures have to be applied and that is presented in the following chapter 5.3.

- **Verification of the shear forces:**

The verification of the shear forces is done according to 4.2.3.3 of EN 1993-1-2 (2004), where the shear resistance of the gross cross-section for normal temperature design is calculated according to EN 1993-1-3 (2004) and it is given in chapter 4.4.1.

-Design shear resistance at room temperature: ($V_{b,Rd}$)

$$V_{b,Rd} = \frac{\frac{h_w}{\sin\phi} \cdot t \cdot f_{bv}}{\gamma_{M0}} = 9.06\ \text{kN}$$

The reduction factor $k_{0.2p,web,\theta}$ is calculated from the following condition:

$$V_{fi,t,Rd} = \mathrm{V}_{fi,Ed,2}$$

$$\frac{k_{0.2p,web,\theta} \cdot V_{b,Rd}}{\gamma_{M,fi}} = \mathrm{V}_{fi,Ed,web} \approx \mathrm{V}_{fi,Ed,2}/2 = 1.055\ \text{kN} \quad \rightarrow \quad k_{0.2p,web,\theta} = 0.1164$$

The corresponding value of the critical temperature is then:

$$\theta_{crit}{}^{(V_{fi,Ed})} = 722.66\ °C \qquad \gg \qquad \theta_{crit}{}^{(M_{fi,Ed})} = 553.5\ °C$$

Since the critical temperature of the web subjected to shear force is significantly higher than the critical temperature of the element subjected to bending ($\theta_{crit}{}^{(V_{fi,Ed})} > \theta_{crit}{}^{(M_{fi,Ed})}$), the required fire resistance time is certainly higher and thus shear forces are not the governing ones for the overall design.

## 5.4 Protected steel beam at elevated temperatures

The procedure for calculation of the resistance of the insulated members is thoroughly the same as for the non-protected and the only possible difference will be shown here.

### 5.4.1 Simply supported beam

- **Calculation of the critical temperature:**

Since it is assumed that all four sides of the purlin are exposed to fire as a safety side strategy, and the static system is determinate, the adaption factors may be taken as:
$\kappa_1 = 1.0$
$\kappa_2 = 1.0$

and thus the critical temperatures have the same values as for the unprotected beam:

Eurocode: $\theta_{crit} = 503.5$ ℃

French Annex: $\theta_{crit} = 549$ ℃

- **Fire resistance verification:**

Calculation of thermal response of the insulated steel member when subjected to fire is done and the distribution of the temperature inside the steel is presented (*Figure 5.3*). The fire curve, which presents the thermal action of fire, is given in chapter 4.3 (*Figure 4.4*), and the thermal response is manually calculated in Excel according to the procedure described in chapter 3.4. For the insulation, intumescent coating is used which thermal properties ($\rho$, $\lambda$, $c$) are given in chapter 3.6. Here is presented only one case in which the coating is 1 mm thick ($d_p$=1 mm).

In the *Figure 5.3*, beside the thermal response of the insulated steel member (continuous line), the thermal response of the member without fire protection is plotted (dashed line). As it may be seen, at the low temperatures (< 400°C), these two responses are almost the same. Then in the range between 400°C and 800°C, the intumescent coating starts to show its effectiveness, which is manifested by response which is scaled and translated rightwards. The reason for this is the particular thermal conductivity that this coating possesses (see *Table 3.6*). In this range, the thermal conductivity of the coating declines significantly, which leads to slower heating of the steel material. However, for the temperatures even higher than 800°C, there is a sudden jump in the thermal conductivity of the coating which results in abrupt change of the slope of the thermal response (both in heating and cooling phase). The information on the thermal conductivity of the coating above 950°C is not provided by the producers Therefore, for extremely high temperatures (> 950°C) the steel responses as though there is no insulation, so the highest temperature is reached at the same moment of time. As this coating is produced to protect steel members, which critical temperatures are usually in the range between 400°C and 800°C, the information on the thermal conductivity of the coating for extremely high

temperatures is not necessary. In the cooling phase, also, around the temperature of 700°C, there is a sudden deviation in the thermal response curve due to the changes in the thermal conductivity of the coating.

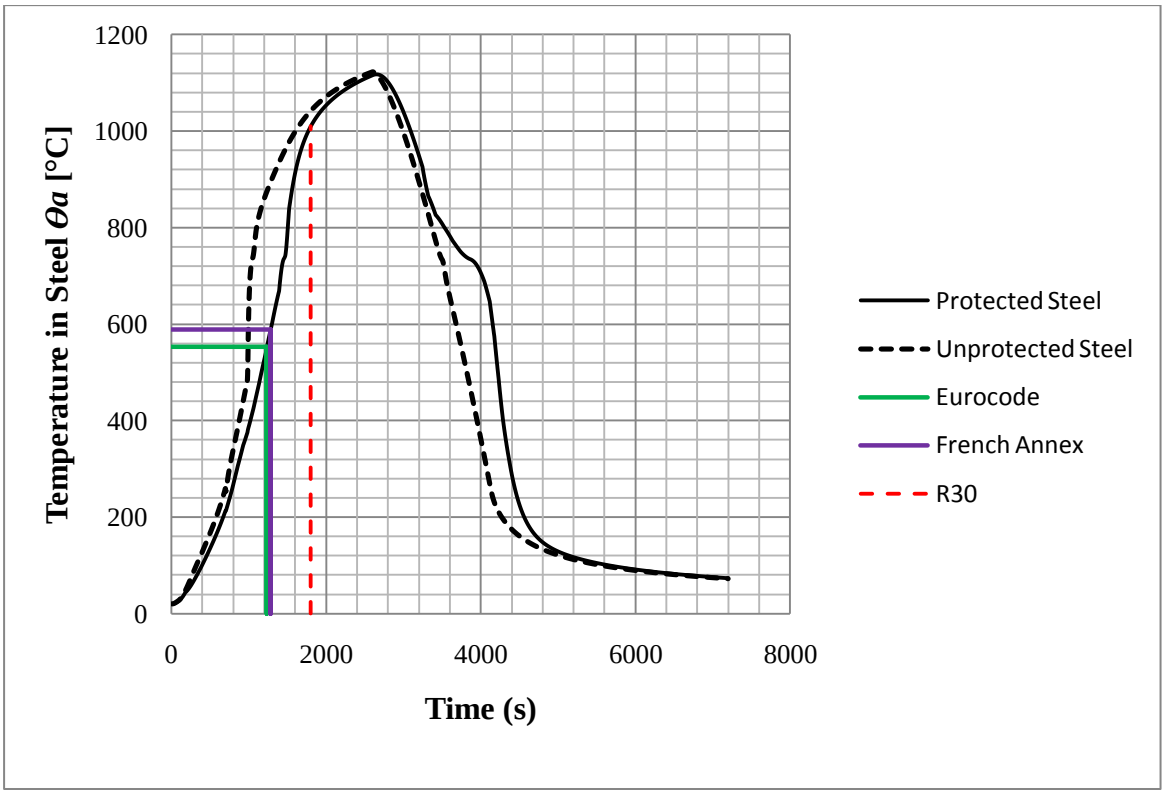


*Figure 5.3* - Thermal response of the insulated Ω160 subjected to fire

Where

- Section factor: $A_p/V = O/A = 1042mm/5.158\,cm^2 = 2020.16\,m^{-1}$

- As the intumescent coating is not a heavy material, it is considered that $\Phi = 0$.

- The thermal conductivity of the fire protection material ($\lambda_p$) depends on the temperature of the fire protection, which is more precisely calculated as an average value of gas temperature $\theta_{g,t}$ and steel temperature $\theta_{a,t}$:

$$\theta_{p,t} = \frac{\theta_{g,t} + \theta_{a,t}}{2}$$

The resistance of the purlin is checked and presented also in the *Figure 5.3*, and the following results are obtained:

Eurocode: $t_{fi,d} = 1166s = 19.43\,min \leq t_{fi,req} = 30\,min$

French Annex: $t_{fi,d} = 1230s = 20.5\,min \leq t_{fi,req} = 30\,min$

In both cases the required fire resistance time is not satisfied, which means that fire protection of 1mm is not enough to provide desired resistance. However, the increase in thickness of the coating above 1 mm is not recommended as it would lead to rather uneconomical solutions, so some other changes have to be done. For that reason it is more likely to expect better results if the thickness of the steel section is increased instead of this expensive insulating coating. Those two parameters (thickness of the coating ($d_p$), thickness of the steel ($t$)) are therefore studied until the optimal economical solution is found, and the results will be presented in the section 5.5, where all the results are given and compared.

### 5.4.2 Continuous beam

- **Calculation of the critical temperature:**

Since it is assumed that all four sides of the purlin are exposed to fire as a safety side strategy, and the static system is indeterminate, the adaption factors are taken as

$\kappa_1 = 1.0$

$\kappa_2 = 0.85$

and thus the critical temperatures have the same values as for the unprotected beam:

Eurocode: $\theta_{crit} = 553.5℃$

French Annex: $\theta_{crit} = 588.5℃$

- **Fire resistance verification:**

Calculation of thermal response of the insulated steel member when subjected to fire is done and the distribution of the temperature inside the steel is presented (*Figure 5.4*). Here is presented only one case in which the coating is 1mm thick ($d_p$ = 1 mm). All parameters needed for calculation of heat transfer are the same as for protected simple supported beam, so the thermal response is completely the same.

The resistance of the continuous purlin is checked and presented also in the *Figure 5.4*, and the following results are obtained:

Eurocode: $t_{fi,d} = 1234s = 20.6min \leq t_{fi,req} = 30\ min$

French Annex: $t_{fi,d} = 1280s = 21.33min \leq t_{fi,req} = 30\ min$

In both cases the required fire resistance time is not satisfied, which means that fire protection of 1 mm is not enough to provide desired resistance. Also in this case, two parameters (thickness of the coating ($d_p$), thickness of the steel ($t$)) are therefore varied until the optimal economical solution is found (section 5.5).

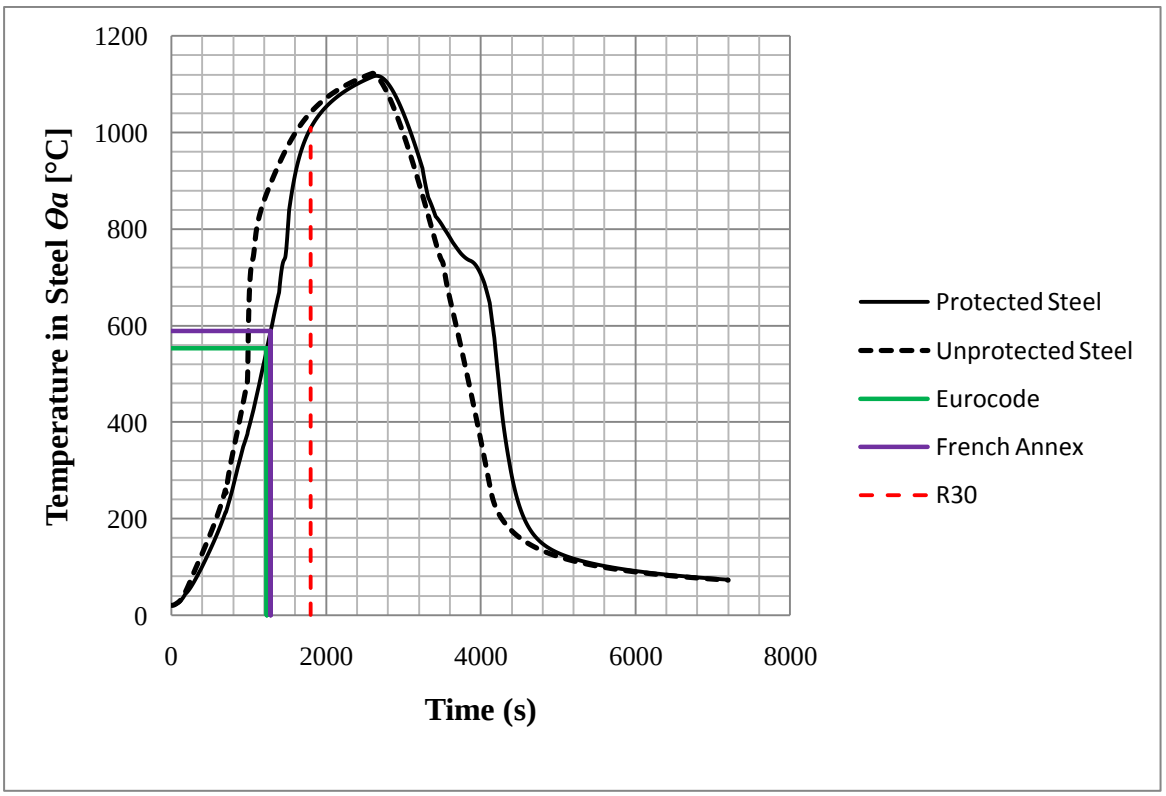


*Figure 5.4* - Thermal response of the insulated continuous beam subjected to fire

## 5.5 Comparison and discussion of the analytical results

In this section are presented the analytical results of simply supported and continuous beams both at ambient and elevated temperatures, where the thickness of steel and insulation coating are varied. The analytical results for one case ($t$ = 1 mm and $d_p$ = 1 mm) are calculated in detail in chapters 5.2, 5.3 and 5.4, while for the other cases only the final results are shown in this section. First, the values of the critical temperatures are provided in Table 5.5 and Table 5.6.

As it can be seen, the critical temperatures are slightly higher in case of continuous beams than in a case of simply supported beams, whereas in both cases French Annex provides higher results in comparison with the values obtained by EN 1993-1-2 (2004). Another interesting conclusion is that the critical temperatures vary between 500°C and 700°C, which is considerably higher than 350°C as it is recommended in the Eurocode.

*Table 5.5*- Critical temperatures of steel for simply supported beams

| | **Critical temperature (°C)** | |
|---|---|---|
| $t_{steel}$ (mm) | *Eurocode* | *French Annex* |
| 1.0 | 503.5 | 549 |
| 2.0 | 635.6 | 668 |
| 2.4 | 662 | 690 |

*Table 5.6*- Critical temperatures of steel for continuous beams

| | **Critical temperature (°C)** | |
|---|---|---|
| $t_{steel}$ (mm) | *Eurocode* | *French Annex* |
| 1.0 | 553.5 | 588 |
| 1.6 | 639 | 669 |
| 1.8 | 655 | 682 |
| 2.0 | 668 | 695 |
| 2.4 | 686 | 722.5 |

Furtermore, the measured resistances are presented (Table 5.7 and Table 5.8). For the ambient temperatures the design buckling moment resistance and design shear resistance are given, while for the elevated temperatures the resistance of the purlin measured in time is shown.

*Table 5.7* - Analytical results of simply supported beam for Ω160 cross-section

| | | | | **Elevated Temperature** | | | |
|---|---|---|---|---|---|---|---|
| | | | | **Unprotected Steel Member** | | **Insulated Steel Member** | |
| | | **Ambient Temperature** | | *Eurocode* | *French Annex* | *Eurocode* | *French Annex* |
| $t_{steel}$ *[mm]* | $d_p$ *[mm]* | $M_{b,Rd}$ *[kNm]* | $V_{b,Rd}$ *[kN]* | $t_{fi,d}$ *[min]* | $t_{fi,d}$ *[min]* | $t_{fi,d}$ *[min]* | $t_{fi,d}$ *[min]* |
| **1.0** | **1.0** | 4.77 | 9.06 | 16.35 | 16.45 | 19.43 | 20.5 |
| **2.0** | **1.0** | 10.435 | 45.5 | 16.92 | 17.1 | 26.55 | 27.0 |
| **2.4** | **0.75** | 12.82 | 61.2 | 17.16 | 17.42 | 26.16 | 26.58 |
| **2.4** | **0.8** | 12.82 | 61.2 | 17.16 | 17.42 | 26.6 | 27.05 |
| **2.4** | **1.0** | 12.82 | 61.2 | 17.16 | 17.42 | 28.3 | 28.7 |

*Table 5.8* - Analytical results of continuous beam for Ω160 cross-section

| | | | | **Elevated Temperature** | | | |
|---|---|---|---|---|---|---|---|
| | | | | **Unprotected Steel Member** | | **Insulated Steel Member** | |
| | | **Ambient Temperature** | | *Eurocode* | *French Annex* | *Eurocode* | *French Annex* |
| $t_{steel}$ *[mm]* | $d_p$ *[mm]* | $M_{b,Rd}$ *[kNm]* | $V_{b,Rd}$ *[kN]* | $t_{fi,d}$ *[min]* | $t_{fi,d}$ *[min]* | $t_{fi,d}$ *[min]* | $t_{fi,d}$ *[min]* |
| **1.0** | **1.0** | 5.18 | 9.06 | 16.45 | 16.55 | 20.57 | 21.33 |
| **1.6** | **1.0** | 8.91 | 29.26 | 16.8 | 16.96 | 25.15 | 25.52 |
| **1.8** | **1.0** | 10.07 | 36.93 | 16.95 | 17.2 | 26.1 | 26.5 |
| **2.0** | **1.0** | 11.23 | 45.5 | 17.1 | 17.3 | 27.0 | 27.42 |
| **2.4** | **0.5** | 13.49 | 61.2 | 17.42 | 17.75 | 24.16 | 24.66 |
| **2.4** | **1.0** | 13.49 | 61.2 | 17.42 | 17.75 | 28.66 | 29.1 |

As it may be observed, even with the maximum thickness of the steel and coating, the fire resistance of 30 minutes by analytical approach can not be achieved. In case of continuous beam, however, slightly higher resistance is reached than in the case of simply supported beam.

# 6 NUMERICAL ANALYSIS

## 6.1 Introduction

As it is already stated, the program ABAQUS (ABAQUS, 2014) based on the finite element method is used for numerical analysis. Being one of the most commonly used software in the academic research of material and geometric nonlinear analysis, it offers to user a wide range of materials models, and an extensive database of various elements that can model practically any desired geometry in a rather simple way, using interactive graphical interface. Beside structural (stress-displacement) problems, which are probably the most commonly analyzed, this simulation tool also allows user to study different problems such as heat transfer, which is necessary for analyzing of elements exposed to elevated temperatures. Therefore this powerful software is used also in this thesis for analysis on the structural behaviour of cold-formed steel beams subjected to fire.

In this chapter are explained into details all the steps and techniques used in 3D nonlinear finite element model of cold-formed purlins, with particular reference to some general issues in creating the model such as – element type, mesh size, load increment, material stress-strain curve model, magnitude and type of geometrical imperfections etc. The numerical results are later compared with ones obtained by analytical results.

## 6.2 Description of the thermal and mechanical analysis

Thermal response of the structure may be time dependant (“transient”) and non-dependant (“steady-state”). Transient thermal response considers that external heat fluxes and boundary conditions do not remain constant in time, usually with considerable initial temperature variations, while in a long run those changes may be neglected and therefore transient response turns into a steady-state. Since fire conditions highly depend on time, the structures subjected to fire normally show transient response, and thus also in this application transient analysis will be done in Abaqus.

Generally, there are two ways through which the thermal response of a structure can be studied in Abaqus: (ABAQUS Analysis - User’s Manual, version 6.14-1)

- Uncoupled thermal response (pure heat transfer analysis)
- Coupled response (thermal-stress analysis)
  a) Sequentially coupled
  b) Fully coupled

Since the gravity and imposed load, as well as second order effects do not affect crucially the thermal resistance of steel beams, and thus the temperature distribution in steel sections, it is allowed to perform so-called sequentially coupled thermal-stress analysis instead of fully coupled in which possible effect of the displacements over the temperature evolution in fire may not be neglected. This is a great convenience since the fully coupled analysis requires exquisitely powerful computer station and even then the computation time can be enormously long. On the other hand, the sequentially coupled thermal-stress analysis is simplified method which actually consists of two steps:

***1) Thermal Analysis*** – in which temperature distribution (temperature field) inside the structural members is separately obtained, without taking into consideration effects of mechanical load. For this purpose *Transient Heat Transfer Analysis* was used in Abaqus software. In this analysis the basic variable (degree of freedom) at the nodes of the elements is a scalar quantity temperature which is in Abaqus denoted by the degree of freedom 11 and is presented as nodal output variable NT11.

***2) Structural analysis*** –in which the response of the structure is calculated, when subjected to both static (mechanical) loading and thermal loads that have been previously obtained in the first step as temperature field in time domain. For this analysis it is possible to use several procedure types in Abaqus depending on the considered study case and material, such as Abaqus/Standard's general static, visco, Riks or even the dynamic implicit procedure (quasi-static). In this thesis, the *General Static* procedure type is used as it is proven to give convergent solution (Mago *et al*, 2014). The nonlinear geometric parameter (*NLGEOM=ON) was also set to account for geometrical imperfections and this way geometric nonlinear analysis is performed. In order to obtain geometrical imperfections needed for geometrical nonlinear static analysis, first the elastic buckling (eingenvalue) analysis was performed. This analysis (*Linear perturbation, Buckle*) as a result gives buckling modes which shapes are used as an input to geometric nonlinear analysis. The exact and detailed definition of geometric imperfections will be explained in the following chapter, where structural model is described.

For each of these two analysis a separate model was made (thermal and structural), and all the parameters and assumptions that have been used for modelling each of them will be explained into details in the following chapter.

## 6.3 Definition of the numerical models

In this chapter will be described both models used for the sequentially coupled thermal-stress analysis. The geometry of the analyzed trapezoidal Omega 160 purlins are the same in both models and the shape and the dimensions are already presented in the section

4.4.1 (*Figure 4.5*). Two different static schemes are analyzed as it is already stated in section 5.1.

### 6.3.1 Thermal model

In this research steel purlins are analyzed both unprotected and insulated by fire protection coating. The thermal response of the steel element is normally changed when protection is added. Here will be explained also all the additions in modelling of the fire protection.

- ***Material Modelling*:**

1) Unprotected steel:

For the heat transfer analysis there are three relevant thermal properties of steel - density, thermal conductivity and specific heat. The thermal conductivity ($\lambda$) and specific heat ($c$) are temperature dependant properties which are modelled according to relevant standard (EN 1993-1-2, 2004), or here chapter 3.3.4.

2) Insulated steel:

For the insulation, the intumescent coating is used and it is applied around the whole cross section, on every possible surface of the purlin (*Figure 6.1*). The thermal properties of the applied coating are provided in chapter 3.6, and the thickness of the coating is varied in the range between 0.5 mm and 1 mm, which is recommended by the producers to be the maximum thickness of the coating in order to meet the economical solution.

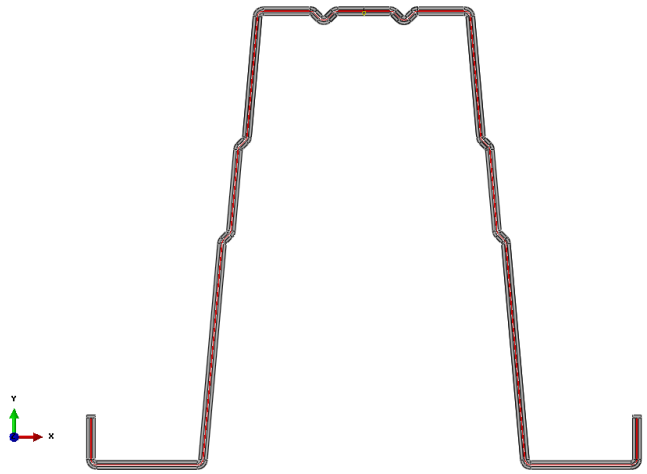

*Figure 6.1* - Application of insulation coating around the steel profile

**- *Loads and Boundary Conditions*:**

Heat transfer is a complex process in which thermal energy of two physical systems is exchanged through one or combination of three basic mechanisms: convection, radiation and conduction (diffusion). To understand how the thermal load and thermal boundary conditions are applied in Abaqus here will be briefly explained each of these three mechanisms.

***1) Conduction***: This mechanism considers heat transfer within an object or between two objects that are in contact, and it is described through Fourier's law (Eq. 6.1), where the rate of transferred heat (heat flux) depends on the temperature difference and thermal conductivity of the material ($\lambda$), which is temperature dependant.

$$\dot{Q} = -\lambda \frac{dT}{dx} \tag{6.1}$$

***2) Convection***: In this process the heat is transferred over the surface of the element by movements of heated gases or liquids. The convective part of the heat flux to the surface depends on the difference between the gas temperature ($\theta_g$) near the element subjected to fire and the temperature of the element ($\theta_m$), and the film conditions on the surface which is taken into account through so-called film coefficient of convection $\alpha_c$ (Eq. 6.2). This coefficient depends on the fire curve that is used (standard, parametric, natural, etc) and on the situation of the surface, whether the surface is directly exposed to fire on it is unexposed. (Franssen, 2010).

$$\dot{h}_{net,c} = \alpha_c \cdot \left(\theta_{g,t} - \theta_{m,t}\right) \tag{6.2}$$

In this case, it is assumed that in the fire condition all the surfaces of the purlin are thoroughly exposed to fire, so the only considered value of the film coefficient is 35 W/m$^2$K (clause 3.3.2 of EN 1991-1-2 (2002)), which is safety-side assumption.

***3) Radiation***: Unlike the conduction and convection, this mechanism does not necessarily require medium, as the thermal energy is actually transferred by electromagnetic waves. This mechanism is taken into account by the other component of the heat flux (radiative heat flux), which beside temperatures of the gas and material, depend also on the thermal emissivity of the surface. In this case it is taken the value of 0,8 for thermal emissivity of the surface both for cold-formed steel and intumescent coating. Beside this, it is necessary in the Abaqus (*Model Attributes*) to define Stephan Boltzmann constant as 5,67x10$^{-8}$ W/m$^2$K$^4$, as well as absolute zero temperature which is applied as -273 K.

There are several types of the thermal boundary conditions in Abaqus (ABAQUS, 2014):

- Prescribed temperatures
- Prescribed fluxes
- Film conditions
- Radiation conditions
- Natural boundary condition (default)

Prescribed temperatures are commonly used when the temperature of a surface is known. In this case, the temperature evolution in time is obtained from OZone program (Cadorin and Franssen, 2001), and this fire curve is used in Abaqus to vary the magnitude of the temperature with step time by means of "amplitude curves".

The thermal load which in heat transfer analysis refers to convection and radiation (convective and radiative heat flux) is in Abaqus applied as *Interaction* between gas temperature and surface of the element and not explicitly as for any other mechanical *Load*. To do so, it is necessary first to define *Interaction properties* of the film condition for convection. As it is already noted, it is assumed that under fire condition all surfaces of the element are uniformly exposed to both radiation and convection.

For the steel purlins protected by intumescent coating it is necessary to model in Abaqus thermal contact between the surfaces of insulation and steel to allow heat flow across contact surfaces. The exact thermal contact properties (gap conductance) are not explicitly given in relevant standards. However, Abaqus allows definition of the thermal contact as a function of clearance, regardless of real existence of clearance. To do so, it is necessary to specify at least two data lines. When gap conductance is defined as a function of clearance, the value of the conductance drops to zero immediately after the last data point; therefore, there is no heat conductance when the clearance is greater than the value corresponding to the last data point, which makes the thermal conductance practically independent from the distance between the closely positioned surfaces. In this case, the thermal conductance is specified as (Table 6.1):

*Table 6.1* - Definition of thermal contact as a function of clearance

| **Conductance** | **Clearance** |
|---|---|
| 50 | 0 |
| 0 | 0.01 |

**- *Finite Element Type*:**

Abaqus has an extensive heat transfer element library (ABAQUS, 2014):

- Continuum solid elements (1D, 2D, Axisymmetric and 3D heat trasfer elements)
  - First order interpolation
  - Second order interpolation
- Conventional shell elements
- Point elements

In this case, the solid element (DC3D8) is chosen for modelling both the steel purlins, and insulation material, which denotes an 8-node heat transfer brick element with first-order (linear) interpolation (*Figure 6.2*). By using this element it is aimed to obtain more accurate and realistic results with a clear picture of the temperature distribution within the cross section due to heat transfer in particular.

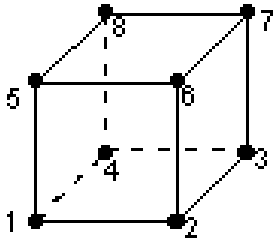


*Figure 6.2* - Scheme of the DC3D8 element (ABAQUS, 2014)

**- *Finite Element Mesh*:**

The finite element size may have a huge impact on the behavior of cold-formed beams, and thus a parametric study was first performed in order to analyze the sensitivity of the mesh density. For heat transfer analysis, beside the finite element size along the beam (a and b dimensions) it is also important to analyze the third "through-thickness" dimension (c), because otherwise the distribution of temperature would be considered uniform along the thickness of the steel cross-section which is not the case in reality, despite the small thickness of the cold-formed profiles. This can affect the structural response of the purlins as the temperature of each node of the element (NT11 output variable) obtained in thermal model is then applied to the nodes of the structural model, and the inner parts of the section having the lower values of the temperature may contribute to higher overall capacity of the purlin.

For this reason, firstly, three different meshes are analyzed - 5 x 5 mm, 10 x 10 mm and 20 x 20 mm (*Figure 6.3*) considering only one element through the thickness, and then

for the adopted solution another study is done on the number of elements through the thickness. For this study, three solutions are compared, with two, three and four elements through the thickness (*Figure 6.4*), which is recommended for the solid elements in ABAQUS Analysis - User's Manual, 6.14-1.

In Figure 6.3, the temperature distribution in time is presented for three studied sizes of meshes, measured in the same point (middle of the span) of the purlin.

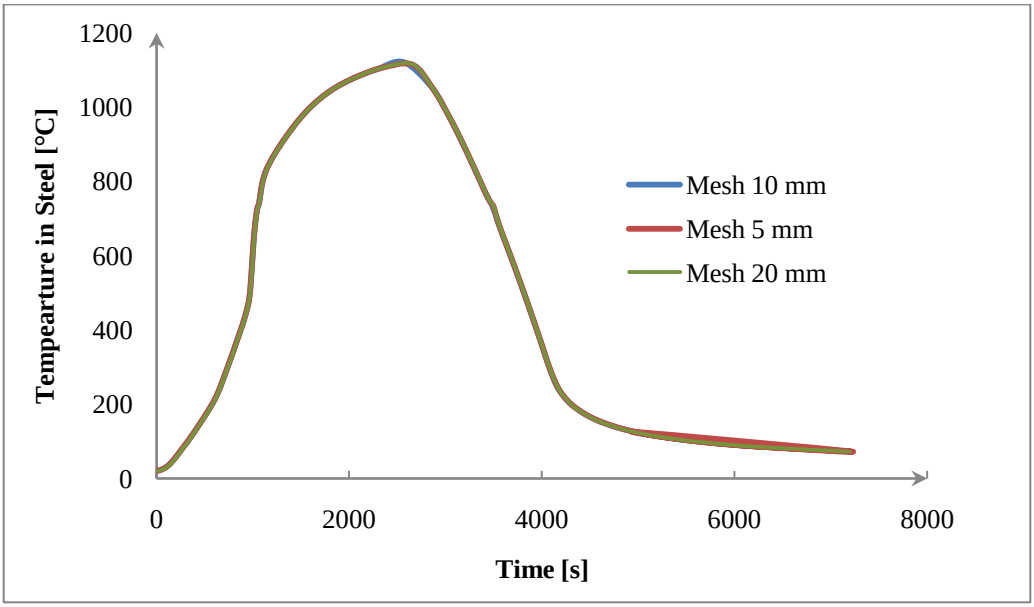


*Figure 6.3* - Influence of the mesh size on the thermal response

In Figure 6.4, in order to understand the influence of the number of the elements through the steel cross-section, it is presented the distribution of the temperature through the steel thickness measured in the top flange at the same moment of time, for instance, 1100 seconds after the ignition of fire. Expectedly, the more elements there are the more refined temperature distribution is obtained. However, the difference is almost imperceptible in case of non-massive cold-formed profiles.

Taking everything into consideration, in a case of the thin-gauge profiles, the temperature distribution is practically the same, regardless of the mesh size and the number of the finite elements through the thickness. However, in the stress-strain analysis, these variations play an important role and the decision on the size of the mesh will be made only after the mechanical analysis is done.

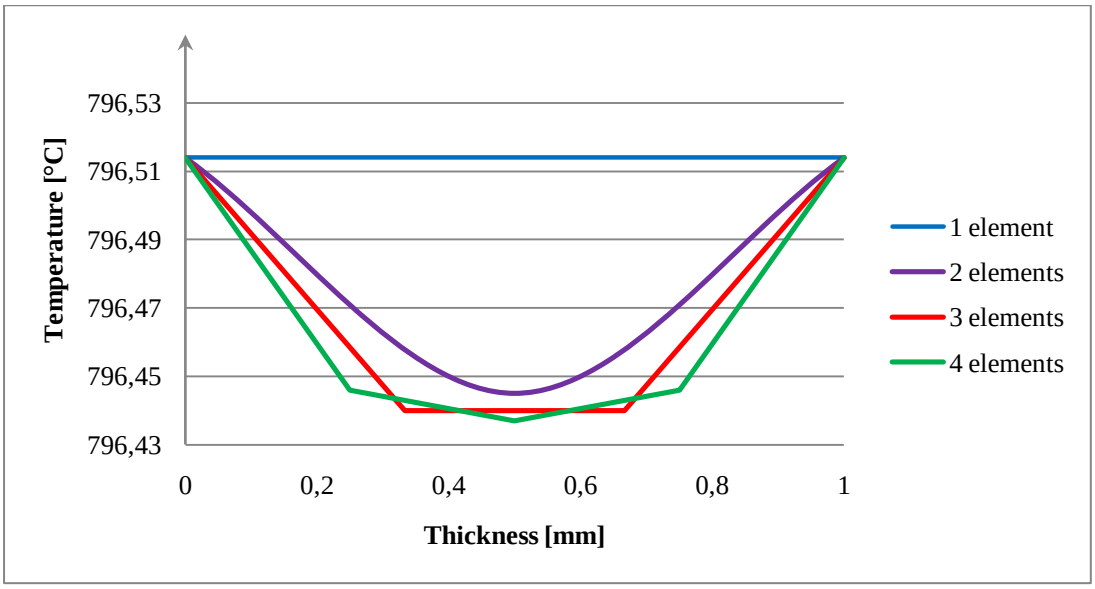


*Figure 6.4* - Influence of the number of finite elements through the thickness on the thermal response

### 6.3.2 Mechanical model

- ***Material Modelling*:**

1) Ambient temperature: ($t$ = 20 °C)

At the ambient temperature, the material behaviour of cold-formed profiles is modelled by multi-linear stress-strain curve in an attempt to account for the gradual yielding behaviour followed by a significant period of strain hardening, which occurs due to cold-forming process. Due to the lack of experimental results of the tensile test on steel grade S280GD+Z, the nominal values for yielding strength, tensile strength and Young's modulus are used, which are prescribed in Table 3.1b of the EN 1993-1-3 (2004) as $f_{yb} = 280\ \mathrm{N/mm^2}$, $f_u = 360\ \mathrm{N/mm^2}$ and $E = 210\ \mathrm{GPa}$. The stress-strain curve for cold-formed profiles which is used in the numerical model is shown below (*Figure 6.5*).

The initial slope of the curve is defined by the Young's elastic modulus ($E$), while the second, third and fourth slope is described by tangent modulus which have the values of $E_1$=*38% E*, $E_2$=*10% E* and $E_3$=*0,5% E*. This way gradual yielding is achieved by bilinear approximation with $E_1$ tangent modulus in the range between 70% and 87,5% of $f_{yb}$, and $E_2$ in the range between 87,5% and 100% of yielding strength. However, these stress-strain curves are given as engineering input, and should be converted into true stress-strain curves (see *Figure 6.5*), using the Equations 6.3 and 6.4 which are given in the Annex C of the EN 1993-1-5 (2006).

$$\sigma_{true} = \sigma_{nom} \cdot (1 + \varepsilon_{nom}) \quad (6.3)$$

$$\varepsilon_{true} = \ln(1 + \varepsilon_{nom}) \quad (6.4)$$

Where $\sigma_{true}$ and $\varepsilon_{true}$ are true values of stress and strain, while $\sigma_{nom}$ and $\varepsilon_{nom}$ are the nominal values.

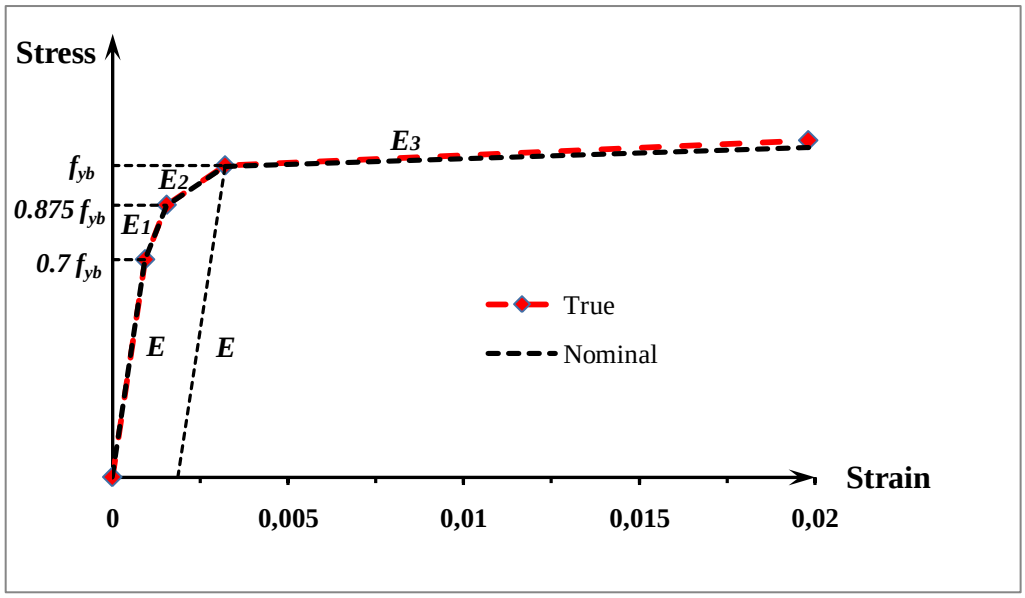


*Figure 6.5* - Stress-strain relationship of the cold-formed profile at ambient temperature

All the values needed for the definition of the stress-strain curve for steel S280GD+Z in Abaqus are provided below (*Table 6.2*). The true stain values ($\varepsilon_{true}$) have to be additionally converted into plastic strains ($\varepsilon_{pl}$) by Equation 6.5, and these values are used as input in Abaqus (ABAQUS, 2014).

$$\varepsilon_{pl} = \varepsilon_{true} - \frac{\sigma_{true}}{E} \quad (6.5)$$

Where E presents the Young's module of elasticity ($E$ =210 GPa).

*Table 6.2* - Properties of steel S280GD+Z at the ambient temperature applied in Abaqus

| Points | E (MPa) | $\sigma_{nom}$ (MPa) | $\varepsilon_{nom}$ | $\sigma_{true}$ (MPa) | $\varepsilon_{true}$ | $\varepsilon_{pl}$ |
|---|---|---|---|---|---|---|
| **1** | 210000 | 196 | 0.000933 | 196.18 | 0.0009328 | 0 |
| **2** | 79800 | 245 | 0.001547 | 245.38 | 0.0015461 | 0.000378 |
| **3** | 21000 | 280 | 0.003214 | 280.9 | 0.0032088 | 0.0018713 |
| **4** | 1050 | 297.63 | 0.02 | 303.58 | 0.0198026 | 0.018357 |

2) Elevated temperatures:

Mechanical properties of the steel (Young's modulus, thermal expansion, metal plasticity) that are temperature dependent are modelled in Abaqus as material properties according to EN 1993-1-2 (2004), or here chapters 3.3.1, 3.3.2 and 3.3.3. Also at the elevated temperatures the stress-strain curves are given as engineering values, and thus the same conversion has to be done using the Equations 6.3 to 6.5.

The Poisson's coefficient is taken as $v$ = 0.3, and it is considered as temperature non-dependant (Kaitila, 2002b).

**- *Loads and Boundary Conditions*:**

In the structural model, unlike in the thermal, the mechanical boundary conditions and loading is applied, in such a way to try to imitate the real situation.

1) Boundary conditions:

In the case of simply supported beam (5.0 m long) one end is supported by so-called double support, where displacements are restrained in longitudinal, vertical and horizontal directions (in Abaqus U1, U2 and U3), whereas the other end is supported by simply support in which only the vertical displacement (U2) and the displacement perpendicular to the plane of the purlin (U1) are restrained. In the case of continuous beam, the simple supports are used in the both ends of the beam, while the double support is placed in the middle of the span (at the distance of 5.0 m from the end of the beam). In order to take into account the fact that purlins require an area on the bottom flanges to be fastened by screws to the rafters, these boundary conditions are applied on a correspondent area which is taken from previous studies (Gonçalo, 2014). This area has a length of 75 mm in the longitudinal direction of purlin and a width which depends on the width of the bottom chord of studied Omega 160 profile (*Figure 6.6*).

2) Loading:

The coupled thermal-stress analysis, which is conducted here, requires two steps in Abaqus. In the first step, the mechanical loading is applied to the purlin and in the second step the temperature field obtained from the thermal model is placed in the structural model. This way the simulation of reality is achieved, as the beam before fire appears was exposed only to the uniform mechanical load, and then fire occurs which affect the structural behaviour of the purlin as the material properties are reduced.

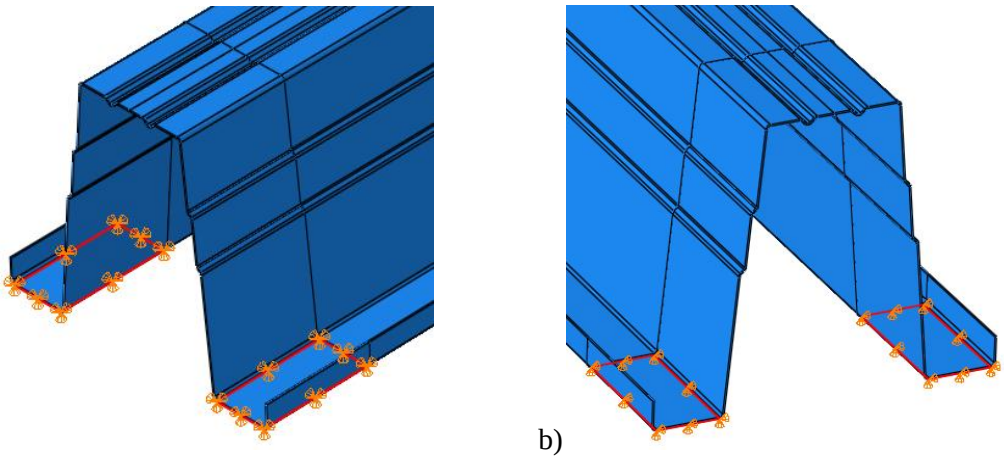

a) b)

*Figure 6.6* - Boundary conditions used in the model a) double support and b) simple support

The mechanical load is uniform and it acts on the top flange of the purlin (*Figure 6.7*). The magnitude of the linear load is obtained from the accidental design situation, according to the EN 1991 (2002) (here chapter 4.3.3), which is then distributed on the top flange of the purlin as a pressure load.

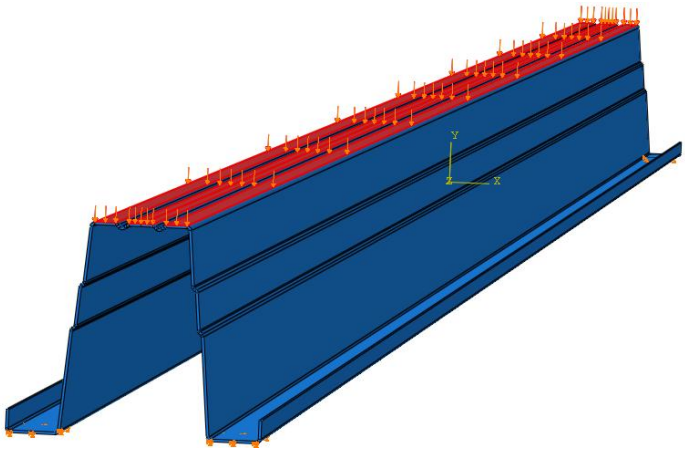

*Figure 6.7* - Mechanical load acting on the purlin at the moment of fire

- ***Finite Element Type*:**

For structural (stress-strain) analysis the solid element (C3D8R) is chosen. This denotation stands for a three-dimensional (3D), continuum (C), hexahedral and an eight-node brick element with reduced integration (R), hourglass control and first-order (linear) interpolation (*Figure 6.8*). This type of finite element has three degrees of freedom in each node - translations in X, Y and Z direction of global coordinate system.

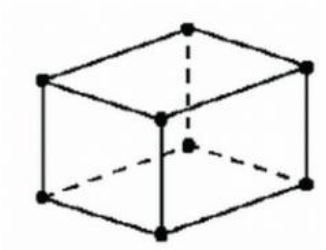

*Figure 6.8* - Scheme of the C3D8R element (ABAQUS Analysis - User's Manual, 6.14-1)

**- *Finite Element Mesh*:**

As it is already explained in the model for the thermal analysis (chapter 6.3.1), the size of the mesh may have significant impact on the response of the beam and overall resistance. Although it is possible to have different size of the mesh in the thermal and structural model, in this case the same parametric study on the sensitivity of the mesh size is done as for the thermal analysis model. So, again, three different mashes are analyzed first (5 x 5 mm, 10 x 10 mm and 20 x 20 mm), and for the adopted mesh size, another set of analyses are performed with two, three and four elements through the thickness (*Figure 6.9 and 6.10*). In these graphs are plotted the displacements against the time obtained in Abaqus for a purlin 1 mm thick, where the displacement is measured in the middle of the beam. It may be seen that the size of the mesh plays a certain role in the final results (*Figure 6.9*). The bigger mesh (20 mm) gives lower magnitudes of the displacements comparing to mash size of 10 mm and 5 mm, which may lead to unsafe results, giving the resistant time of the beam of 1034 seconds. On the other hand, the difference between the mesh size of 10 mm and 5 mm is negligible, with resistant times of 1008 and 998 seconds, respectively ($\Delta < 1.0$ %). For this reason, the adopted size of the elements is 10 mm, which provides at the same time enough fast and accurate computation. Also the number of elements through the thickness showed a huge impact on the overall results (*Figure 6.10*). The more refined the mesh is, the resistance of the beam is increased and this positive effect has to be taken into account, although the computation time is also considerably increased with more finite elements. However, the difference in results between the case with three and four elements through the thickness (1036 s and 1040 s) is practically negligible (0.4 %). Therefore, the final solution is to have a mesh with three elements through the thickness of steel. For the insulated members, it is adopted to have two elements through the thickness of insulation. The reason for this is that the insulation plays only important role in the heat transfer analysis, whereas in the thermal analysis it is completely omitted from model as it does not participate in mechanical resistance of the puriln.

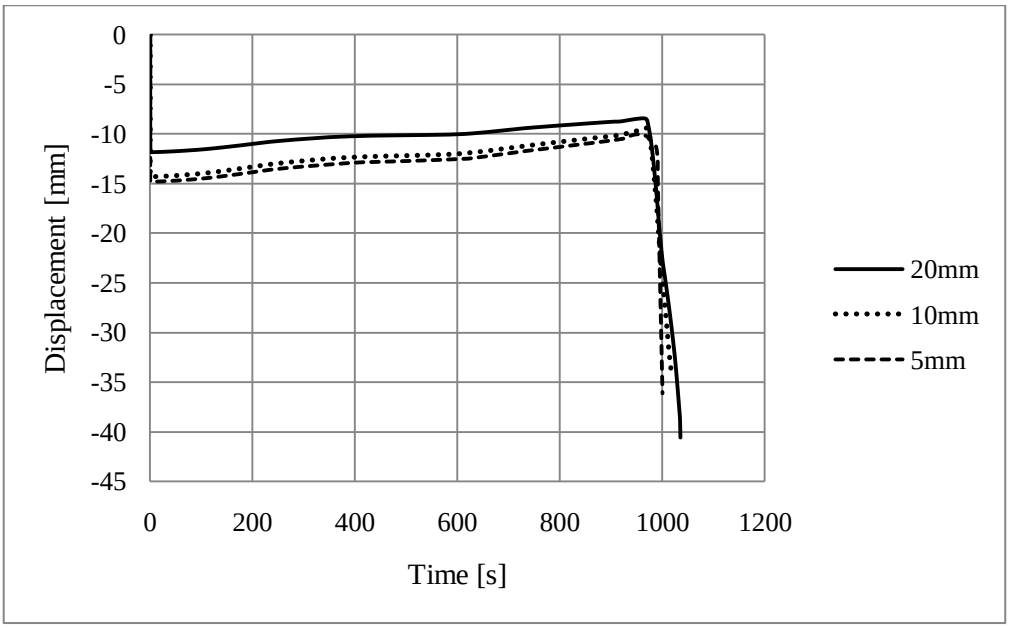


*Figure 6.9* - The influence of the finite element size on the behavior of the purlin under fire

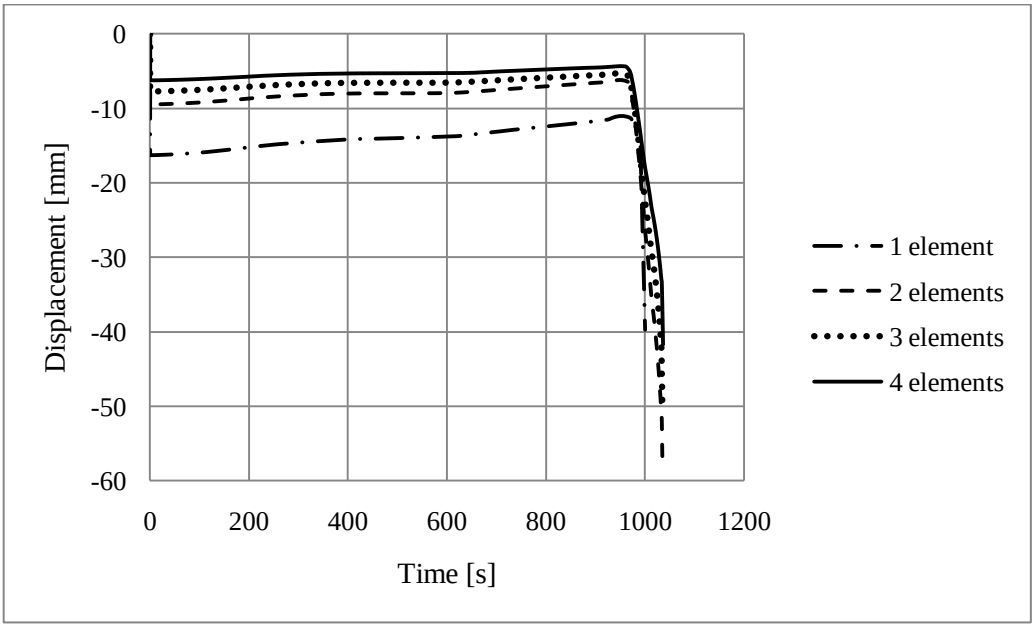


*Figure 6.10* - The influence of the number of finite elements through the thickness of the cross section on the behavior of the purlin under fire

The similar study is performed for the continuous beam, where due to the increased number of elements the examined finite element sizes are 10 x 10 mm, 15 x 15 mm and 20 x 20 mm. The final solution is to use the same mesh size of 10 mm with 3 finite elements through the thickness, whereas for the insulation also 10 mm mesh is used with 2 elements through the thickness (for the same reasons as it is explained for the simply supported beam).

Finally, in the Figure 6.11 and 6.12 is presented the model with the finite element mesh used for the Omega 160 purlin.

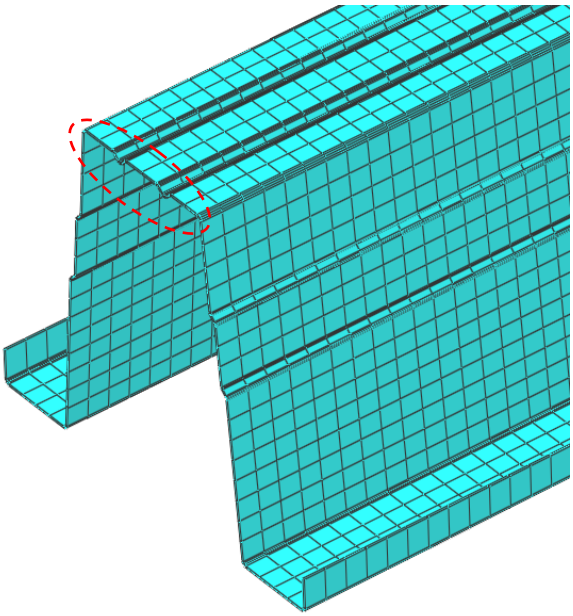

*Figure 6.11*- Finite element mesh used for the numerical model

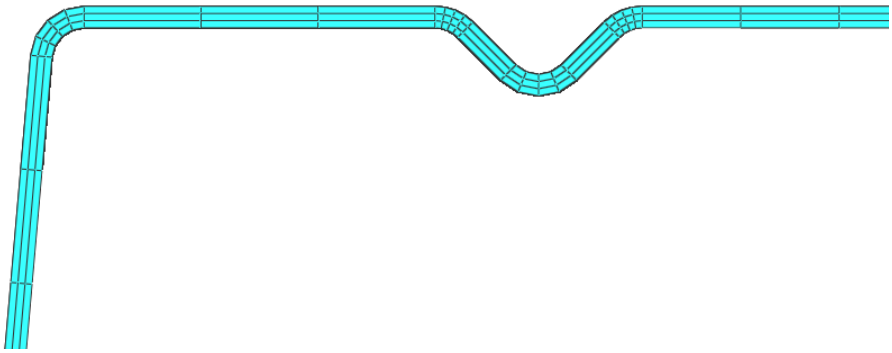

*Figure 6.12*- Finite element mesh through the thickness used for the numerical model

- ***Geometric Imperfections*:**

The influence of geometric imperfections and residual stresses has only recently started to receive more attention (Arrais, 2012; Laim, 2013), and it is proven that it might have a considerable impact on the on the ultimate load bearing capacity of CFS beams under fire conditions.

According to Annex C of EN 1993-1-5 (2006), geometric imperfections may be modelled in FE model as the shapes of the critical plate buckling modes with amplitudes provided in the Table C.2 of the same Annex, which are for this particular study case given in the Table 6.3. Eurocode distinguishes two types of the geometric imperfections – global and

local. The global imperfections are defined as bow imperfections with a sinusoidal shape having the amplitude of $L/1000$, where $L$ is the length of the beam (*Figure 6.13a*). The local imperfections, however, are defined by the buckling shape (eigenmodes) obtained from elastic buckling analysis, having the amplitude of $b/200$, where $b$ stands for the width of the analyzed plate (*Figure 6.13b*). It is important to say that the term "local" refers to both local and distortional buckling modes.

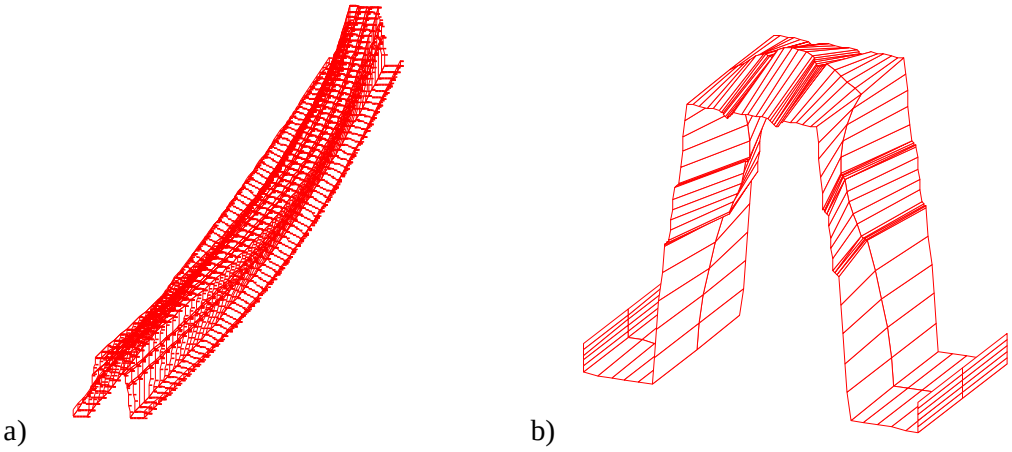

a) b)

*Figure 6.13* - Geometric imperfections of Omega 160 profile (CUFSM): a) global and b) local

Annex C of EN 1993-1-5 also recommends 80% of geometric fabrication tolerances, which leads to 20% reduction of geometric initial imperfections (Eq. 6.6 and 6.7):

$$\delta_{global} = 0.8 \cdot \frac{L}{1000} \tag{6.6}$$

$$\delta_{local} = 0.8 \cdot \frac{b}{200} \tag{6.7}$$

*Table 6.3* - Amplitudes of the geometric imperfections (EN 1993-1-5, Annex C)

| | **Global [*mm*]** | **Local [*mm*]** |
|---|---|---|
| *Simply supported beam* | 4.0 | 0.64 |
| *Continuous beam* | 8.0 | 0.64 |

Where the length of the simply supported beam is 5 m, and of the continuous beam is 10 m, in total, and the height of the web of the purlin is $b$ = 160 mm.

Also, according to EN 1993-1-5 (2006), these geometric imperfections should be combined in the numerical model. In the Annex C of the same Eurocode it is stated that in combining imperfections, a leading imperfection should be chosen and the accompanying imperfections may have their value reduced to 70%. In mentioned previous studies (Arrais, 2012) it is obtained that combination of local and global imperfections gives the lowest resistance of the beam. It is also proven in an extensive parametric study that the

slender beams are more sensible to global imperfections, and subsequently the local imperfections have a negative impact on the resistance of the stocky beams. Following this studies, in this work, both combinations are studied, first when the global imperfections are dominant (100% global + 70% local) and secondly when the local imperfections are dominant (100% local + 70% global), and it is then concluded which case gives the lower resistance of the purlin.

In order to obtain the local and global buckling modes (shapes) needed for the definition of geometric imperfections of the studied Omega 160 cross-section, the program CUFSM (Schafer *et.al.*, 2006) is used. As it is mentioned before, this program performs elastic buckling analysis of thin-gauge elements using the finite strip method (FSM). Moreover it allows the user to predict the possible buckling modes (local, distortional and global) and their importance on the overall behaviour of the beam. The shapes of the corresponding buckling modes (with the lowest Eigen value for each instability mode) are then used to define geometric imperfections on the finite element models in ABAQUS with magnitudes given in the Table 6.3. In order to generate geometric imperfections in ABAQUS, first the elastic buckling analysis (*Liner perturbation, Buckle*) was performed on a separate numerical model. After computation of buckling modes, they are compared with ones obtained in CUFSM (with the lowest Eigen value for local and global buckling modes) and the corresponding modes in Abaqus are then combined and used to input the geometric imperfections in the structural model in which nonlinear analysis is later performed.

- *Residual stresses*:

Residual stresses are commonly appeared in CFS due to the cold-forming manufacturing process (chapter 2.4). These stresses may have significant impact on the load bearing capacity of the element. The stresses are equilibrated (resultant is equal to zero) and captured inside the cross section so this effect is in the most cases neglected as it has no huge impact on the overall global behaviour, but as a local effect this has to be taken into account, especially when local buckling phenomenon is analysed. However, these stresses depend on many parameters, which make it difficult to take them into account properly. So, residual stresses and cold-work of forming (where the yield stress in the corners is evidently increased) were ignored in these analyses (Laim, 2013).

## 6.4 Calibration of the mechanical numerical model

Due to the lack of the experimental results for this particular cross-section under elevated temperatures, the validation of the finite element model is done using the results from the previous numerical study (Salgueiro, 2015) on structural performance at ambient temperature of Omega (Ω160) cross-section. Calibration study is done in order to have

practice with the program and confidence with the results. Here will be presented only the final results.

### 6.4.1 Consideration about the calibration model

The numerical models for simply supported and continuous beams are defined as it is described and the results are compared with the results of the models M17 and M21 of the previous research (Salgueiro, 2015). Both M17 and M21 models correspond to the Omega 160 (see *Figure 4.5*) with the thickness of cross section equal to 1 mm. Two different cases of purlins are analyzed: simply supported beam (3.0 m) and two-span continuous beam (3.0 m + 3.0 m). It is important to stress that the initial geometric imperfections are not considered in these numerical models as well as residual stresses. In this study the steel grade S320GD+Z was used. The boundary conditions used for these models are defined in the chapter 6.3.2. In the case of simply supported beam one end is supported by double support, where displacements are restrained in longitudinal, vertical and horizontal directions, and the other end is supported by simply support in which only the vertical displacement and the displacement perpendicular to the plane of the purlin are restrained. In the case of continuous beam, the simple supports are used in the both ends of the beam, while the double support is placed in the middle of the span, at the distance of 3 m from the end of the beam (see *Figure 6.6*). In both models, the concentrated forces are applied downwards between 1/5 of the total span of the element, so the uniform bending moment is obtained in the central part of the beam.

### 6.4.2 Results with the shell elements

In this section are presented the results of the geometric and material non-linear analysis performed with these two models. In the previous study (Salgueiro, 2015), the shell finite elements were used, so here is aimed to perform completely the same analysis in order to calibrate models.

- *Simply Supported Beam*:

The force-displacement curve is calculated and presented in the Figure 6.14. It is obtained that the maximum load that Omega 160 with the thickness of 1 mm can sustain is 5.42 kN, when the failure occurs in the middle of the span as it is expected. Comparing to the results obtained in the previous study in model M17, where the maximum load is equal to 5.53 kN, the difference is negligible (1.5 %), which proofs that the model is calibrated.

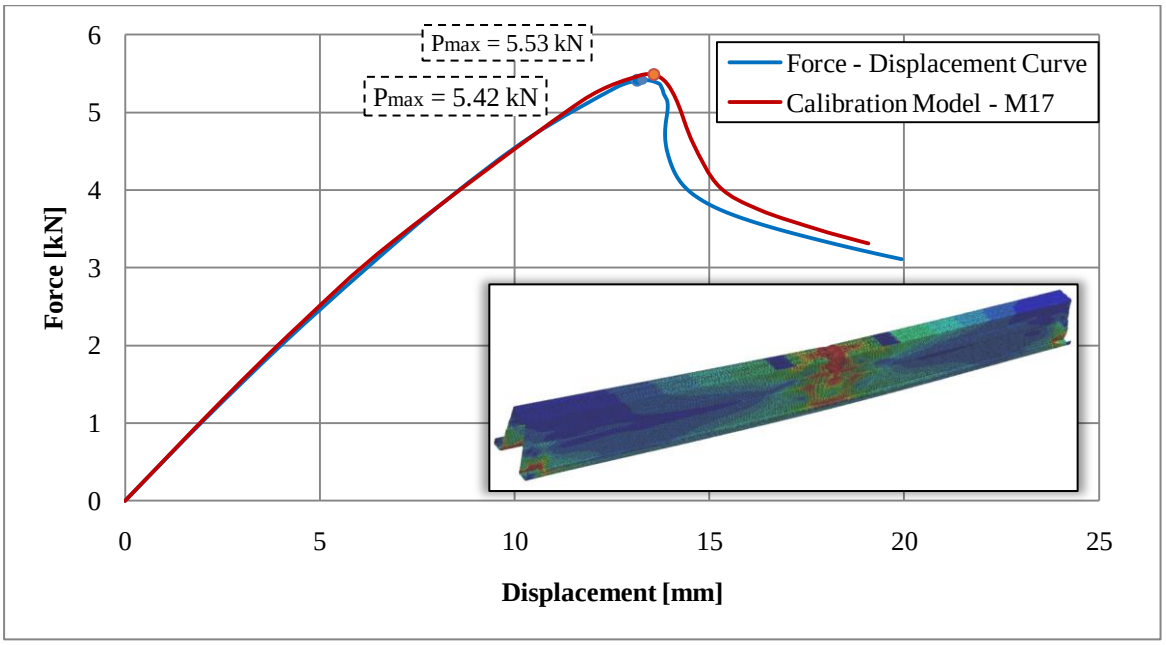


*Figure 6.14* - Force-displacement curve for simply supported beam

- *Continuous Beam*:

The force-displacement curve with corresponding failure mode in case of the continuous Omega 160 purlin with thickness of 1 mm is given in Figure 6.15. In this case the maximum applicable load calculated is 5.58 kN, while in the model M21, this value is equal to 5.48 kN, making the difference of 1.8 %, that can be neglected.

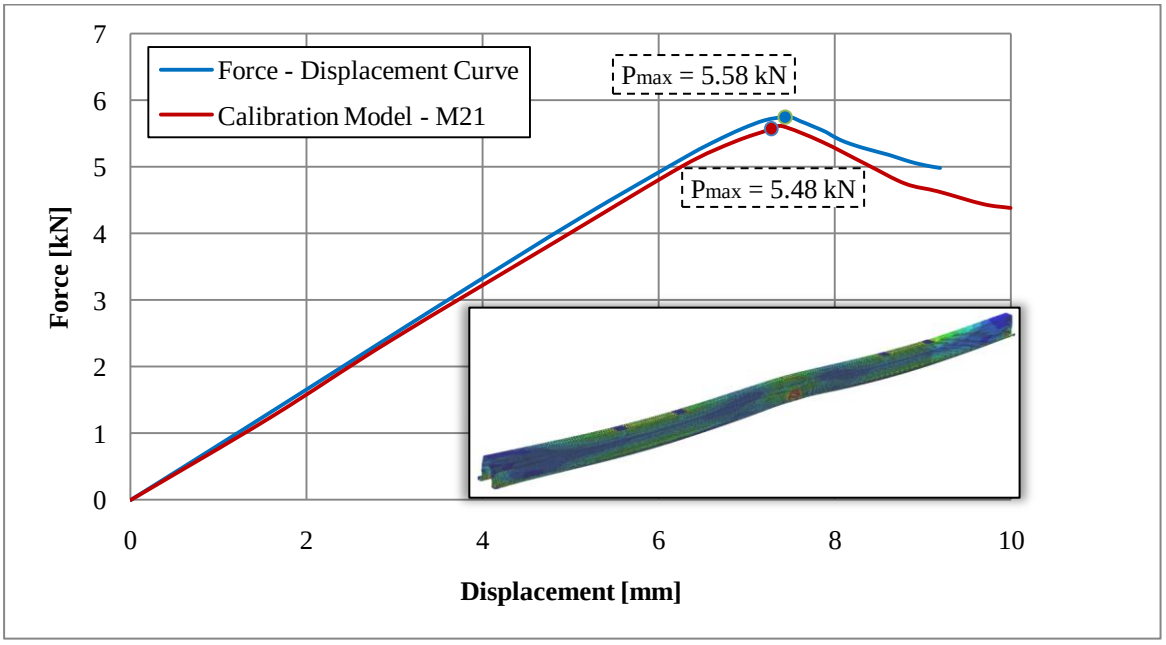


*Figure 6.15*- Force-displacement curve for continuous two-span beam

### 6.4.3 Calibration with solid elements

However, in this work, the heat transfer analysis as well as thermo-mechanical strain-stress analysis has to be done. For this reason, in order to better understand distribution of the temperature across the thickness of the steel, it was decided to use solid elements as it is explained in chapters 6.3.1 and 6.3.2. It is thus necessary to check the validity of the same numerical models but only now with the solid elements. Moreover, it was again analyzed the influence of the number of elements through the thickness of the steel cross-section (*Figure 6.16* and *6.17*). The number of the elements across the cross section showed an exquisite influence on the structural behavior of the studied members. As it is presented in the Figure 6.16, in case of simply supported beam, models with one and two elements through the thickness have significantly reduced both strength and stiffness, while the increased number of elements leads to convergent results, with very small difference between the models with three and four elements across the thickness. It can be also seen that models with solid finite elements (with 3 and 4 elements through thickness) gave slightly higher load bearing capacity comparing to the model with shell finite elements (5.50 kN and 5.57 kN). This study proofs that numerical models with solid finite elements give good results comparing to ones with the shell elements, which allows use of solid-element models for the purpose of this work.

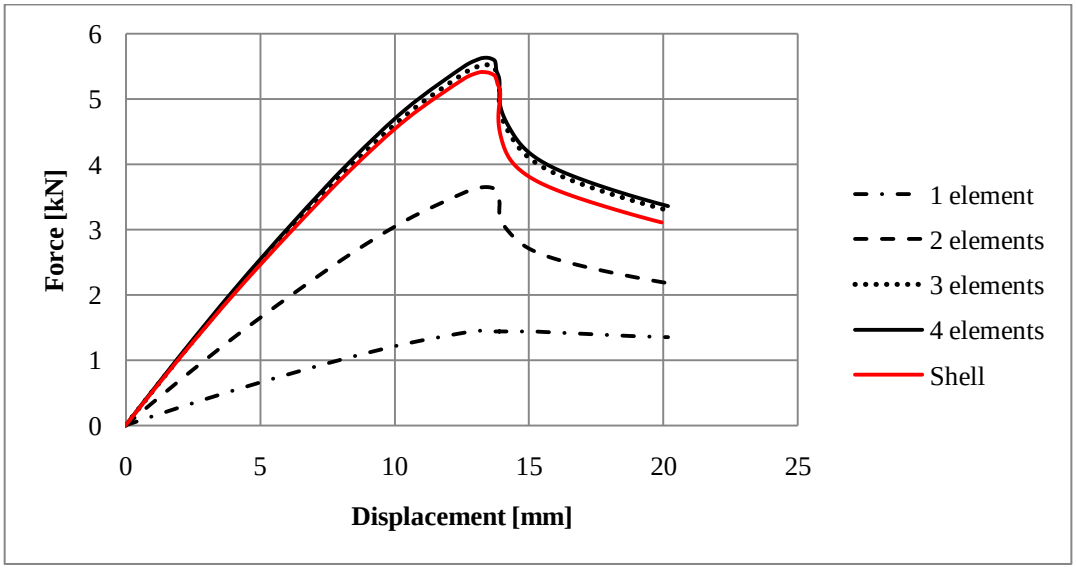


*Figure 6.16* - Validation of numerical model with solid finite elements in case of simply supported beam

A similar study is performed in case of continuous beam (*Figure 6.17*). Also, in this case it is obtained that at least 3 elements through thickness are needed in order to get results comparable to the ones obtained with the shell finite elements.

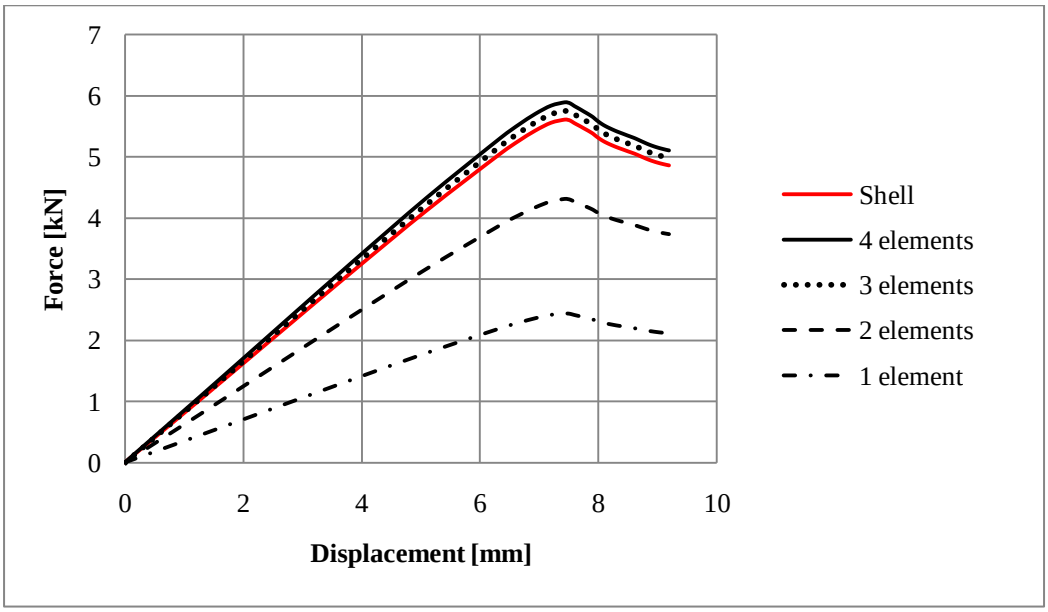


*Figure 6.17* - Validation of numerical model with solid finite elements in case of continuous beam

## 6.5 Unprotected steel beam

In this chapter, the results from Abaqus will be presented for unprotected steel beam, both for the simply supported purlins and for the continuous beams. Finally, the numerical results are compared with the analytical ones, separately for thermal analysis and for thermo-mechanical analysis. For unprotected steel beams, several study cases are considered, where the thickness of the steel profile ($t_{steel}$) varies between 1.0 mm and 2.4 mm.

### 6.5.1 Thermal Results

In order to compare results from thermal analysis, the distribution of temperature in steel during the period of 7200 seconds is considered, as it is the total duration of the fire load. In analytical approach according to Eurocode, the distribution of temperature is considered to be uniform in each point of the member. In numerical analysis, however, this is not the case as the distribution of temperature varies along the thickness of the steel member. The point in the middle of the top flange is taken as a reference point for this comparison. The Figure 6.18 presents the distribution of the temperature in time for the case of unprotected beam with the thickness of 1 mm.

It may be seen that for such a thin element, there is no difference in thermal response of the element between analytical and numerical approach and both curves are affine to the zone model fire curve. Since the thermal boundary conditions are completely the same for the simply supported and continuous beam, the thermal response is also the same.

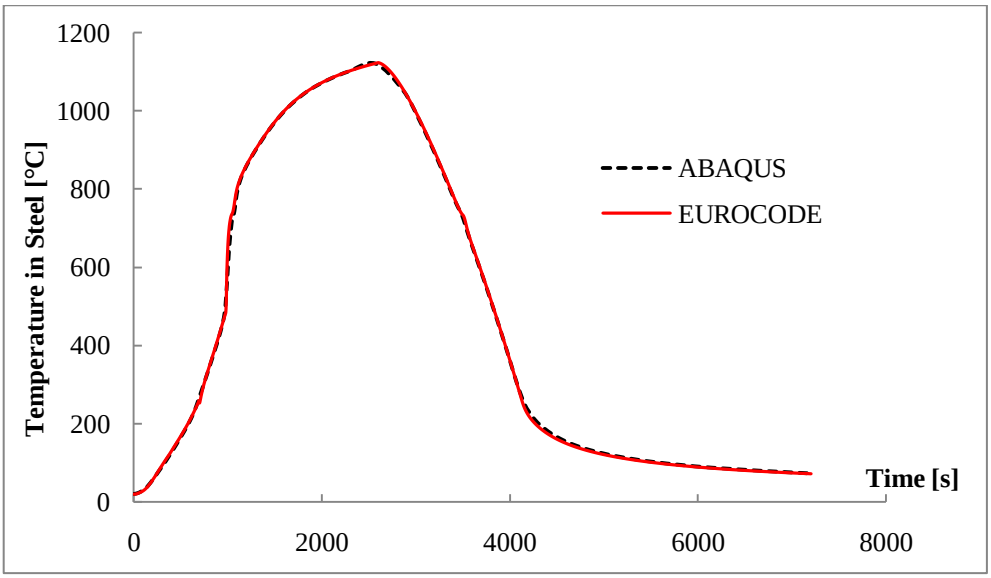


*Figure 6.18* - Thermal response of the unprotected purlin subjected to fire

### 6.5.2 Mechanical Results

In order to obtain the resistance of the beam in Abaqus, the displacement of the purlin in time is considered. In the beginning, at the room temperature, the purlin shows elastic behaviour, and later as the fire load increases, the purlin starts to behave plastically due to the degradation of the mechanical properties which leads to extensive deformations. At the moment when the system is no longer able to maintain equilibrium with the external forces, the collapse of the beam occurs abruptly, with a drastic increase of the deflections and the program Abaqus stops working. The time of resistance is therefore taken as the moment when the software stops working (*Figure 6.19* and *6.20*).

It is important to say that in the part 1 of the ISO 834 standard, the limiting deflection is given, which if exceeded, it may be considered that the failure of the system occurs. However, this criteria is valid only for the elements exposed to Standard ISO 834 fire curve, whereas for the natural fire curves (zone curve), no prescription is provided. Therefore, for the resistant time it is adopted the time when the program stops working due to the extensive displacements.

*Figure 6.19* - Simply supported purlin at the moment of failure

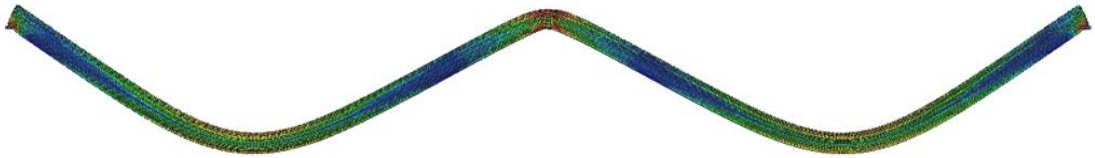

*Figure 6.20* - Continuous two-span purlin at the moment of failure

- *Simply Supported Beam*:

The deformation in time is measured in the middle of the span of the purlin (*Figure 6.21*), where the sudden drop in curve presents actually the collapse of the system. Here are presented the results for the thicknesses that were considered in this research on the way to obtain the optimal solution.

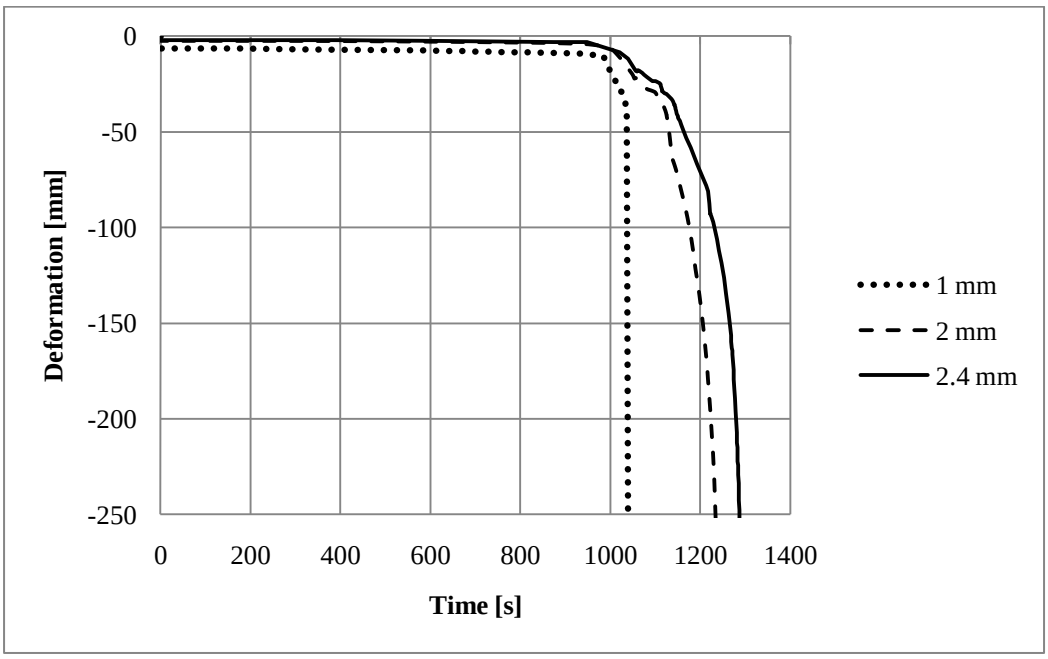


*Figure 6.21* - Behavior of simply supported purlins subjected to fire

As it can be seen, for the simply supported beam, three different study cases are analyzed. In all three cases, the maximal deflection, at which the program stopped working, is approximately 250 mm. As it is expected, the profile with the lowest thickness of steel (1 mm) undergoes collapse after only 1035 seconds (≈ 17.3 min), which is read from the x-axis. Then the profile with the thickness of 2 mm is analyzed, and no huge improvement is achieved, sustaining less than 21 minutes under fire conditions. Therefore, the values between 1 mm and 2 mm of steel are omitted from the analysis, and it is tried with the maximum thickness of the steel (2.4 mm). However, even with the maximum thickness of the steel, the resistance of 21.5 minutes is obtained which is still far away from the demand of 30 minutes.

Also, for the case where thickness of the steel is 2.4 mm, the displacements in axial direction are measured and analyzed. More precisely, the distance between two nodes of one finite element are measured in time in axial direction. These two nodes are located in the top flange of the cross-section (*Figure 6.22*).

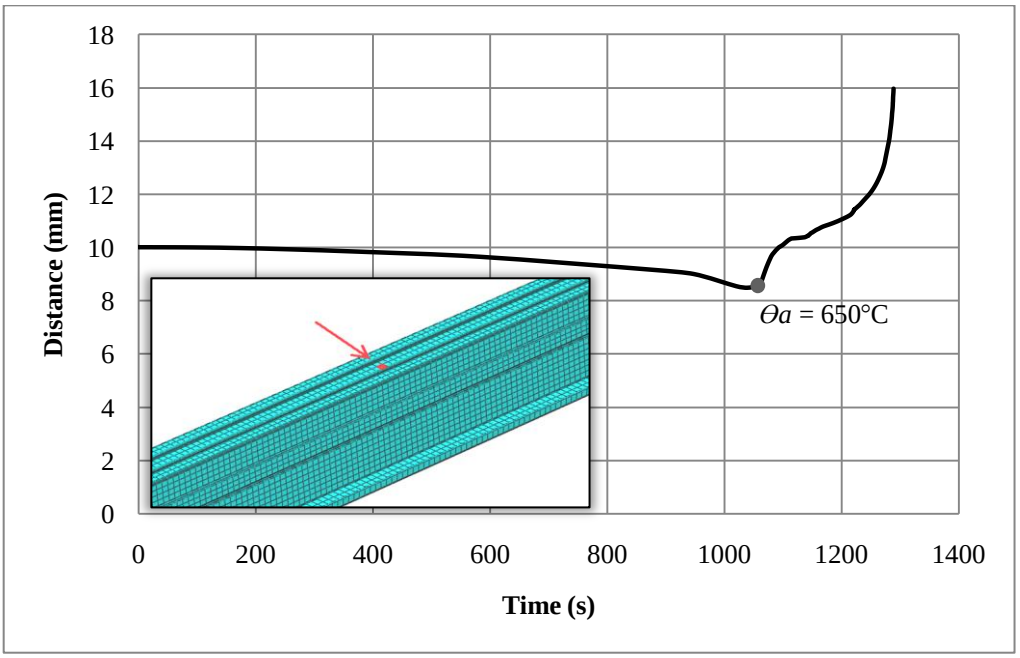


*Figure 6.22*- Distance variation between two nodes in axial direction

Initially, before the loads are applied, the distance between two nodes is 10 mm (see Figure 6.22). Afterwards, the loads are applied and the compression appears in the upper flange, which leads to the reduction in the distance between two nodes. In the beginning, this reduction is low, but as the temperature rises, it becomes more significant. Then, when the temperature in steel reaches the value of approximately 650°C, due to the degradation of the material properties of steel, large displacement appear. Large vertical displacements induce the development of membrane (tension) forces in the beam. These tensile stresses subsequently lead to the extension of the finite element and thus to the increase of the distance between two nodes (see Figure 6.22). At the moment of collapse, when the critical temperature is reached (≈690°C), the distance between nodes is equal to 16 mm, which is 6 mm more than under initial conditions.

- *Continuous Beam*:

The deformation in time is measured in the section of the purlin where the largest deformations are expected (*Figure 6.23*). Also in this case are presented the results for the thicknesses that were considered in this research on the way to obtain the optimal solution for continuous beam.

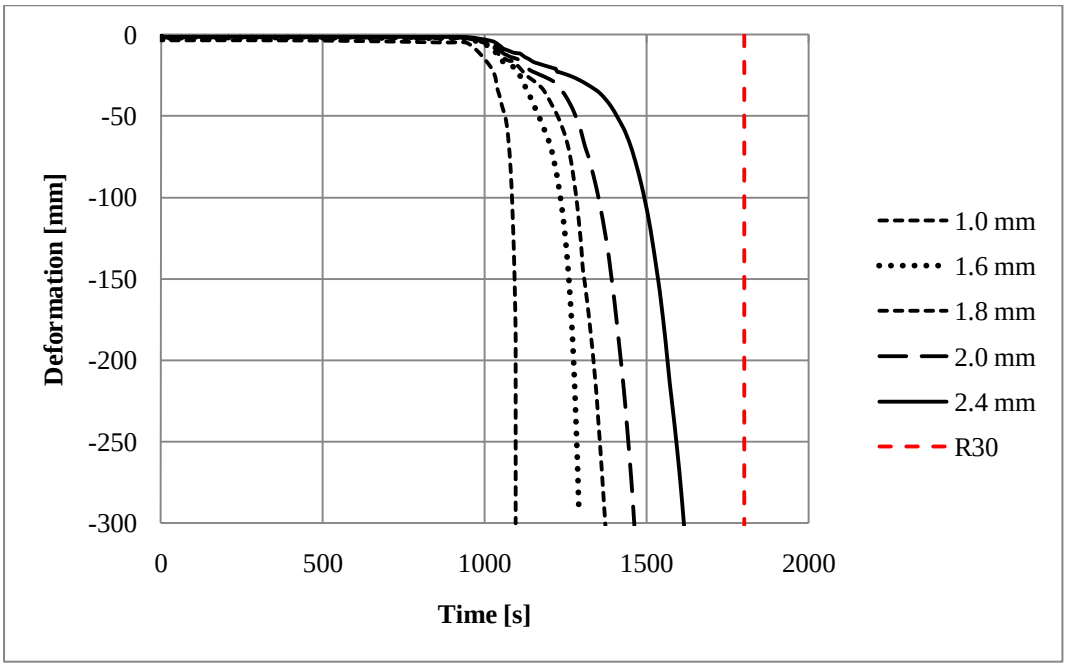


*Figure 6.23* - Behavior of continuous purlins subjected to fire

In the case of the continuous beam, five different study cases are considered, with the thickness of the steel in the range between 1 mm and 2.4 mm. It may be observed that the continuous beam shows better structural behaviour under the fire conditions than simply supported beam. The main reason for that is that continuous beam, being the statically indeterminate system, is actually stiffer system which results in lower displacements and therefore higher fire resistance time. However, even in this case, with the maximum thickness of the steel (2.4 mm), the required resistant time is not satisfied, reaching around 27 minutes at the time of collapse. The other intermediate values are provided in the section 6.7, where all the results are listed and compared.

## 6.6 Steel beam with fire protection

In this chapter, the results from Abaqus will be presented for protected steel beam, both for the simply supported purlins and for the continuous beams. Finally, the numerical results are compared with the analytical ones, separately for thermal analysis and for thermo-mechanical analysis. For protected steel beams, several study cases are considered, where the thickness of the steel profile ($t_{steel}$) and intumescent coating ($d_p$) varies (*Table 6.4* and *Table 6.5*).

*Table 6.4* - Studied cases for simply supported beams with fire protection

| $t_{steel}$ [mm] | $d_p$ [mm] |
|---|---|
| **1.0** | **1.0** |
| **2.0** | **1.0** |
| **2.4** | **0.75** |
| **2.4** | **0.8** |
| **2.4** | **1.0** |

*Table 6.5*- Studied cases for continuous beams with fire protection

| $t_{steel}$ [mm] | $d_p$ [mm] |
|---|---|
| **1.0** | **1.0** |
| **1.6** | **1.0** |
| **1.8** | **0.8** |
| **2.0** | **0.75** |
| **2.4** | **0.4** |
| **2.4** | **0.5** |
| **2.4** | **0.6** |

### 6.6.1 Thermal Results

As it is expected, the thermal response of the steel purlin is modified due to the presence of the instumescent coating (*Figure 6.24*).

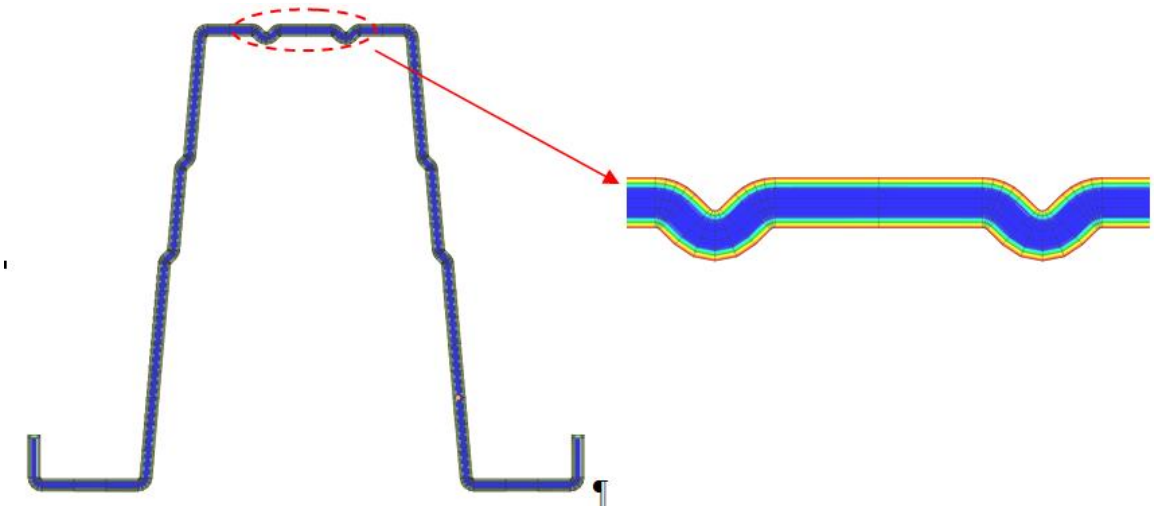

*Figure 6.24* - Heat transfer of protected purlins subjected to fire

The comparison between thermal responses between unprotected and protected steel purlins, as well as between analytical and numerical results is presented in the *Figure 6.25*. In this example the comparison is made for the case when the thickness of the steel cross-section is 1 mm, and also the thickness of the coating is 1 mm.

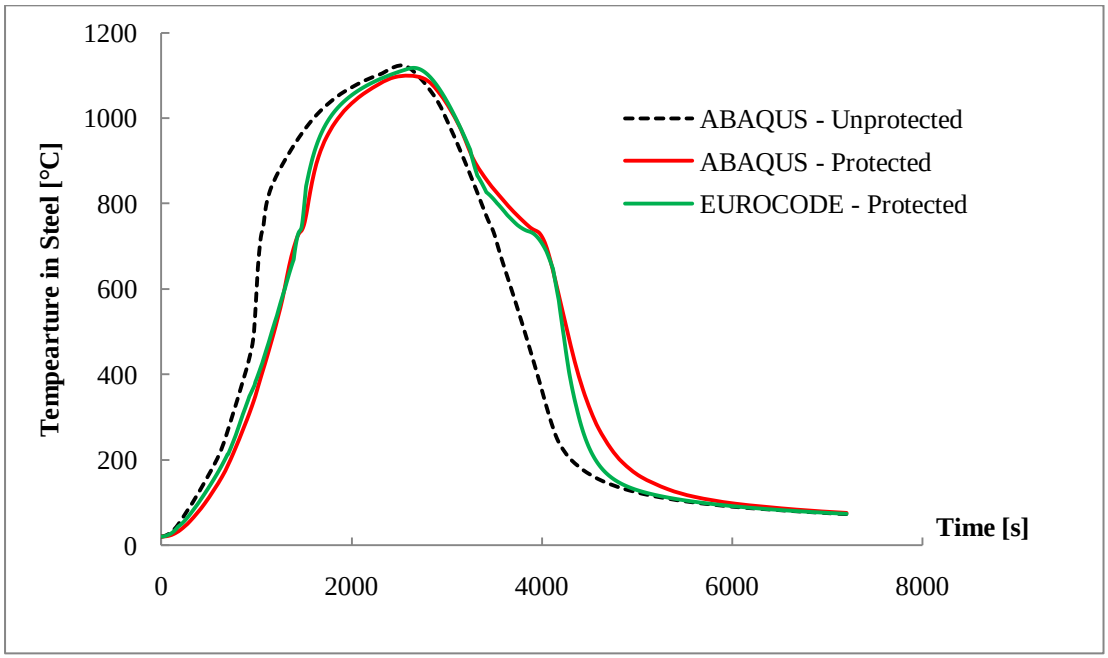


*Figure 6.25* - Comparison of the analytical and numerical results of the thermal response on the studied insulated steel purlin

This graph proves again really good matching between analytical and numerical results of the thermal analysis. It may be seen again that the insulation affects the thermal response of the steel members only in the range between 400 and 800 °C. Due to the lack of data regarding the thermal conductivity for the temperatures above 950°C, the thermal response for protected steel beam at the temperatures higher than 950°C is almost the same as for the unprotected. Also, similar to the analytical results, there is abrupt deviation of the heat transfer curve around 700 °C both in cooling and heating phase, due to the sudden change in the thermal conductivity of the coating at this temperature.

In the *Figure 6.26* is presented how the thermal response is changed for several considered case studies, where both steel thickness and the thickness of the coating are varied. The first number in the legend denotes the thickness of the steel, whereas the second number presents the thickness of the intumescent coating.

It may be noticed that both the increase of the steel thickness and coating thickness leads to better thermal response, the response which is slightly scaled and translated rightwards. It means that for a certain (critical) temperature in steel, in case of thicker steel members with the thicker layer of coating, the collapse time is postponed (translated on the x-axis rightwards).

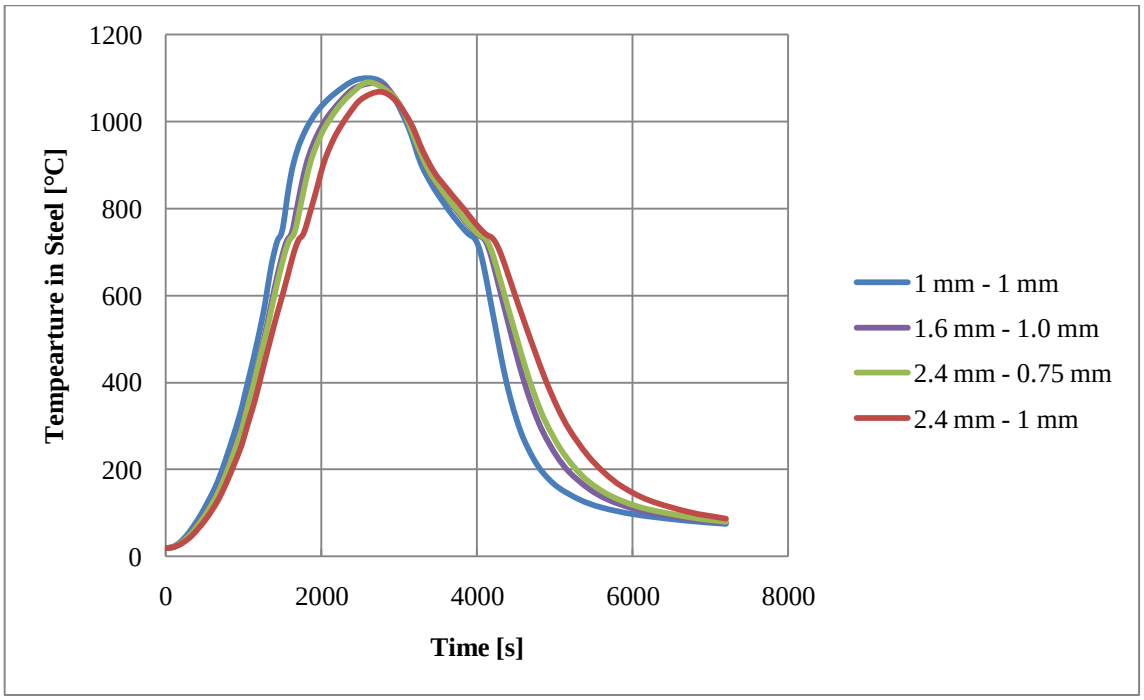


*Figure 6.26* - Thermal response of purlins subjected to fire obtained by ABAQUS

It may be also seen that it is much more favourable to increase thickness of the steel, rather than the thickness of the expensive coating. For instance, in the case when the thickness of the steel is equal to 1.6 mm and the thickness of the coating is 1.0 mm, the thermal response is practically the same as for the case where the steel has thickness equal to 2.4 mm, and the coating is reduced to 0.75 mm. This way, significant economical savings may be achieved.

### 6.6.2 Mechanical Results

The boundary conditions for stress-strain analysis in the case of simply supported and continuous beam are different, unlike the thermal analysis, and thus these two cases will be analyzed separately. The time that a purlin is able to sustain under fire condition is obtained in Abaqus as the moment when abrupt increment in displacements appears, which presents actually the moment when the static system loses equilibrium.

- *Simply Supported Beam*:

In the case of the simply supported beams, the displacements are measured in the middle of the span at the bottom of the top flange. In the *Figure 6.27*, the behaviour of the purlins for all considered case studies (*Table 6.4*) is presented, where both steel thickness and the thickness of the coating is varied. The first number in the legend again denotes the thickness of the steel, whereas the second number presents the thickness of the intumescent coating.

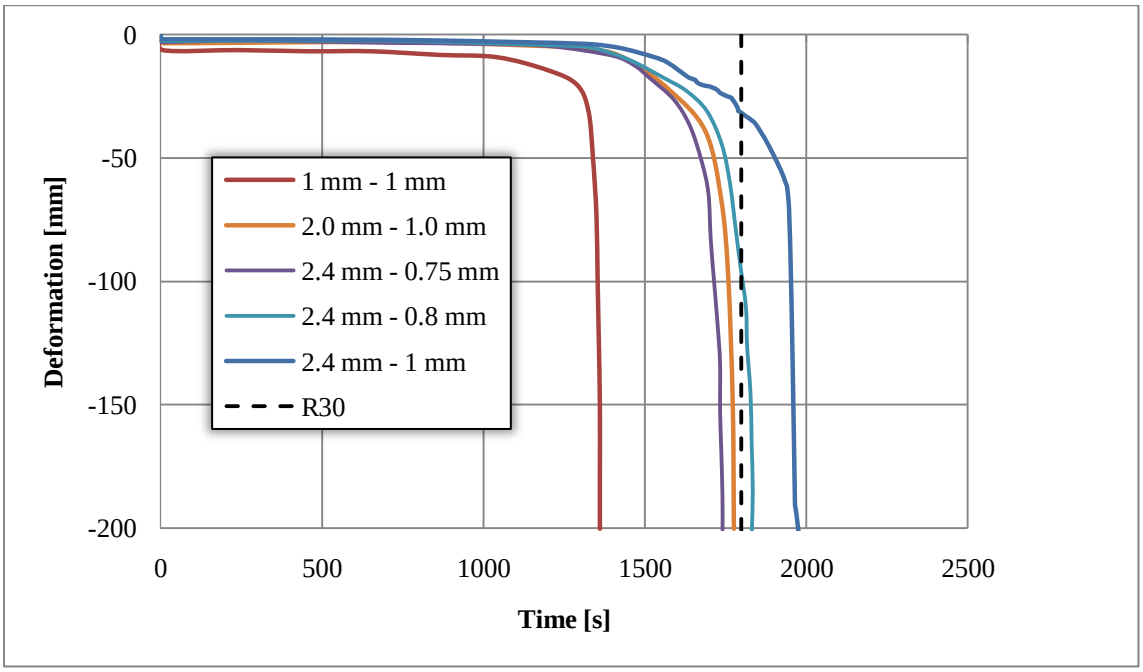


*Figure 6.27* - Thermo-mechanical response of simply supported purlin subjected to fire

It may be noticed that with the lowest thickness of the steel (1.0 mm) and highest thickness of the coating (1.0 mm), the resistance time is insufficient, sustaining only around 1330 seconds under fire (≈ 22 min < 30 min). In other words, the displacement curve for this case is not intersecting the vertical dashed line that presents the 30 minutes demand (R30). Since the goal is to find such a combination of these two parameters that may provide sufficient fire resistance, the thickness of the steel is varied at the first place. Eventually, with the maximum thickness of the steel (2.4 mm) and maximum thickness of the coating (1.0 mm), the requirement is satisfied. In this case, the displacement curve intersects the R30 line, and at that moment the displacement is only around 40 mm. Soon afterwards, the large displacements appear and the collapse occurs approximately 34 minutes after the ignition of fire. Furthermore, the more economical solution is sought, both by reducing the thickness of the steel and the thickness of the coating. Finally, another solution satisfies the requirement, with the steel thickness equal to 2.4 mm and the thickness of the coating equal to 0.8 mm. In this case, the collapse occurs after 31 minutes almost, but the displacements are already 100 mm after 30 minutes, which is 2.5 times more than in the previously mentioned case. All the other results are presented and compared in the section 6.7 in a tabular manner.

- *Continuous Beam*:

In the case of the continuous beams, the displacements are also measured at the bottom of the top flange but only this time at the cross section where the largest displacements are expected for this static scheme. In the *Figure 6.28* is presented the behaviour of the purlins for all considered case studies (see *Table 6.5*).

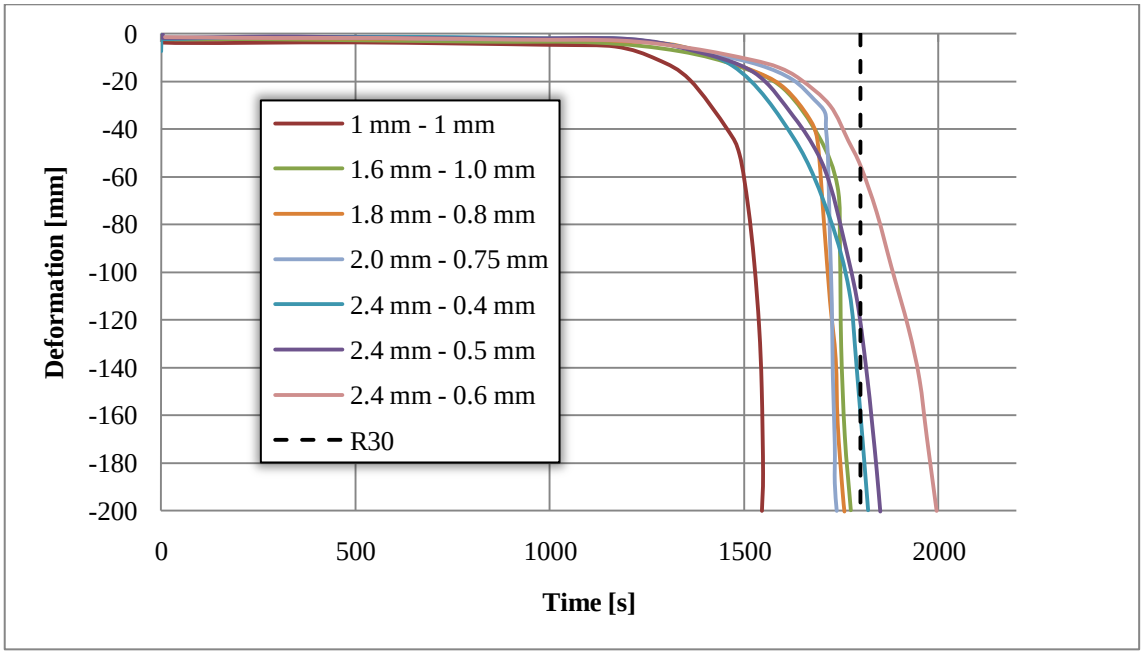


*Figure 6.28* - Thermo-mechanical response of continuous purlins subjected to fire

Similarly to the case of simply supported beam, here also the solutions that are able to sustain 30 minutes under fire are sought and as it can be noticed from the figure, three different solutions provide this requirement. In all three cases, the thickness of the steel is the same and it is equal to 2.4 mm, whereas the thickness of the coating varies (0.4 mm , 0.5 mm and 0.6 mm). The collapse of these three solutions occurs after 30.5, 31.83 and 33.32 minutes, successively, which exceeds 30 minutes requirement. However, the main difference is the magnitude of the displacement at that moment, or in other words, where the displacement curves (on the graph), for these three solutions, intersect the R30 line (demand line). So, in the case with 0.4 mm thickness of the coating the displacement after 30 minutes is around 160 mm, for the case with 0.5 mm thickness of the coating, the displacement is equal to 120 mm and finally in the case where the coating has the thickness equal to 0.6 mm, the displacement is the lowest and has the value equal to 60 mm. All the other solutions and their resistances are provided in the following section, where these results are compared with the analytical results.

## 6.7 Comparison and discussion between numerical and analytical results

In this chapter is presented the comparison between analytical and numerical results of simply supported beams (*Table 6.6*) and continuous beams (*Table 6.7*) both at ambient and elevated temperatures, where the thickness of steel and insulation coating are varied. In this comparison, the presence of initial geometric imperfection is omitted and the influence of possible local and global imperfections is analyzed in the following chapter.

*Table 6.6* - Resistance of simply supported Omega160 profiles

| | | **Unprotected Steel Member** | | | **Insulated Steel Member** | | |
|---|---|---|---|---|---|---|---|
| | | *Eurocode* | *French Annex* | *Abaqus* | *Eurocode* | *French Annex* | *Abaqus* |
| $t_{steel}$ *[mm]* | $d_p$ *[mm]* | $t_{fi,d}$ *[min]* | $t_{fi,d}$ *[min]* | $t_{fi,d}$ *[min]* | $t_{fi,d}$ *[min]* | $t_{fi,d}$ *[min]* | $t_{fi,d}$ *[min]* |
| **1.0** | **1.0** | 16.35 | 16.45 | 17.26 | 19.43 | 20.5 | 22.17 |
| **2.0** | **1.0** | 16.92 | 17.1 | 20.85 | 26.55 | 27.0 | 28.52 |
| **2.4** | **0.75** | 17.16 | 17.42 | 21.5 | 26.16 | 26.58 | 28.25 |
| **2.4** | **0.8** | 17.16 | 17.42 | 21.5 | 26.6 | 27.05 | **30.7** |
| **2.4** | **1.0** | 17.16 | 17.42 | 21.5 | 28.3 | 28.7 | **34.0** |

*Table 6.7* - Resistance of continuous Omega160 profiles

| | | **Unprotected Steel Member** | | | **Insulated Steel Member** | | |
|---|---|---|---|---|---|---|---|
| | | *Eurocode* | *French Annex* | *Abaqus* | *Eurocode* | *French Annex* | *Abaqus* |
| $t_{steel}$ *[mm]* | $d_p$ *[mm]* | $t_{fi,d}$ *[min]* | $t_{fi,d}$ *[min]* | $t_{fi,d}$ *[min]* | $t_{fi,d}$ *[min]* | $t_{fi,d}$ *[min]* | $t_{fi,d}$ *[min]* |
| **1.0** | **1.0** | 16.45 | 16.55 | 18.25 | 20.57 | 21.33 | 25.67 |
| **1.6** | **1.0** | 16.8 | 16.96 | 21.5 | 25.15 | 25.52 | 29.85 |
| **1.8** | **0.8** | 16.95 | 17.2 | 22.95 | 24.75 | 25.1 | 28.95 |
| **2.0** | **0.75** | 17.1 | 17.3 | 24.5 | 25.12 | 25.45 | 28.58 |
| **2.4** | **0.4** | 17.42 | 17.75 | 27.28 | 23.13 | 23.56 | **30.5** |
| **2.4** | **0.5** | 17.42 | 17.75 | 27.28 | 24.16 | 24.66 | **31.83** |
| **2.4** | **0.6** | 17.42 | 17.75 | 27.28 | 25.1 | 25.7 | **33.32** |

As it can be seen, the numerical results obtained in Abaqus give higher resistance of the purlins than the analytical ones, which is expectable as the standard should be on the safety side. However, French Annex of the EN 1993-1-2 (2004) has provided better and less conservative results.

## 6.8 Influence of Geometric Imperfections

Finally, in this section, the influence of the geometric imperfections on the structural behaviour of the purlins subjected to fire is examined. The way how these initial imperfections (global and local) are defined and combined in the numerical model as well as their magnitudes, is described into detail in the chapter 6.3.2 of this work. In previous studies (Arrais, 2012) it is obtained that combination of local and global imperfections gives the lowest resistance of the beam. In this work, both combinations are studied, first when the global imperfections are dominant (100% global + 70% local) and secondly when the local imperfections are dominant (100% local + 70% global), and it is then concluded which case gives the lower resistance of the purlin.

- *Simply Supported Beam*:

Without taking into account geometric imperfections, the adopted solution for simply supported beam, according to Table 6.6 is the one with the thickness of steel cross-section equal to 2.4 mm and insulation thickness equal to 0.8 mm. For this Omega 160 cross-section, the buckling mode instability curve is calculated (*Figure 6.29*) using the program CUFSM (Schafer *et.al.*, 2006), where the buckling modes with the lowest Eigen value for local and global buckling modes are obtained.

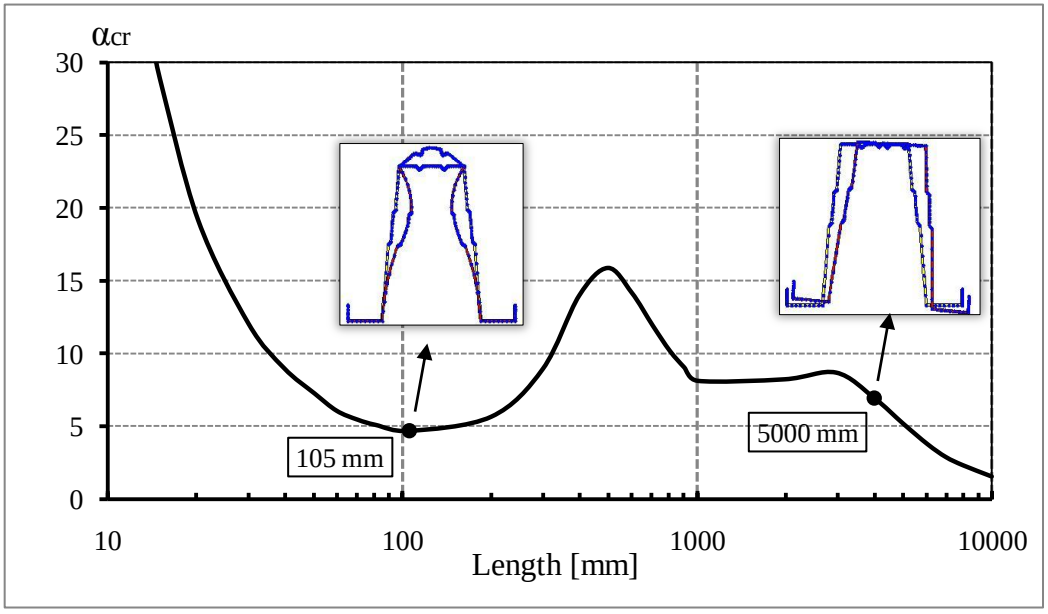


*Figure 6.29* - Buckling mode instability curve of Omega 160 cross-section with the thickness of 2.4 mm (CUFSM)

In order to generate geometric imperfections in ABAQUS, first the elastic buckling analysis (*Liner perturbation, Buckle*) was performed. After computation of buckling modes, they are compared with ones obtained in CUFSM and the corresponding modes in Abaqus are then combined and used to input the geometric imperfections in the structural model. The corresponding buckling shapes (local and global) obtained in Abaqus are presented in the Figure 6.30.

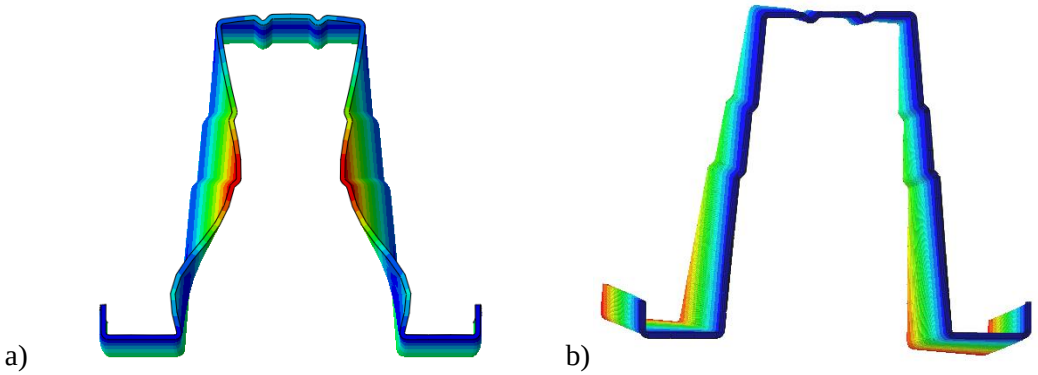


*Figure 6.30* - Corresponding buckling modes obtained in Abaqus: a) local and b) global

After the implementation of these modes as the initial imperfections in numerical model, the results are compared with perfect case – without geometric imperfections (*Figure 6.31*).

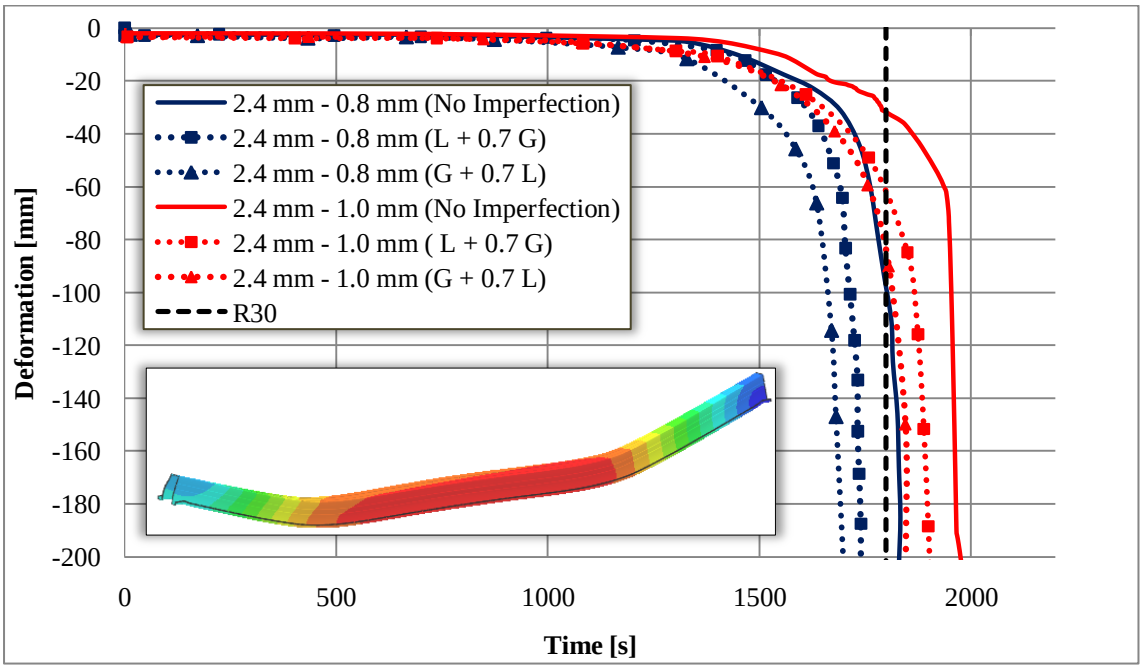


*Figure 6.31* - Influence of geometric imperfections on the resistance of simply supported purlin

In the Figure 6.31, it can be seen that the geometric imperfections affect the resistance of the purlins, and the resistance is reduced mostly for the case with dominant global

imperfections and corresponding local imperfections (G + 0.7L), where G denotes "global" and L stands for "local". The thickness of 0.8 mm of intumescent coating which seemed sufficient when geometric imperfections were not accounted for, is not longer enough to provide required time resistance of 30 minutes. Therefore, this thickness is increased to 1.0 mm and this way the desired resistance is reached even if the worst possible imperfection scenario is taken into account. All the results from the Figure 6.31 are given in the Table 6.8.

*Table 6.8* - Influence of geometric imperfections on the resistance of simply supported purlin

| Steel - Insulation | No Imperfections | Global + 70% Local | Local + 70%Global |
|---|---|---|---|
| **2.4 mm - 0.8 mm** | 30.7 min | 28.16 min | 28.56 min |
| **2.4 mm - 1.0 mm** | 34.0 min | 32. 23 min | 32.78 min |

- *Continuous Beam*:

In case of the continuous beam the adopted solution when the geometric imperfections are not considered is the one with the thickness of steel cross-section equal to 2.4 mm and insulation thickness equal to 0.4 mm. The buckling mode instability curve is calculated for continuous beam by CUFSM (*Figure 6.32*), where the buckling modes with the lowest Eigen values for local and global buckling modes are obtained.

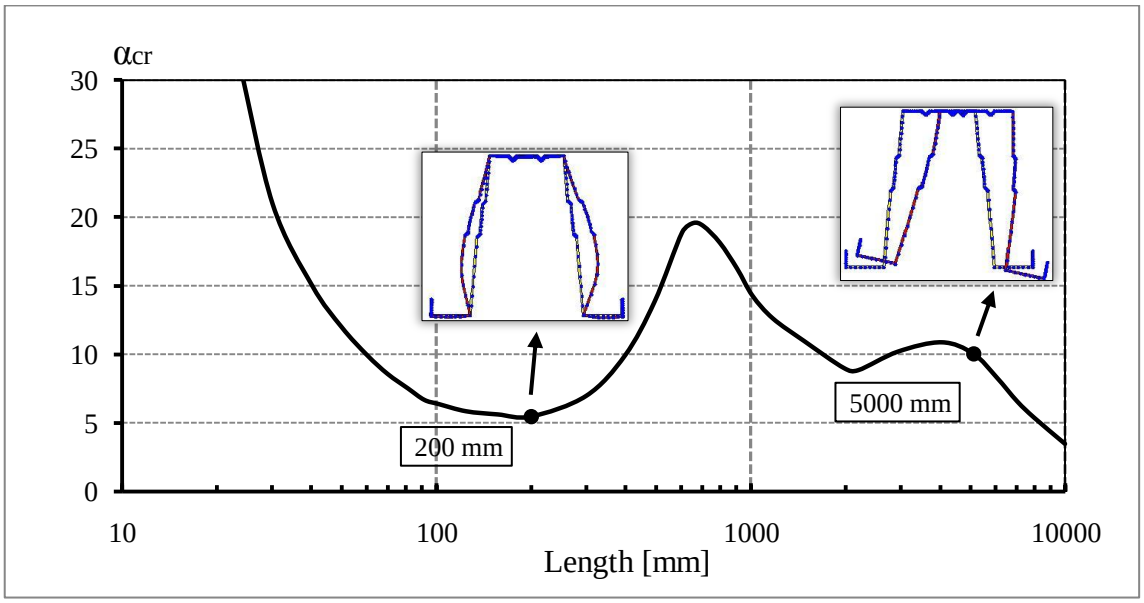


*Figure 6.32* - Buckling mode instability curve of Omega 160 cross-section with the thickness of 2.4 mm (CUFSM)

The corresponding buckling shapes (local and global) obtained in Abaqus are presented in the Figure 6.33.

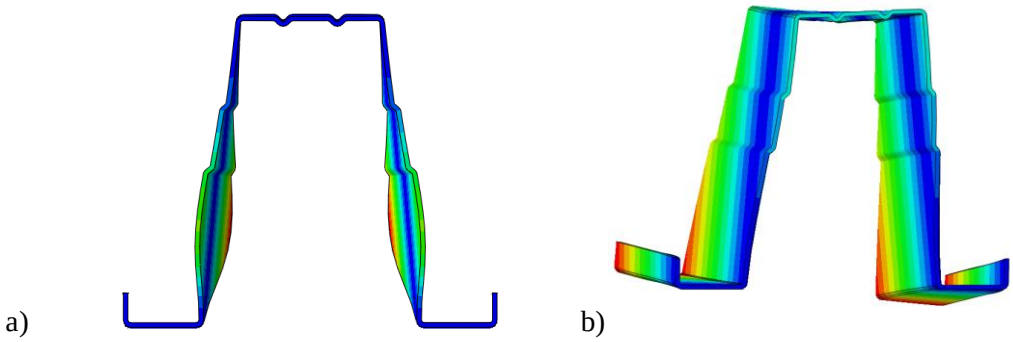


*Figure 6.33* - Corresponding buckling modes obtained in Abaqus: a) local and b) global

After the implementation of these modes as the initial imperfections in numerical model, the results are compared with perfect case – without geometric imperfections (*Figure 6.34*).

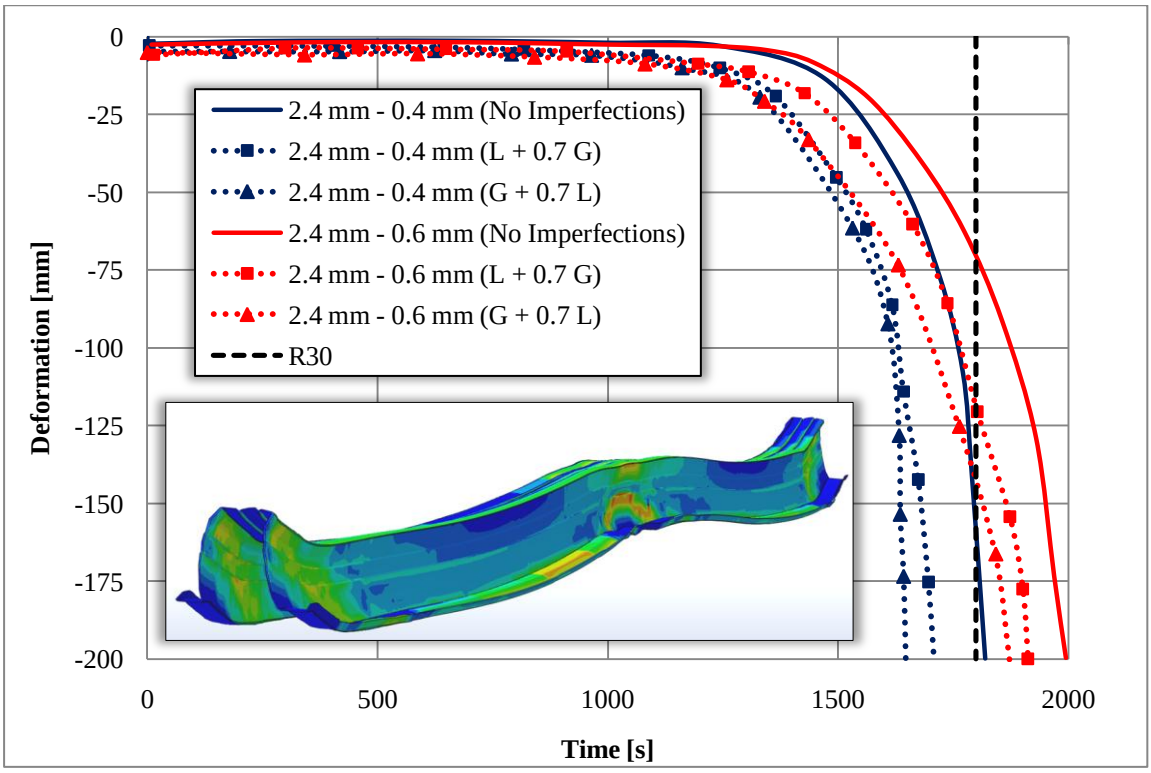


*Figure 6.34* - Influence of geometric imperfections on the resistance of continuous purlin

In the Figure 6.34, it can be seen that the geometric imperfections reduce the resistance of the purlins, and again the resistance is reduced mostly for the case with dominant global imperfections and corresponding local imperfections (G + 0.7L). The thickness of 0.4 mm of intumescent coating does not provide required time resistance of the purlin if imperfections are taken into consideration. Therefore, this thickness is increased to 0.6

mm and this way the demands are satisfied. All the results from the Figure 6.34 are given in the Table 6.9.

*Table 6.9* - Influence of geometric imperfections on the resistance of continuous purlin

| Steel - Insulation | No Imperfections | Global + 70% Local | Local + 70%Global |
|---|---|---|---|
| **2.4 mm - 0.4 mm** | 30.5 min | 28.33 min | 28.88 min |
| **2.4 mm - 0.6 mm** | 33.32 min | 31.22 min | 31.81 min |

# 7 CONCLUSIONS AND FUTURE WORK

## 7.1 Conclusions

In this thesis the structural behaviour of cold-formed steel purlins under the fire condition was examined, Omega 160 cross-sections in particular. For this purpose an industrial building located in Portugal was taken as a study case, where 30 minutes resistance is requested by the Portuguese Legislation. Two typical static systems for purlins were studied – simply supported beam and continuous (two-span) beam. The calculation of the fire resistance of the purlins was performed both analytically and numerically.

The analytical calculation of the fire resistance was done in two ways - according to EN 1993-1-2 (2004) and according to French Annex of the same part of the Eurocode. It was obtained that the French Annex gives slightly higher resistance of the purlins but the difference in the results in case of thin-gauge profiles between these two approaches is practically negligible. However, in both cases, it was obtained that in this kind of application, cold-formed steel beams generally have low fire resistance (lower than requested 30 minutes) but at the same time the critical temperatures are commonly higher than 350 ºC which is the critical temperature proposed for the calculation by EN 1993-1-2 (2004).

The numerical analysis was carried out by the use of finite element analysis software – ABAQUS. In order to obtain more accurate results, a study on the mesh size was firstly done. In was obtained that in the case of the thin-gauge profiles, the temperature distribution is practically the same and uniform, regardless of the mesh size and the number of the finite elements through the thickness. However, in the stress-strain analysis, these variations play an important role and the decision on the size of the mesh was made only after mechanical analysis. Models with one and two elements through the thickness have significantly reduced both strength and stiffness, while the increased number of elements leads to convergent results, with very small difference between the models with three and four elements across the thickness.

The numerical results were compared with the analytical ones and it was established that there is no difference in thermal response of the element between analytical and numerical approach, but when it comes to thermo-mechanical response, the numerical analysis gave higher resistances of the purlins in comparison with the analytical results. However, neither analytical nor numerical approach did not provide sufficient fire resistance time in case of unprotected purlins, being the maximum thickness of the steel section equal to 2.4 mm. Therefore, in order to meet the required fire resistance, the

SteelProst intumescent coating was used. The main idea was to find a solution with as less as possible usage of expensive protection material, which would make these purlins a competitive solution on the market and hopefully initiate their mass production. It was concluded that continuous beams are much better solution than simply supported beam, making the savings in expensive fire protection material up to 50%. In case of simply supported beam, the resistance of 30 minutes was achieved with the thickness of the steel equal to 2.4 mm, whereas the thickness of the coating was 0.8 mm. On the other hand, in case of the continuous beam, for the same thickness of the steel section (2.4 mm), the required thickness of the coating was only 0.4 mm, which makes this solution two times more economical.

Finally, the influence of the initial geometric imperfections was also analyzed and it was deduced that they indeed play an important role in overall behavior of the cold-formed profiles subjected to fire, which is reflected in reduced fire resistance. Both for the simply supported and continuous beam the resistance was reduced mostly for a combination of imperfections with dominant global and corresponding local imperfections. Therefore, in case of simply supported beam, the thickness of the coating of 0.8 mm was no longer sufficient to satisfy 30 minutes demand, but this value had to be increased to 1.0 mm. Also, in case of continuous beam, the thickness of protection material had to be increased from 0.4 mm to 0.6 mm, which still makes a significant saving in protection material of 40% in comparison with simply supported beam.

## 7.2 Future work

The main purpose of this study, beside scientific reasons, was also of the practical nature as it aimed to obtain an economically acceptable solution for cold-formed Omega160 steel purlin which is able to provide required fire resistance. For that reason, the contribution of one particular intumescent coating (SteelProst) to the overall resistance was examined. However, this might be only one possible way how to protect the CFS purlins, and thus numerous studies regarding different fire protection typologies should be done in order to obtain really most competitive solution.

First of all, different intumescent coatings available on the market (mineral fibre, vermiculite cement, perlite, high-density sprays, etc.) with different thermal properties but also different prices should be verified. On the other hand, the improvement of fire resistance for an open cross-section, such as Omega cross-section, might be also achieved using a boards or even steel plate as a fire protection, which may be placed in the bottom part of the cross-section in order to prevent direct exposure of steel to fire (*Figure 7.1*). For that matter, also, boards made of different materials are now available on the market (gypsum boards, fibre-silicate or fibre calcium-silicate boards, vermiculite and cement), and the optimal solution should be searched for.

*Figure 7.1* - Solution with the board on the bottom of the purlin

Using a fire protection (board or steel plate) on the bottom of the profile in this way, it would be possible to "close" cross-section and thus to reduce section factor, which is enormously huge for jagged Omega profiles and the steel section would be exposed to fire only from the lateral and top sides.

Furthermore, in case that this solution is not sufficient to provide the desired resistance, it would be interesting to carry out a study in which two different fire protection materials will be used together: board and intumescent coating. In such a case, the board would be again used in the bottom part of the cross-section, whereas the intumescent coating would be applied on the outer surface of the remaining three sides (*Figure 7.2*). In this way a parametric study should be performed in which the thickness of board, coating and steel section would be varied until the most convenient solution is found.

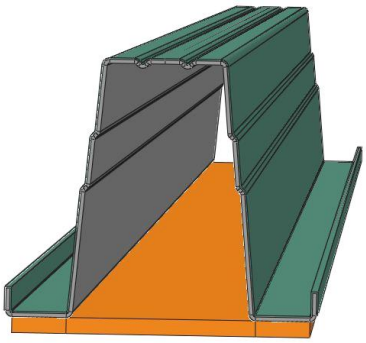

*Figure 7.2* – Solution with the board and intumescent coating

In EN 1993-1-2 (2004), it assumed that the temperature distribution is uniform within the cross-section insulated by fire protection material. However, in these cases where the board is placed only on the bottom of the purlin, this assumption can not be considered as a correct one (*Figure 7.3*). Moreover, the standard does not provide neither design values of the section factor for partially protected cross-section (e.g. board on the bottom of the Omega purlin), nor the prescription how to calculate the temperature development in steel section protected by means of two different fire protection materials. It would be

necessary to perform series of experimental tests and numerical analysis which would eventually lead to improved analytical equations that are suitable for wider range of application.

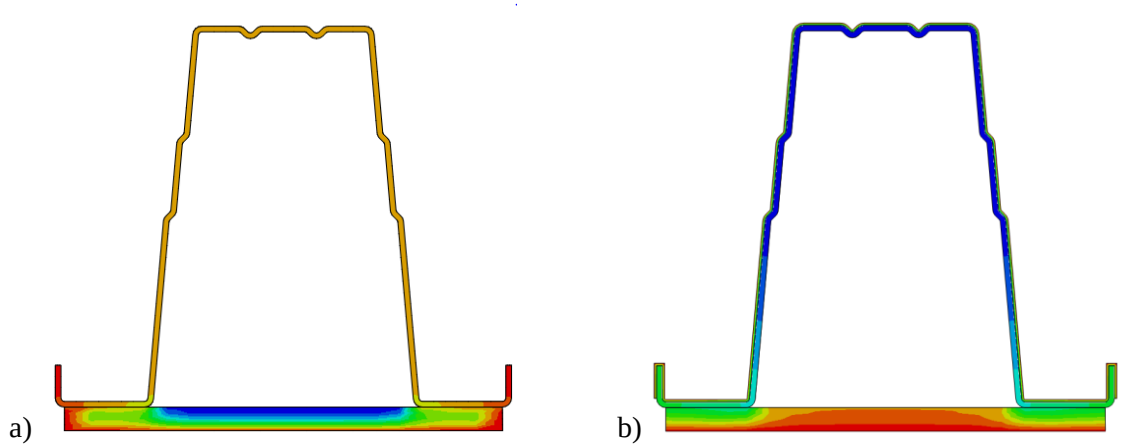


*Figure 7.3* - Temperature distribution of purlin (ABAQUS):
a) protected by gypsum board only
b) protected by board and intumescent coating

It is important to remember that this work research was limited to purlins with Omega 160 cross-sections, with the length of 5.0 meters between the supports and with a certain degree of utilization ($\mu_0$). But in practice, depending on a study case, all these parameters might be very different. Hence, an extensive parametric study which takes into account all these parameters is highly recommended. The final goal would be to obtain a catalogue of purlins in which various Omega profiles are sorted, so a user can choose easily a profile according to desired performance of purlin both at the ambient and elevated temperatures.

# REFERENCES

Arrais, F., 2012. *Comportamento de elementos enformados a frio em situação de incêndio*, Aveiro: PhD Thesis - Universidade de Aveiro, Portugal.

Arrais, F., Lopes, N., Vila Real, P., 2015. *Behavior and resistance of cold-formed steel beams with lipped channel sections under fire conditions,* United Kingdom: Journal of Structural Fire Engineering, Multi-Science Publishing Co. Ltd.

Cadorin, J-F., Franssen, J-M., 2002. *A tool to design steel elements submitted to compartment fires -OZone V2 -Part 1: Pre and post flashover compartment fire model*, Fire Safety Journal.

CEN, European Committee for Standardisation, NF EN 1993-1-2, Eurocode 3: Calcul des structures en acier – Annexe Nationale à la NF EN 1993-1-2: Calcul du comportment au feu, Brussels, Belgium, 2007.

Dassault Systèmes Simulia Corp., 2010, http://www.3ds.com/products/simulia/overview/, Abaqus Analysis – User's Manual, version 6.14-1, USA.

Dubina, D., 2001. *The ECBL approach for interactive buckling of thin-walled steel members*, Steel & Composite Structures. 1(1):75-96.

Dubina, D., Ungureanu, V., Landolfo, R., 2012. *Design of Cold-formed Steel Structures*, Berlin: Ernst & Sohn.

EN 1991-1-2 (2002), Eurocode 1: Actions on structures, Part 1-2: General actions – Actions on structures exposed to fire, European Committee for Standardisation, Brussels, Belgium.

EN 1993-1-1 (2004), Eurocode 3: Design of steel structures, Part 1-1: General rules and rules for buildings, European Committee for Standardisation, Brussels, Belgium.

EN 1993-1-2 (2004), Eurocode 3: Design of steel structures, Part 1-2: General rules, Structural fire design, European Committee for Standardisation, Brussels, Belgium.

EN 1993-1-3 (2004), Eurocode 3: Design of steel structures, Part 1-3: General rules, Supplementary rules for cold-formed members and sheeting, European Committee for Standardisation, Brussels, Belgium.

EN 1993-1-5 (2006), Eurocode 3: Design of steel structures, Part 1-5: Plated structural elements, European Committee for Standardisation, Brussels, Belgium.

Ferraz G, 2014. *Thermal analysis of steel columns exposed to localized fires*, Coimbra: Master Thesis of Steel and Composite Construction - University of Coimbra.

Franssen, J-M., Vila Real, P., 2010. *Fire Design of steel Structures*, ECCS, ISBN & Ernst & Sohn a Wiley Company.

Ghersi, A., Landolfo, R. and Mazzolani, F.M., 2001. *Design of metallic cold-formed thin-walled members*, London: E & FN Spon.

Laím, L., 2013. *Experimental and Numerical Analysis on the Structural Behaviour of Cold-Formed Steel Beams Subjected to Fire*, Coimbra: PhD Thesis - Universidade de Coimbra, Portugal.

Lopes, N., Vila Real, P.M.M., 2014. *Class 4 stainless steel I beams subjected to fire*, Aveiro: LABEST – Department of Civil Engineering, University of Aveiro, Portugal.

Mago, N., Hicks, S., Ian Simms, W., 2014. New Zealand Heavy Engineering Research Association, Freelance Consultant (UK) SIMULIA Customer Conference.

Vila Real, P.M.M., Franssen, J-M., 2001. *Numerical modelling of lateral buckling of steel I beams under fire conditions - comparison with Eurocode 3*, London: J Fire Prot Eng;11(2):112–28.

Vila Real, P., Lopes, N., Silva, L., Franssen, J-M., 2007. *Parametric analysis of the lateral-torsional buckling resistance of steel beams in case of fire*, Fire Saf J;42(6–7):416–24.

Yu, W.W., 2000. *Cold-Formed Steel Design, Third Edition*, New York: John Wiley & Sons.

Yu, W.W., Laboube, R.A., 2010. *Cold Formed Design (4th Edition)*, New York: John Wiley & Sons.

# APPENDIX A – Parametric fire curve

In this appendix, the detailed analytical calculation of the parametric fire curve is provided. This calculation method for a parametric temperature-time curve is given in Annex A and Annex E of EN 1991-1-2 (2002).

The input data is listed below:

| | |
|---|---|
| Floor area: | $A_f$ = 85 m² |
| Total area of enclosures | $A_t$ = 275.7 m² |
| Total area of vertical openings: | $A_v$ = 19.2 m² |
| Height (average): | $H \approx$ 2.5 m |
| Average window height: | $h_{eq}$ = 1.15 m |
| | |
| Floor: | |
| Normalweight concrete: | $\rho$ = 2300 kg/m$^3$ |
| | $c$ = 1000 J/kgK |
| | $\lambda$= 1.0 W/mK |
| Walls Inside: | |
| Lightweight concrete: | $\rho$ = 1600 kg/m$^3$ |
| | $c$ = 840 J/kgK |
| | $\lambda$ = 0.8 W/mK |
| Walls Outside: | |
| Gypsum board: | $\rho$ = 900 kg/m$^3$ |
| | $c$ = 1000 J/kgK |
| | $\lambda$ = 0.25 W/mK |
| Ceiling: | |
| Gypsum board: | $\rho$ = 900 kg/m$^3$ |
| | $c$ = 1000 J/kgK |
| | $\lambda$ = 0.25 W/mK |
| Glass wool and rockwool: | $\rho$ = 60 kg/m$^3$ |
| | $c$ = 1030 J/kgK |
| | $\lambda$ = 0.037 W/mK |

Fire growth rate: medium (for offices)

- DETERMINATION OF FIRE LOAD DENSITY

For the calculation of the fire load density the Annex E of EN 1991-1-2 (2002) provides a calculation model and it can be calculated by using the following equation

$$q_{f,d} = q_{f,k} \cdot m \cdot \delta_{q1} \cdot \delta_{q2} \cdot \delta_n \qquad (A.1)$$

Where

$q_{f,k}$ is characteristic value of fire load density
$m$ is combustion efficiency factor (recommended value is 0.8)
$\delta_{q1}$ is the factor which considers the risk of fire activation by size of the compartment
$\delta_{q2}$ is the factor which considers the fire activation risk due to the type of occupancy
$\delta_n$ is the factor which considers the different active protection measures

The factor $\delta_{q1}$ depends on the compartment area and can be calculated according the following table (*Table A.1*) which is provided in EN 1991-1-2 (2002). Since the floor area in this case is approximately 85 m$^2$, using the linear interpolation the factor is calculated

$$\delta_{q1} = 1.33$$

The factor $\delta_{q1}$ depends on the compartment type of occupancy and can be calculated using the same table (*Table A.1*) which is provided in EN 1991-1-2 (2002). The considered compartment is office so the parameter is obtained accordingly

$$\delta_{q2} = 1.0$$

*Table A.1* - Factors $\delta_{q1}$ and $\delta_{q2}$ (Annex E of EN 1991-1-2, 2002)

| Compartment floor area $A_f$ [m²] | Danger of Fire Activation $\delta_{q1}$ | Danger of Fire Activation $\delta_{q2}$ | Examples of Occupancies |
|---|---|---|---|
| 25 | 1,10 | 0,78 | artgallery, museum, swimming pool |
| 250 | 1,50 | 1,00 | offices,residence, hotel, paper industry |
| 2 500 | 1,90 | 1,22 | manufactory for machinery & engines |
| 5 000 | 2,00 | 1,44 | chemical laboratory, painting workshop |
| 10 000 | 2,13 | 1,66 | manufactory of fireworks or paints |

The correction factor $\delta_n$ which takes into account different usual active measures if exist is calculated according to *Table A.2* by the following equation, provided in Annex E of EN 1991-1-2 (2002). If a certain measure does not exist, the corresponding factor should be taken as 1.0.

$$\delta_n = \prod_{i=1}^{10} \delta_{ni} \qquad (A.2)$$

*Table A.2* - Factors $\delta_{ni}$ (Annex E of EN 1991-1-2)

| Automatic Fire Suppression | | Automatic Fire Detection | | | Manual Fire Suppression | | | | |
|---|---|---|---|---|---|---|---|---|---|
| Automatic Water Extinguishing System | Independent Water Supplies | Automatic fire Detection & Alarm | | Automatic Alarm Transmission to Fire Brigade | Work Fire Brigade | Off Site Fire Brigade | Safe Access Routes | Fire Fighting Devices | Smoke Exhaust System |
| | 0 \| 1 \| 2 | by Heat | by Smoke | | | | | | |
| $\delta_{n1}$ | $\delta_{n2}$ | $\delta_{n3}$ | $\delta_{n4}$ | $\delta_{n5}$ | $\delta_{n6}$ | $\delta_{n7}$ | $\delta_{n8}$ | $\delta_{n9}$ | $\delta_{n10}$ |
| 0,61 | 1,0 \| 0,87 \| 0,7 | 0,87 or 0,73 | | 0,87 | 0,61 or 0,78 | | 0,9 or 1 or 1,5 | 1,0 or 1,5 | 1,0 or 1,5 |

In this case, it is considered that the only measure existing is Off-site fire brigade ($\delta_{n7} = 0.78$), and safe access routes are also present ($\delta_{n8} = 1.0$), so the overall correction factor is

$$\delta_n = \prod_{i=1}^{10} \delta_{ni} = 1.0 \cdot 1.0 \cdot 1.0 \cdot 1.0 \cdot 1.0 \cdot 1.0 \cdot 0.78 \cdot 1.0 \cdot 1.0 \cdot 1.5 = 1.17$$

According to Annex E (Table E.4) of the same standard, the characteristic value of the fire load density for offices is

$$q_{f,k} = 511 \ \frac{MJ}{m^2}$$

Finally, the design value of the fire load density is calculated as

$$q_{f,d} = q_{f,k} \cdot m \cdot \delta_{q1} \cdot \delta_{q2} \cdot \delta_n = 511 \cdot 0.8 \cdot 1.33 \cdot 1.0 \cdot 1.17 = 636.1 \frac{MJ}{m^2}$$

- CALCULATION OF THE PARAMETRIC TEMPERATURE-TIME CURVE

It has to be checked whether the fully engulfed fire is fuel or ventilation controlled. Annex A of the EN 1991-1-2 (2002) gives procedure for this calculation which consists of several steps.

First, the so-called opening factor ($O$) and the design value of the fire load density which refers to the total surface ($q_{t,d}$) are required.

$$O = \sqrt{h_{eq}} \cdot \frac{A_v}{A_t} = \sqrt{1.15} \cdot \frac{19.2}{275.7} = 0.07468 \ m^{1/2} \quad \begin{cases} \geq 0.02 \\ \leq 0.2 \end{cases}$$

$$q_{t,d} = q_{f,d} \cdot \frac{A_f}{A_t} = 636.1 \cdot \frac{84.968}{275.7} = 196.04\ \frac{MJ}{m^2} \quad \begin{cases} \geq 50 \\ \leq 1000 \end{cases}$$

Now, whether the fire is fuel or ventilation controlled depends on the time corresponding to the maximum temperature developed in compartment, and it is calculated with the following expression

$$t_{max} = \max \begin{cases} 0.2 \cdot 10^{-3} \cdot \frac{q_{t.d}}{O} = 0.2 \cdot 10^{-3} \cdot \frac{196.04}{0.07468} = 0.525h = 31.5\text{min} \\ t_{lim} = 0.33\text{h} = 20\text{min}\ (\text{for medium fire growth rate} - \text{office}) \end{cases}$$

Since $t_{max} \geq t_{lim}$ it means that the fire is ventilation controlled.

The following step in this procedure is to calculate separately heating and cooling phase, which are given as two separate functions.

- Heating phase:

The temperature-time curve which presents the heating phase is given by

$$\theta_g = 20 + 1325 \cdot \left(1 - 0.324 \cdot e^{-0.2 \cdot t^*} - 0.204 \cdot e^{-1.7 \cdot t^*} - 0.472 \cdot e^{-19 \cdot t^*}\right) \qquad (A.3)$$

Where the time $t^*$ for ventilation controlled fire is calculated as

$$t^* = t \cdot \Gamma \qquad (A.4)$$

and factor Γ is given by

$$\Gamma = \frac{(\text{O}/\text{b})^2}{(0.04/1160)^2} \qquad (A.5)$$

In order to calculate factor Γ, parameter b has to be calculated by following expression

$$b = \sqrt{\rho \cdot \lambda \cdot c} \qquad (A.6)$$

where $\rho, \lambda, c$ are density, thermal conductivity and specific heat of the corresponding boundary, which values may be taken at ambient temperature. If any of the boundaries of compartment (walls, floor or ceiling) are consisted of severeal layers, then this parameter has to be calculated as follows

- If $b_1 < b_2$ then $b = b_1$

- If $b_1 > b_2$ then limit thickness $s_{lim}$ has to be calculated for the exposed material as

$$s_{lim} = \sqrt{\frac{3600 \cdot t_{max} \cdot \lambda_1}{c_1 \cdot \rho_1}} \qquad (A.7)$$

$$\text{if } s_1 > s_{lim} \quad \text{then} \quad b = b_1$$
$$\text{if } s_1 < s_{lim} \quad \text{then} \quad b = b_1 \cdot \frac{s_1}{s_{lim}} + \left(1 - \frac{s_1}{s_{lim}}\right) \cdot b_2 \qquad (A.8)$$

where the denotation 1 refers to the layer which is directly exposed to fire, the denotation 2 refers to the next adjacent layer, etc.

Finally the factor b, as an avarage value has to be calculated, using the given formula

$$b = \frac{\sum(b_i \cdot A_i)}{A_t - A_v} \qquad (A.9)$$

- Floor: (normalwight concrete)

$$b_{floor} = \sqrt{2300 \cdot 1.6 \cdot 1000} = 1918.33 \; \frac{J}{m^2 \cdot s^{\frac{1}{2}} \cdot K} \begin{cases} \geq 100 \\ \leq 2200 \end{cases}$$

- Ceiling: (Layer 1- Glass wool and rockwool)

$$b_{ceil,1} = \sqrt{60 \cdot 0.037 \cdot 1030} = 47.82 \; \begin{cases} \geq 100 \\ \leq 2200 \end{cases} \Rightarrow 100 \; \frac{J}{m^2 \cdot s^{\frac{1}{2}} \cdot K}$$

- Ceiling: (Layer 2- Gypsum board)

$$b_{ceil,2} = \sqrt{900 \cdot 0.25 \cdot 1000} = 474.34 \; \frac{J}{m^2 \cdot s^{\frac{1}{2}} \cdot K} \begin{cases} \geq 100 \\ \leq 2200 \end{cases}$$

- Walls inside: (Lightweight concrete)

$$b_{wall,in} = \sqrt{1600 \cdot 0.8 \cdot 840} = 1036.92 \; \frac{J}{m^2 \cdot s^{\frac{1}{2}} \cdot K} \begin{cases} \geq 100 \\ \leq 2200 \end{cases}$$

- Walls outside: (Gypsum board)

$$b_{wall,out} = \sqrt{900 \cdot 0.25 \cdot 1000} = 474.34 \; \frac{J}{m^2 \cdot s^{\frac{1}{2}} \cdot K} \begin{cases} \geq 100 \\ \leq 2200 \end{cases}$$

Finally, the factor b is calculated as

$$b = \frac{\sum(b_i \cdot A_i)}{A_t - A_v} = \frac{b_{floor} \cdot A_f + b_{ceiling} \cdot A_c + b_{walls} \cdot (A_{walls} - A_v)}{A_t - A_v}$$

$$b = \frac{1918.33 \cdot 84.97 + 100 \cdot 84.97 + 1036.92 \cdot 58.68 + 474.34 \cdot 47.1}{275.7 - 19.2}$$

$$b = 992.89 \; \frac{J}{m^2 \cdot s^{\frac{1}{2}} \cdot K} \begin{cases} \geq 100 \\ \leq 2200 \end{cases}$$

And now, the factor Γ and time $t^*$ may be calculated as

$$\Gamma = \frac{(O/b)^2}{(0.04/1160)^2} = \frac{(0.07468/992.89)^2}{(0.04/1160)^2} = 4.7577$$

$$t^* = t \cdot \Gamma = 4.7577 \cdot t \approx 4.76 \cdot t$$

Now the heating phase can be calculated:

$$\theta_g = 20 + 1325\left(1 - 0.324e^{-0.2(4.76 \cdot t)} - 0.204e^{-1.7(4.76 \cdot t)} - 0.472e^{-19(4.76 \cdot t)}\right)$$

or

$$\theta_g = 20 + 1325 \cdot (1 - 0.324 \cdot e^{-0.95 \cdot t} - 0.204 \cdot e^{-8.1 \cdot t} - 0.472 \cdot e^{-90.4 \cdot t})$$

- Cooling phase:

The temperature-time curves in the cooling phase depend on the maximum temperature and the time when the maximum temperature occurs ($t^*_{max}$), so this has first to be calculated as follows

$$t^*_{max} = t_{max} \cdot \Gamma = 0.525h \cdot 4.7577 = 2.498h$$

Since $t^*_{max} = 2.498h > 2h$ the function that represents the cooling phase is given by the following expression (Annex A, EN 1991-1-2)

$$\theta_g = \theta_{max} - 250 \cdot (t^* - t^*_{max} \cdot x) \qquad (A.10)$$

Where $x = 1.0$ if $t_{max} > t_{lim}$ which is the case here (ventilation controlled fire), and $\theta_{max}$ is calculated using the function for heating phase from the condition that these two curves are intersected in this point $\theta_{max} = \theta_g(t^*_{max})$

$$\theta_{max} = 20 + 1325\left(1 - 0.324e^{-0.2t^*_{max}} - 0.204e^{-1.7t^*_{max}} - 0.472e^{-19t^*_{max}}\right)$$
$$\theta_{max} = 1080.63℃$$

Finally, the cooling phase curve can be expressed as:

$$\theta_g = 1080.63 - 250 \cdot (4.76 \cdot t - 2.498)$$

Combination of the heating and cooling curves leads to the parametric temperature-time curve shown in *Figure A.1*.

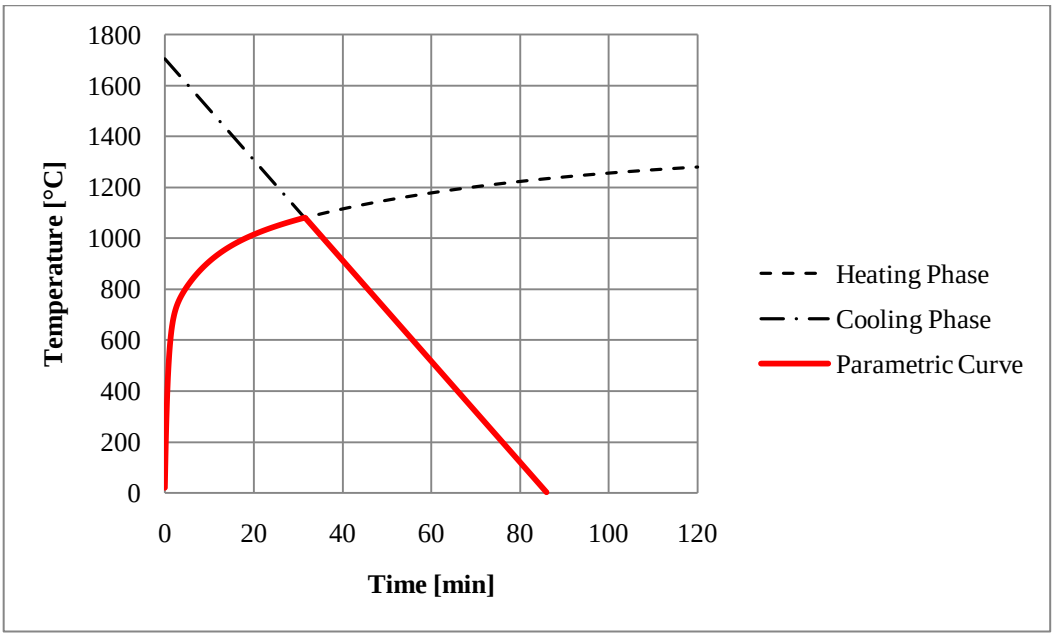


*Figure A.1* - Parametric temperature-time curve for the study case

- **<u>OZone V2 fire curve</u>:**

Here are added parameters which were used in calculation of fire zone curve in OZone program (Figure A.2 and Figure A.3).

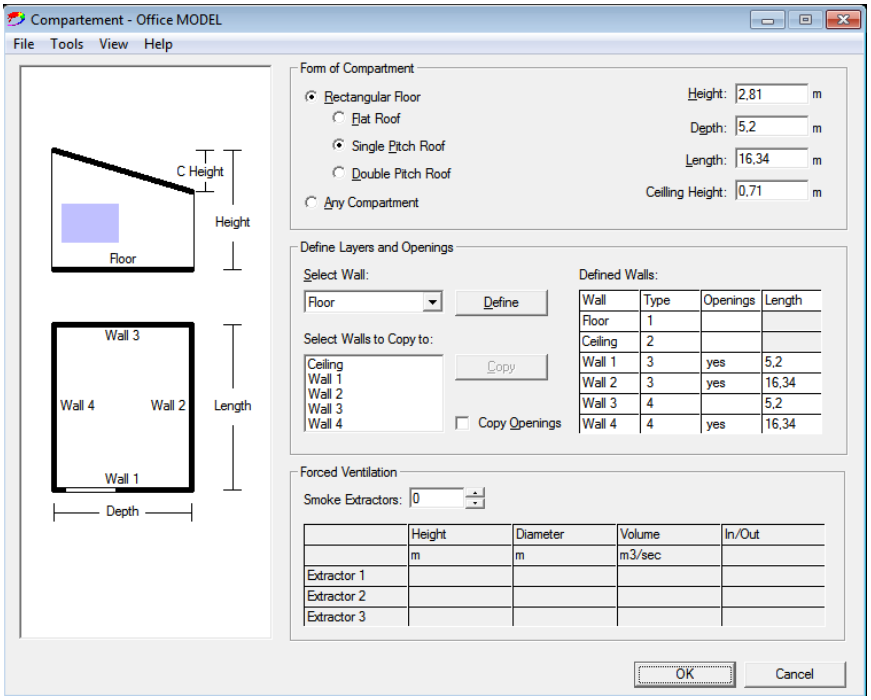


*Figure A.2* - Compartment parameters

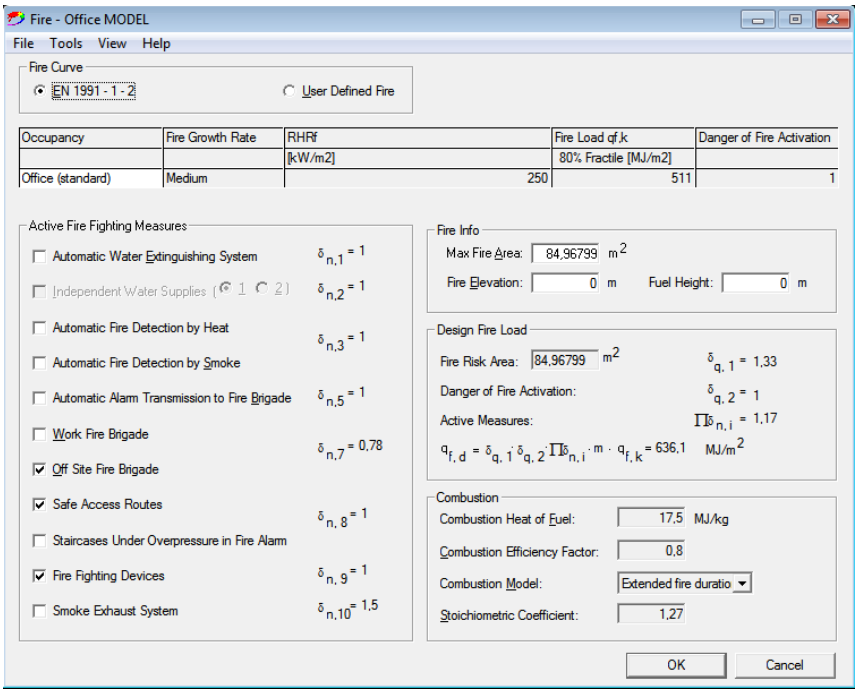


*Figure A.3* - Fire characteristics

# APPENDIX B – Effective cross sectional properties

In this appendix, the detailed analytical calculation of the effective cross section properties of Ω160 subjected to positive and negative bending moment is provided. The thickness of the cross section is constant and has value of 1 mm.

- **Cross-sectional dimensions:**

-Height of the section: $H = 160\ mm$

-Width of the bottom flange: $B = 195\ mm$

-Width of the top flange: $b = 75\ mm$

-Nominal thickness: $t_n = 1.0\ mm$

-Material core thickness: $t_c = t_n - t_{zinc}$ $t_c = 0.96mm$

$t_{zinc} = 0.04mm$ (Z275)

-Height of the section: (centre line) $H_c = 160\ mm$

-Width of the bottom flange: (centre line) $B_c = 194\ mm$

-Width of the top flange: (centre line) $b_c = 74\ mm$

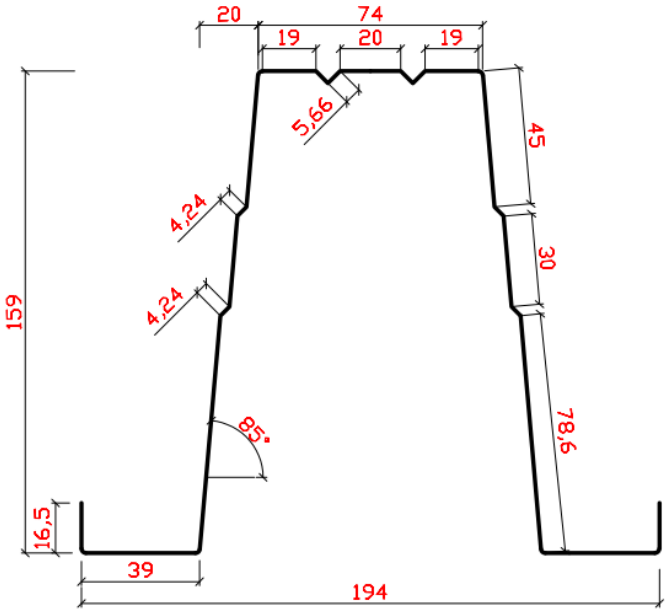


*Figure B.1* - Cross section dimensions

- **Material properties:**

-Young's module of elasticity: $E$ = 210000 N/mm$^2$

-Poisson ratio: $\nu$ = 0.3

-Shear modulus: $G$= 80770 N/mm$^2$

-Nominal yield strength (S280GD+Z): $f_{yb}$ = 280 N/mm$^2$

-Elastic strain: $\varepsilon = \sqrt{235/f_{yb}}$ $\varepsilon$ = 0.92

## B.1 Cross section subjected to positive bending moment

This calculation method follows the procedure given in 5.5.3.4 of EN 1993-1-3 (2004).

- **LOCAL BUCKLING**

First, the local buckling of the parts of the cross section that are subjected to compression has to be checked. Local buckling is accounted for by using effective cross-sectional properties, based on the concept of effective widths given in the EN 1993-1-5 (2006).

***1) <u>Flange</u>:***

- Stress ratio: (uniform compression) $\psi = \sigma_{min}/\sigma_{max}$ $\psi = 1.0$

- Buckling factor: $k_\sigma = 4.0$

[Table 4.1 of EN 1993-1-5, or here *Table 3.4*]

- Relative plate slenderness:

$$\overline{\lambda_p} = \frac{\bar{b}/t}{28.4\varepsilon\sqrt{k_\sigma}} = \frac{20/0.96}{28.4 \cdot 0.92 \cdot \sqrt{4}} = 0.3987$$

-Reduction factor:

$\overline{\lambda_p} = 0.3987 < 0.673$ $\rightarrow$ $\rho = 1.0$

-Effective flange widths: $b_{eff} = \rho \cdot \bar{b}$ $b_{1,eff} = b_{2,eff} = b_{eff}/2 = 10\ mm$

[Table 4.1 of EN 1993-1-5, or here *Table 3.4*]

The whole flange is effective in terms of local buckling!

***2) <u>Web</u>:***

- Stress ratio: (longest part in compression) $\psi = \sigma_{min}/\sigma_{max}$ $\psi = 0.47$

- Buckling factor: $k_\sigma = 8.2/(1.05 + \psi)$ $k_\sigma = 5.395$

[Table 4.1 of EN 1993-1-5, or here *Table 3.4*]

- Relative plate slenderness:

$$\overline{\lambda_p} = \frac{\bar{b}/t}{28.4\varepsilon\sqrt{k_\sigma}} = \frac{45/0.96}{28.4 \cdot 0.92 \cdot \sqrt{5.395}} = 0.772$$

-Reduction factor:

$$\overline{\lambda_p} = 0.772 > 0.7432 \quad \rightarrow \quad \rho = \frac{\overline{\lambda_p} - 0.055(3+\psi)}{\overline{\lambda_p}^2} = 0.975 < 1.0$$

-Effective web widths: $b_{eff} = \rho \cdot \bar{b}$ $b_{eff} = 43.88\ mm$

[Table 4.1 of EN 1993-1-5, or here *Table 3.4*]

This means that the web is not fully effective, and for the web with intermediate stiffeners the effective parts are calculated not according to Table 4.1 of EN 1993-1-5 (2006), but according to 5.5.3.4.3 of the EN 1993-1-3 (2004), as a special case.

- **DISTORTIONAL BUCKLING**

Distortional buckling for trapezoidal sheeting profiles with intermediate stiffeners is accounted for in Clause 5.5.3.4 of EN 1993-1-3 (2004), where the concept of reduced thickness of stiffeners or other parts of the cross-section undergoing distortional buckling according to the minimum distortional buckling stress is used.

***1) <u>Flanges with intermediate stiffeners</u>:*** (Clause 5.5.3.4.2 of EN 1993-1-3, 2004)

-Critical buckling stress: ($\sigma_{cr,s}$)
For two symmetrically placed flange stiffeners, the elastic critical buckling stress should be obtained from:

$$\sigma_{cr,s} = \frac{4.2 \cdot k_w \cdot E}{A_s} \cdot \sqrt{\frac{I_s \cdot t^3}{8 \cdot {b_1}^2 \cdot (3 \cdot b_e - 4 \cdot b_1)}} \qquad (B.1)$$

with

$$b_e = 2 \cdot b_{p,1} + b_{p,2} + 2 \cdot b_s \qquad (B.2)$$

$$b_1 = b_{p,1} + 0.5 \cdot b_r \qquad (B.3)$$

Where

$b_{p,1}$ is the notional flat width of an outer plane element (*Figure B.2*)

$b_{p,2}$ is the notional flat width of the central plane element (*Figure B.2*)

$b_r$ is the overall width of a stiffener (*Figure B.2*)

$b_r$ is the overall width of a stiffener (*Figure B.2*)

$A_s$ is the cross section area of the stiffener cross section (*Figure B.2*)

$I_s$ is the cross section second moment of area of the stiffener (*Figure B.2*)

$k_w$ is a coefficient that takes into account the partial rotational restraint of the flange by the webs

a)

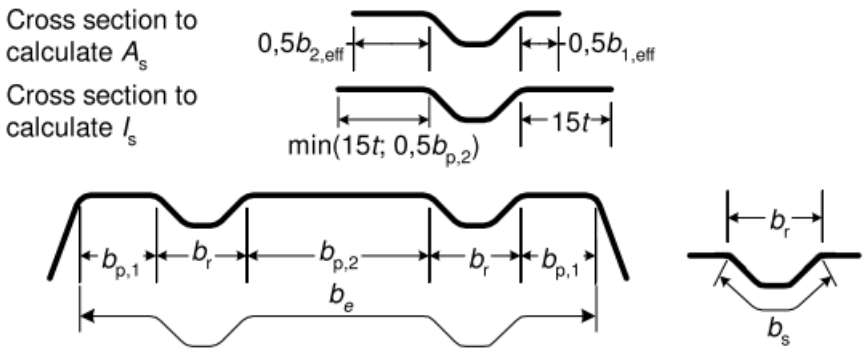


b)

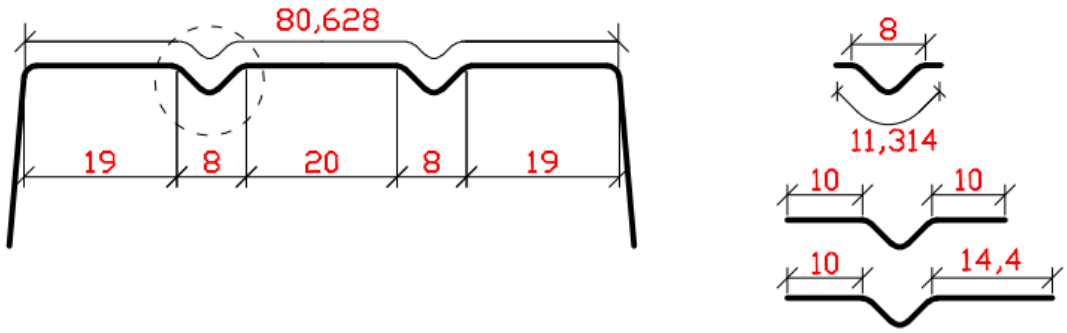


*Figure B.2* - Parameters for compression flange with two stiffeners
a) General according to 5.5.3.4.2 of EN 1993-1-3 and b) For Ω160

All these values are calculated according to *Figure B.2*, and presented below:

$$b_e = 2 \cdot b_{p,1} + b_{p,2} + 2 \cdot b_s = 2 \cdot 19 + 20 + 2 \cdot 11.314 = 80.628\ mm$$

$$b_1 = b_{p,1} + 0{,}5 \cdot b_r = 19 + 0.5 \cdot 8 = 23\ mm$$

$$A_s = 30.814\ mm^2$$

$$I_s = 49.861\ mm^4$$

-Flange buckling wavelength:

$$l_b = 3.65 \sqrt[4]{\frac{I_s \cdot {b_1}^2 \cdot (3b_e - 4b_1)}{t^3}} = 167.82\ mm$$

- Slant height of the web: (*Figure B.3*) $s_w = 160.1\ mm$

- Parameter $k_{wo}$ for a compression flange with two intermediate stiffeners:

$$k_{wo} = \sqrt{\frac{(3b_e - 4b_1) \cdot (3b_e - 4b_1)}{b_1 \cdot (4b_e - 6b_1) + (3b_e - 4b_1) \cdot s_w}} = 1.306$$

For $l_b / s_w = 1.048 < 2$, the value of $k_w$ may be calculated as follows:

$$k_w = k_{wo} - (k_{wo} - 1)\left[\frac{2l_b}{s_w} - \left(\frac{l_b}{s_w}\right)^2\right] = 1.0$$

Finally, the elastic critical buckling stress for compressed flange with two intermediate stiffeners is calculated:

$$\sigma_{cr,s} = \frac{4.2 \cdot k_w \cdot E}{A_s} \cdot \sqrt{\frac{I_s \cdot t^3}{8 \cdot {b_1}^2 \cdot (3b_e - 4b_1)}} = 238.71\ \text{MPa}$$

This value will be later used for the interaction between the distortional buckling (flexural buckling of the flange stiffeners and the web stiffeners), according to 5.5.3.4.4 of EN 1993-1-3 (2004).

***2) <u>Web with intermediate stiffeners</u>:*** (Clause 5.5.3.4.3 of EN 1993-1-3, 2004)

According to Clause 5.5.3.4.3 of EN 1993-1-3, the effective cross-section of a web should include: (*Figure B.3*)

a) a strip of width $s_{eff,1}$, adjacent to the compression flange

b) the reduced effective area $A_{s,red}$ of each web stiffener

c) a strip of width $s_{eff,n}$ adjacent to the effective centroidal axis

d) the part of the web in tension.

The effective areas of the stiffeners should be obtained from the following figure (*Figure B.3*).where all important dimensions are presented:

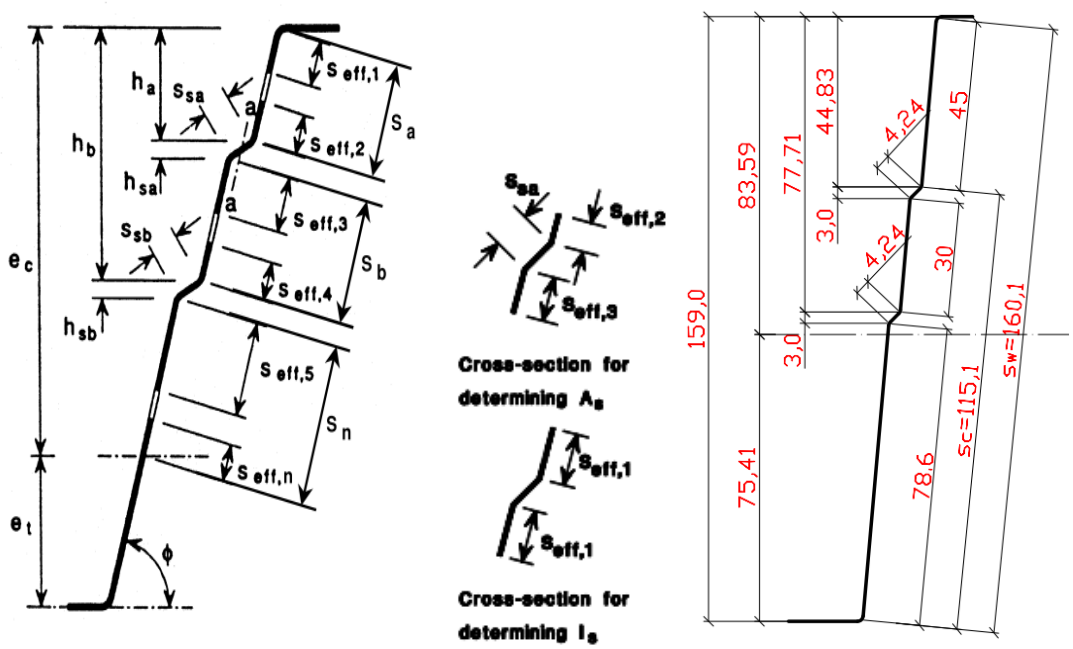


a) b) c)

*Figure B.3* - Parameters for web subject to stress gradient with two stiffeners
a) General according to 5.5.3.4.3 of EN 1993-1-3
b) Web stiffeners according to 5.5.3.4.3 of EN 1993-1-3
c) For Ω160

The dimensions $s_{eff,1}$ to $s_{eff,n}$ should be determined as follows:

$$s_{eff,0} = 0.76 \cdot t \cdot \sqrt{\frac{E}{\sigma_{com,Ed}}} = 0.76 \cdot 0.96 \cdot \sqrt{\frac{210 \cdot 10^3}{280}} = 19.98mm$$

$$s_{eff,1} = s_{eff,0} = 19.98mm$$

$$s_{eff,2} = (1 + 0.5 \cdot h_a/e_c) \cdot s_{eff,0} = 25.34mm$$

$$s_{eff,3} = [1 + 0.5(h_a + h_{sa})/e_c] \cdot s_{eff,0} = 25.7mm$$

$$s_{eff,4} = (1 + 0.5 \cdot h_b/e_c) \cdot s_{eff,0} = 29.27mm$$

$$s_{eff,5} = [1 + 0.5(h_b + h_{sb})/e_c] \cdot s_{eff,0} = 29.63mm$$

$$s_{eff,n} = 1.5 s_{eff,0} = 29.972mm$$

Where in expression for $s_{\text{eff},0}$ the stress in the compression flange, when the cross-section resistance is reached, is taken as: $\sigma_{com,\text{Ed}} = f_{yb} = 280\ N/mm^2$.

The dimensions $s_{eff,1}$ to $s_{eff,n}$ should be then corrected if the considered plane element is fully effective, using the following expressions given in Clause 6 of 5.5.3.4.3 of EN 1993-1-3 (2004):

(I) $s_{eff,1} + s_{eff,2} = 45.32mm > s_a = 45mm$

$$s_{eff,1} = \frac{s_a}{2 + 0.5 \cdot h_a/e_c} = 19.84\ mm$$

$$s_{eff,2} = s_a \cdot \frac{1 + 0.5 \cdot h_a/e_c}{2 + 0.5 \cdot h_a/e_c} = 25.16\ mm$$

(II) $s_{eff,3} + s_{eff,4} = 54.97mm > s_b = 30mm$

$$s_{eff,3} = s_b \cdot \frac{1 + 0.5(h_a + h_{sa})/e_c}{2 + 0.5(h_a + h_{sa} + h_b)/e_c} = 14.025\ mm$$

$$s_{eff,4} = s_b \cdot \frac{1 + 0.5 \cdot h_b/e_c}{2 + 0.5(h_a + h_{sa} + h_b)/e_c} = 15.975\ mm$$

(III) $s_{eff,5} + s_{eff,n} = 59.6mm > s_n = 2.86mm$

$$s_{eff,5} = s_n \cdot \frac{1 + 0.5(h_b + h_{sb})/e_c}{2.5 + 0.5(h_b + h_{sb})/e_c} = 1.426\ mm$$

$$s_{eff,n} = \frac{1.5 s_n}{2.5 + 0.5(h_b + h_{sb})/e_c} = 1.434\ mm$$

-Critical buckling stress: ($\sigma_{cr,sa}$)

For a single stiffener, or for the stiffener closer to the compression flange in webs with two stiffeners, the elastic critical buckling stress $\sigma_{cr,sa}$ should be obtained from:

$$\sigma_{cr,sa} = \frac{1.05 \cdot k_f \cdot E \cdot \sqrt{I_s \cdot t^3 \cdot s_1}}{A_{sa} \cdot s_2 \cdot (s_1 - s_2)} \qquad (B.4)$$

with

$$s_1 = s_a + s_{sa} + s_b + 0{,}5(s_{sb} + s_c) = 45 + 4.24 + 30 + 0.5(4.24 + 115.1) = 138.91\ mm$$

$$s_2 = s_1 - s_a - 0{,}5 s_{sa} = 138.91 - 45 - 0.5 \cdot 4.24 = 91.79\ mm$$

$A_{sa} = 43.4276\ mm^2$ (Figure B.3, b)

$I_{sa} = 96.3293\ mm^4$ (Figure B.3, b)

$k_f$ is a coefficient that takes into account partial rotational restraint of the web by the flanges (may be conservatively taken as 1.0)

Finally, the elastic critical buckling stress for compressed web with two intermediate stiffeners is calculated:

$$\sigma_{cr,sa} = \frac{1.05 \cdot k_f \cdot E \cdot \sqrt{I_s \cdot t^3 \cdot s_1}}{A_{sa} \cdot s_2 \cdot (s_1 - s_2)} = 127.73\ \text{MPa}$$

This value will be later used for the interaction between the distortional buckling (flexural buckling of the flange stiffeners and the web stiffeners), according to 5.5.3.4.4 of EN 1993-1-3 (2004).

***3) <u>Sheeting with flange stiffeners and web stiffeners</u>:***

According to 5.5.3.4.2 (10) and 5.5.3.4.3 (11), if both the webs and flanges are stiffened the reduction factor ($\chi_d$), which takes into account distortional buckling of both web and flange, should be calculated using the methodology described in this thesis (chapter 3.4.1), but with the modified elastic critical stress $\sigma_{cr,mod}$ given in 5.5.3.4.4 as

$$\sigma_{cr,mod} = \frac{\sigma_{cr,s}}{\sqrt[4]{1+\left(\beta_s \cdot \frac{\sigma_{cr,s}}{\sigma_{cr,sa}}\right)^4}} = \frac{238.706}{\sqrt[4]{1+\left(0.446 \cdot \frac{238.706}{127.73}\right)^4}} = 216.364 \text{ MPa}$$

Where the interaction factor $\beta_s$ for member in bending is calculated as

$$\beta_s = 1 - (h_a + 0.5 \cdot h_{sa})/e_c = 0.446$$

In 5.5.3.4.3 (16) of EN 1993-1-3 (2004) it is stated: "Optionally, the effective section properties may be refined iteratively by basing the location of the effective centroidal axis on the effective cross-sections of the webs determined by the previous iteration and the effective cross-sections of the flanges determined using the reduced thickness $t_{red}$ for all the elements included in the flange stiffener areas $A_s$." As it is given a freedom to choose if the iterative procedure will be performed, in this case that procedure is not conducted, which may be considered as safety-side solution.

- Relative slenderness: ($\overline{\lambda_d}$)

$$\overline{\lambda_d} = \sqrt{f_{yb}/\sigma_{cr,mod}} = \sqrt{280/216.364} = 1.136$$

- Reduction factor: ($\chi_d$)

$$0.65 < \overline{\lambda_d} = 1.042 < 1.38 \quad \rightarrow \quad \chi_d = 1.47 - 0.723\overline{\lambda_d} = 0.6487$$

The reduced effective area of the stiffener and reduced thickness of effective stiffener section which takes into account distortional buckling (flexural buckling of an intermediate stiffener) is calculated according to chapter 3.4.1 of this thesis separately for stiffened flange and stiffened web, as follows:

***Flange:***

$$A_{s,red} = \chi_d A_s \frac{f_{yb}/\gamma_{M0}}{\sigma_{com,Ed}} = 0.6487 \cdot 30.814 \cdot \frac{280/1.0}{276.22} = 20.26mm^2$$

$$t_{red} = t \cdot \frac{A_{s,red}}{A_s} = 1.0 \cdot \frac{20.26}{30.814} = 0.66\ mm$$

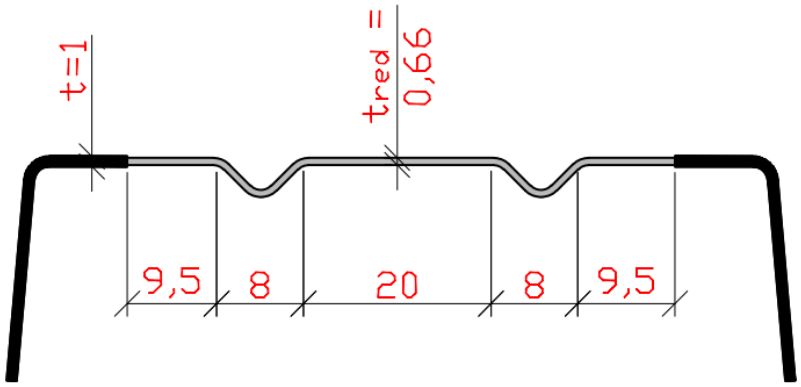


*Figure B.4* - Effective area of the flange

***Web:***

$$A_{sa,red} = \chi_d A_{sa} \frac{f_{yb}/\gamma_{M0}}{\sigma_{com,Ed}} = 0.6487 \cdot 43.4276 \cdot \frac{280/1.0}{123.34} = 63.96mm^2$$

$$t_{red} = t \cdot \frac{A_{s,red}}{A_s} = 1.0 \cdot \frac{63.96}{43.4276} = 1.473mm > t \quad \rightarrow \quad t_{red} = t = 1.0mm$$

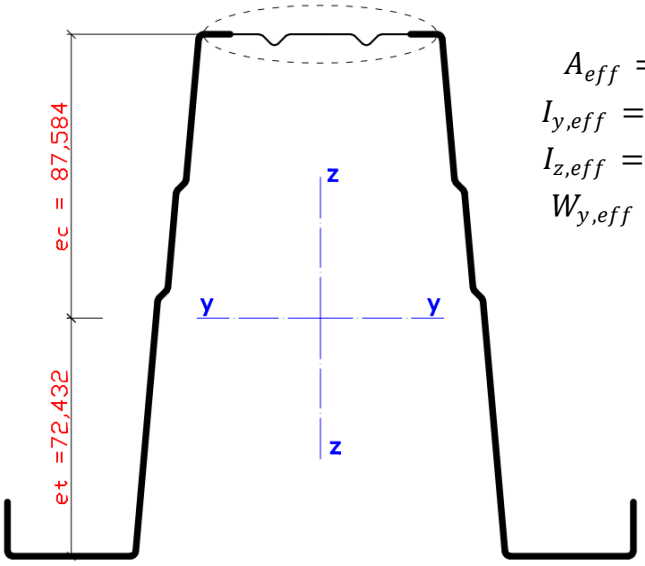


$$A_{eff} = 4.95\ cm^2$$
$$I_{y,eff} = 168.16\ cm^4$$
$$I_{z,eff} = 152.53\ cm^4$$
$$W_{y,eff} = 19.2\ cm^3$$

*Figure B.5* - Schematic layout of effective cross-section

## B.2 Cross section subjected to negative bending moment

(This calculation method follows the procedure given in 5.5.3.2 of EN 1993-1-3)

The concept prescribed in EN 1993-1-3 (2004) considers that first effective properties of the flange with the edge stiffener have to be calculated and then for new position of the neutral axis, the effective properties of the compressed part of the web are calculated.

***1) Flange with edge stiffener:***

The local buckling of the parts of the cross section that are subjected to compression has to be checked. Local buckling is accounted for by using effective cross-sectional properties, based on the concept of effective widths given in the EN 1993-1-5 (2006).

***1.Iteration:*** (Initial effective cross-section for the stiffener)

- FLANGE:

$\bar{b} = b_p = 39\ mm$
$t = 0.96\ mm$

- Stress ratio: (uniform compression) $\psi = \sigma_{min}/\sigma_{max}$ $\psi = 1$

- Buckling factor: $k_\sigma = 4.0$
[Table 4.1 of EN 1993-1-5, or here *Table 3.4*]

- Relative plate slenderness:

$$\overline{\lambda_p} = \frac{\bar{b}/t}{28.4\varepsilon\sqrt{k_\sigma}} = \frac{39/0.96}{28.4 \cdot 0.92 \cdot \sqrt{4}} = 0.777$$

-Reduction factor:

$$\overline{\lambda_p} = 0.777 > 0.673 \quad \rightarrow \quad \rho = \frac{\overline{\lambda_p} - 0.055(3+\psi)}{\overline{\lambda_p}^2} = 0.923$$

-Effective flange widths: $b_{\text{eff}} = \rho \cdot \bar{b}$ $b_{\text{eff}} = 35.98mm$
[Table 4.1 of EN 1993-1-5, or here *Table 3.4*]

- Effective widths:

$b_{e1} = b_{e2} = 0.5 b_{eff} = 17.99mm$

-LIP:

The effective width $c_{eff}$ should be calculated using the corresponding buckling factor $k_\sigma$, $\overline{\lambda_p}$ and $\rho$ expressions as follows: (Clause 5.5.3.2 of EN 1993-1-3)

$b_{p,c} = 16.5mm$

$$\frac{b_{p,c}}{b_p} = \frac{16.5}{39} = 0.423 > 0.35 \quad \rightarrow \quad k_\sigma = 0.5 + 0.83\sqrt[3]{\left[\frac{b_{p,c}}{b_p} - 0.35\right]^2} = 0.645$$

(EN 1993-1-3, Eq. 5.13c)

$$\overline{\lambda_p} = \frac{\bar{b}/t}{28.4\varepsilon\sqrt{k_\sigma}} = \frac{16.5/0.96}{28.4 \cdot 0.92 \cdot \sqrt{0.645}} = 0.819$$

Cold formed outstand elements:

$$\overline{\lambda_p} = 0.819 > 0.748 \quad \rightarrow \quad \rho = \frac{\overline{\lambda_p} - 0.188}{\overline{\lambda_p}^2} = 0.941 < 1.0$$

- Effective width:

$c_{eff} = \rho b_{p,c} = 0.941 \cdot 16.5 = 15.52mm$

The geometrical properties of effective edge stiffener section are calculated after the first iteration according to 5.5.3.2 of EN 1993-1-3 (2004): (*Figure B.6*)

a) b)

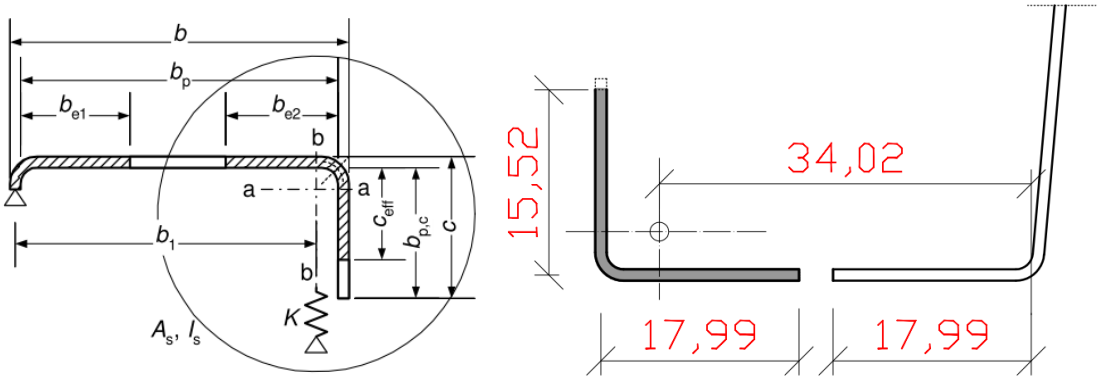


*Figure B.6* - Effective edge stiffener section -1st Iteration
a) Parameters for calculation of stiffness (5.5.3.2 of EN 1993-1-3) and b) For Ω160

$A_s = 32.652\ mm^2$

$I_s = 801.98\ mm^4$

Calculation of linear spring stiffness $K_1$: (EN 1993-1-3, Eq. 5.10b)

$$K_1 = \frac{Et^3}{4(1-\nu^2)} \cdot \frac{1}{{b_1}^2 h_w + {b_1}^3 + 0.5 b_1 b_2 h_w k_f} = 0.23 \text{ MPa}$$

Where:

- $b_1$ = 34.02 mm (the distance from the web-to-flange junction to the gravity centre of the effective area of the edge stiffener, including the efficient part of the flange $b_{e2}$)

- $k_f$ =0 (flange 2 is in tension)

- $h_w$ =*h*-2*t* = 158mm (the web depth)

Elastic critical buckling stress for the effective stiffener section: (EN 1993-1-3, Eq. 5.15)

$$\sigma_{cr,s} = \frac{2\sqrt{KEI_s}}{A_s} = 380.95 \text{ MPa}$$

Reduction factor $\chi_d$ for distortional buckling: (EN 1993-1-3, Eq. 5.12d)

$$\overline{\lambda_d} = \sqrt{\frac{f_{yb}}{\sigma_{cr,s}}} = \sqrt{\frac{280}{380.95}} = 0.8573$$

For $0.65 < \overline{\lambda_d} < 1.38 \quad \rightarrow \quad \chi_d = 1.47 - 0.723\overline{\lambda_d} = 0.85 < 1.0$

***2.Iteration:***

According to 5.5.3.2 of EN 1993-1-3 (2004), if $\chi_d$ < 1 it may be refined iteratively, starting the iteration with modified values of $\rho$ obtained using 5.5.2(5) with $\sigma_{com,Ed,i}$ equal to $\chi_d f_{yb}/\gamma_{M0}$, so that:

- <u>FLANGE</u>:

$$\overline{\lambda_p}^{(2)} = \overline{\lambda_p}\sqrt{\chi_d{}^{(1)}} = 0.777\sqrt{0.85} = 0.7164$$

$$\overline{\lambda_p} = 0.7164 > 0.673 \quad \rightarrow \quad \rho = \frac{\overline{\lambda_p} - 0.055(3+\psi)}{\overline{\lambda_p}^2} = 0.9672 < 1.0$$

- Effective width:

$$b_{eff} = \rho \bar{b} = 0.9672 \cdot 39 = 37.72\, mm$$
$$b_{e1} = b_{e2} = 0.5 b_{eff} = 18.86\, mm$$

-LIP:

$$\overline{\lambda_p}^{(2)} = \overline{\lambda_p}\sqrt{\chi_d{}^{(1)}} = 0.819\sqrt{0.85} = 0.7551$$

$$\overline{\lambda_p} = 0.7551 > 0.748 \quad \rightarrow \quad \rho = \frac{\overline{\lambda_p} - 0.188}{\overline{\lambda_p}^2} = 0.995 < 1.0$$

- Effective width:

$$c_{eff} = \rho b_{p,c} = 0.995 \cdot 16.5 = 16.41mm$$

The geometrical properties of effective edge stiffener section are calculated after the second iteration according to 5.5.3.2 of EN 1993-1-3 (2004): (*Figure B.7*)

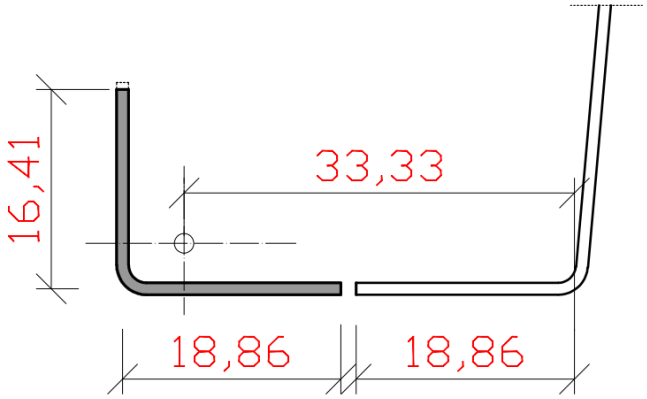


$A_s = 34.412\ mm^2$

$I_s = 946.26\ mm^4$

*Figure B.7* - Effective edge stiffener section -2nd Iteration

Calculation of linear spring stiffness $K_1$: (EN 1993-1-3, Eq. 5.10b)

$$K_1 = \frac{Et^3}{4(1-\nu^2)} \cdot \frac{1}{b_1{}^2 h_w + b_1{}^3 + 0.5 b_1 b_2 h_w k_f} = 0.24 \text{ MPa}$$

Where:

- $b_1$ = 33.33 mm
- $k_f$ =0 (flange 2 is in tension)
- $h_w$ =$h$-2$t$ = 158mm (the web depth)

Elastic critical buckling stress:

$$\sigma_{cr,s} = \frac{2\sqrt{KEI_s}}{A_s} = 401.5 \text{ MPa}$$

$$\overline{\lambda_d} = \sqrt{\frac{f_{yb}}{\sigma_{cr,s}}} = \sqrt{\frac{280}{401.5}} = 0.8351$$

For $0.65 < \overline{\lambda_d} < 1.38 \quad \rightarrow \quad \chi_d = 1.47 - 0.723\overline{\lambda_d} = 0.866 < 1.0$

***3.Iteration:***

- FLANGE:

$$\overline{\lambda_p}^{(3)} = \overline{\lambda_p}\sqrt{\chi_d{}^{(2)}} = 0.777\sqrt{0.866} = 0.723$$

$$\overline{\lambda_p} = 0.723 \ > 0.673 \qquad \rightarrow \qquad \rho = \frac{\overline{\lambda_p} - 0.055(3+\psi)}{\overline{\lambda_p}^2} = 0.9626 < 1.0$$

- Effective width:

$$b_{eff} = \rho\bar{b} = 0.9626 \cdot 39 = 37.54\ mm$$
$$b_{e1} = b_{e2} = 0.5 b_{eff} = 18.77\ mm$$

-LIP:

$$\overline{\lambda_p}^{(3)} = \overline{\lambda_p}\sqrt{\chi_d{}^{(2)}} = 0.819\sqrt{0.866} = 0.762$$

$$\overline{\lambda_p} = 0.762 \ > 0.748 \qquad \rightarrow \qquad \rho = \frac{\overline{\lambda_p} - 0.188}{\overline{\lambda_p}^2} = 0.988 < 1.0$$

$$c_{\text{eff}} = \rho b_{p,c} = 0.988 \cdot 16.5 = 16.32mm$$

The geometrical properties of effective edge stiffener section are calculated after the second iteration according to 5.5.3.2 of EN 1993-1-3 (2004): (*Figure B.8*)

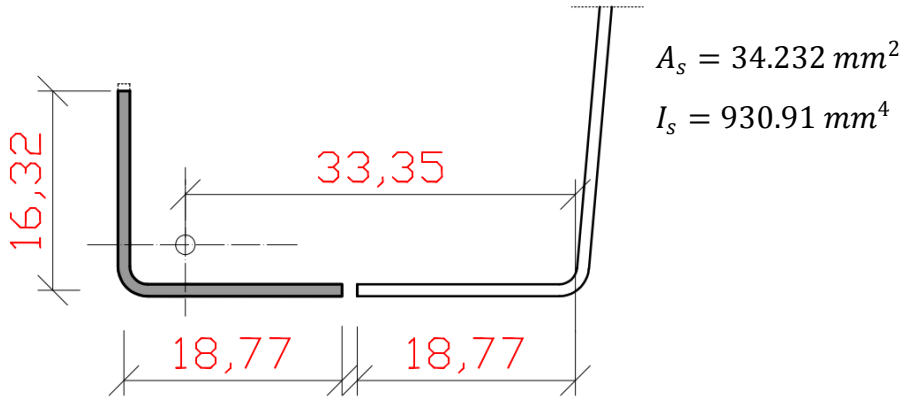


*Figure B.8* - Effective edge stiffener section -3rd Iteration

Calculation of linear spring stiffness $K_1$: (EN 1993-1-3, Eq. 5.10b)

$$K_1 = \frac{Et^3}{4(1-\nu^2)} \cdot \frac{1}{{b_1}^2 h_w + {b_1}^3 + 0.5 b_1 b_2 h_w k_f} = 0.239 \text{ MPa}$$

Where:

- $b_1$ = 33.35 mm
- $k_f$ =0 (flange 2 is in tension)
- $h_w$ =$h$-2$t$ = 158 mm (the web depth)

Elastic critical buckling stress:

$$\sigma_{cr,s} = \frac{2\sqrt{KEI_s}}{A_s} = 400.1 \text{ MPa}$$

$$\overline{\lambda_d} = \sqrt{\frac{f_{yb}}{\sigma_{cr,s}}} = \sqrt{\frac{280}{400.1}} = 0.8366$$

For $0.65 < \overline{\lambda_d} < 1.38 \quad \rightarrow \quad \chi_d = 1.47 - 0.723\overline{\lambda_d} = 0.865 < 1.0$

***4.Iteration:***

- <u>FLANGE</u>:

$$\overline{\lambda_p}^{(4)} = \overline{\lambda_p}\sqrt{\chi_d{}^{(3)}} = 0.777\sqrt{0.865} = 0.723$$

$$\overline{\lambda_p} = 0.723 > 0.673 \quad \rightarrow \quad \rho = \frac{\overline{\lambda_p} - 0.055(3+\psi)}{\overline{\lambda_p}^2} = 0.9626 < 1.0$$

Since the reduction factor $\rho^{(4)} = \rho^{(3)} = 0.9626$ the iterative process stops here and the values of effective widths from the previous iteration are adopted

- Effective width:

$$b_{eff} = \rho\bar{b} = 0.9626 \cdot 39 = 37.54\ mm$$
$$b_{e1} = b_{e2} = 0.5b_{eff} = 18.77\ mm$$

-<u>LIP</u>:

$$\overline{\lambda_p}^{(4)} = \overline{\lambda_p}\sqrt{\chi_d{}^{(3)}} = 0.819\sqrt{0.865} = 0.762$$

$$\overline{\lambda_p} = 0.762 > 0.748 \quad \rightarrow \quad \rho = \frac{\overline{\lambda_p} - 0.188}{\overline{\lambda_p}^2} = 0.988 < 1.0$$

Since the reduction factor $\rho^{(4)} = \rho^{(3)} = 0.988$ the iterative process stops here and the values of effective widths from the previous iteration are adopted

$$c_{eff} = \rho b_{p,c} = 0.988 \cdot 16.5 = 16.32mm$$

- Final geometric properties of effective edge stiffener section are given and for these values the new position of the neutral axis is calculated, which is necessary for calculation of $\sigma_{com,Ed}$ and thus $t_{red}$ (*Figure B.9*).

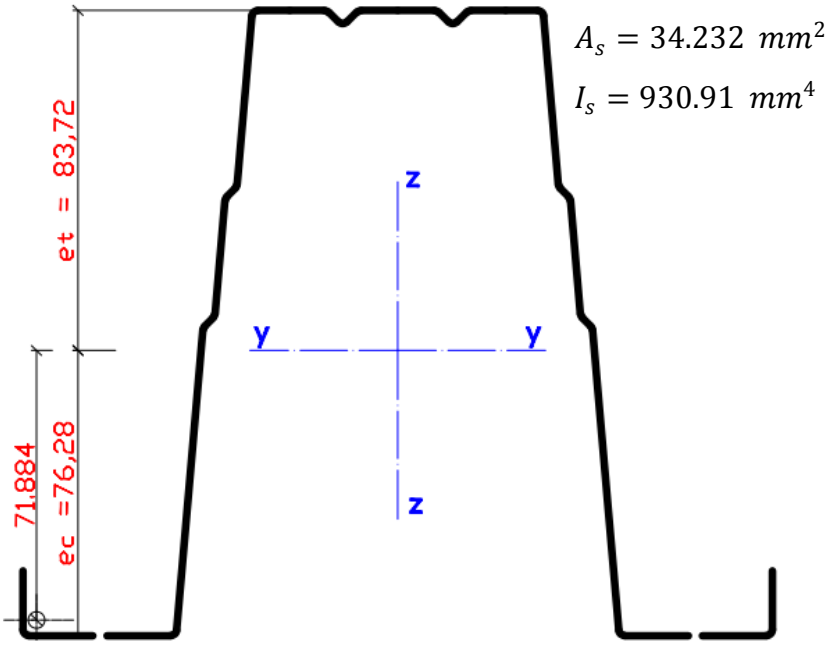


*Figure B.9* - Effective cross section – shifting of the neutral axis

Reduction factor $\chi_d$ for distortional buckling

$\chi_d{}^{(4)} = \chi_d{}^{(3)} \quad \rightarrow \quad \chi_d = 0.865$

Reduced area and thickness of effective stiffener section: (EN 1993-1-3, Eq. 5.17)

$$A_{s,red} = \chi_d A_s \frac{f_{yb}/\gamma_{M0}}{\sigma_{com,Ed}} = 0.865 \cdot 34.232 \cdot \frac{280/1.0}{263.86} = 31.42\ mm^2$$

Where

$\sigma_{com,Ed}$ is compressive stress at the centreline of the stiffener calculated on the basis of the effective cross-section (Figure B.9), obtained from

$$\sigma_{com,Ed} = \frac{71.884}{76.28} \cdot f_{yb} = 263.86\ \text{MPa}$$

The reduced effective area $A_{s,red}$ should be represented by using a reduced thickness $t_{red}$ for all the elements included in $A_s$.

$$t_{red} = t \cdot \frac{A_{s,red}}{A_s} = 1.0 \cdot \frac{31.42}{34.232} \qquad \Rightarrow \qquad \boldsymbol{t_{red} = 0.92\ mm}$$

Finally, the effective cross section with reduced thickness of the edge stiffener is shown in the following figure (*Figure B.10*):

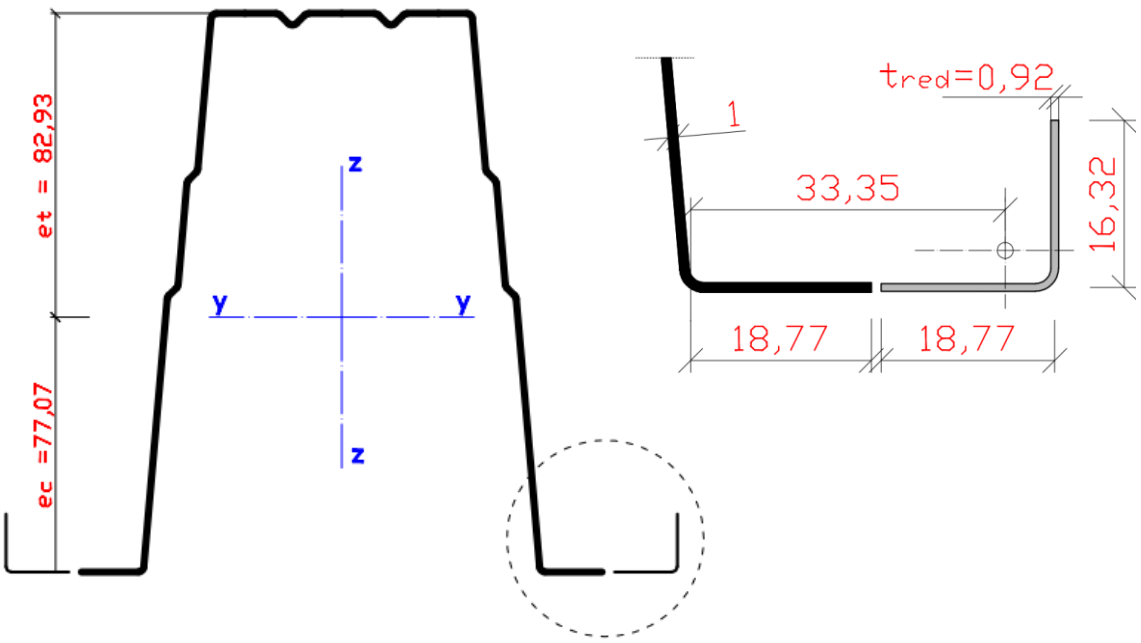


*Figure B.10* - Effective cross section with reduced thickness considering only flanges

***2) <u>Web</u>:***

$\bar{b} = 159\ mm$

$t = 0.96\ mm$

Stress distribution in the web is affected by shifting of neutral axis due to reduction of thickness in compressed flange (*Figure B.10*)

$$\psi = \frac{\sigma_2}{\sigma_1} = \frac{82.93}{-77.07} = -1.076$$

Buckling factor $k_\sigma$ is calculated according to EN 1993-1-5, Table 4.1 (or Table 3.4 in this thesis).

For $-3 < \psi < -1 \quad \rightarrow \quad k_\sigma = 5.98(1-\psi)^2 = 25.77$

$$\overline{\lambda_p} = \frac{\bar{b}/t}{28.4\varepsilon\sqrt{k_\sigma}} = \frac{159/0.96}{28.4 \cdot 0.92 \cdot \sqrt{25.77}} = 1.249$$

$$\overline{\lambda_p} = 1.249 > 0.88 \quad \rightarrow \quad \rho = \frac{\overline{\lambda_p} - 0.055(3+\psi)}{\overline{\lambda_p}^2} = 0.733 < 1.0$$

- Effective widths:

$$b_{eff} = \rho\bar{b}_c = \frac{\rho\bar{b}}{1-\psi} = \frac{0.733 \cdot 159}{1+1.076} = 56.13\ mm$$

$b_{e1} = 0.4b_{eff} = 22.45\ mm$

$b_{e2} = 0.6b_{eff} = 33.68\ mm$

The effective cross section is presented below: (*Figure B.11*)

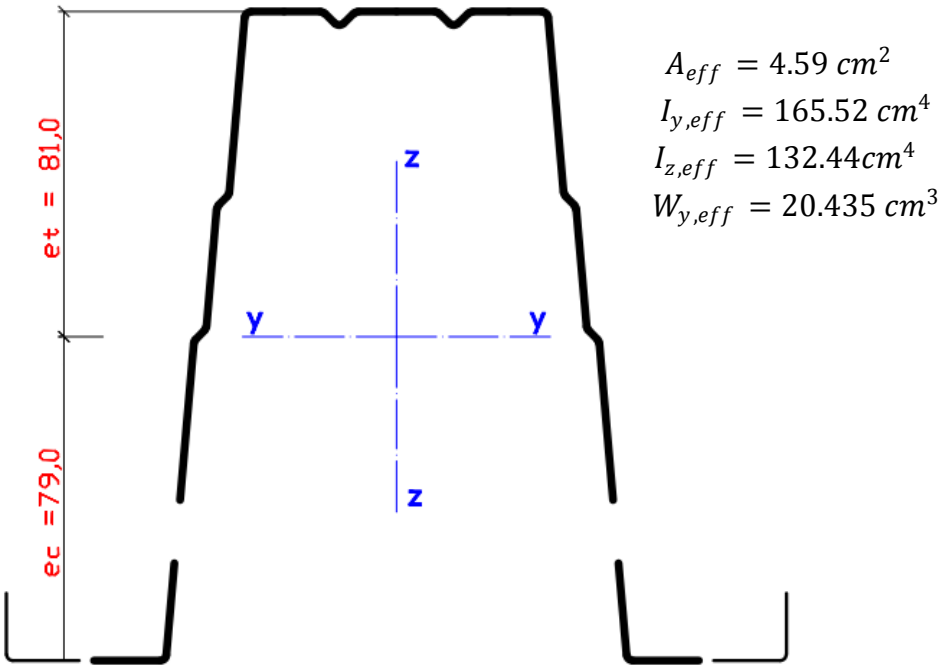


*Figure B.11* - Schematic layout of effective cross-section